REVIEWS OF GEOPHYSICS AND SPACE PHYSICS, VOL. 21, NO. 8, PAGES 1667–1725, NOVEMBER 1983

Bunte Breccia of the Ries: Continuous Deposits of Large Impact Craters

FRIEDRICH HÖRZ

Experimental Planetology Branch, NASA Johnson Space Center

ROLF OSTERTAG

Mineralogisches Institut, Universität Münster

D. A. RAINEY

Lockheed Engineering and Management Services Co., Inc.

The Ries Crater, an impact structure of 26 km diameter in south Germany, is the largest terrestrial crater where substantial amounts of ejecta are preserved, on occasion >100 m deep. Further, the target stratigraphy is well known, and it is possible to relate specific clasts and breccia lithologies to initial target depth. As a consequence the continuous deposits of the Ries, also known as Bunte Breccia, may be studied with exceptional field control. We report field observations and laboratory analyses obtained from 560-m core materials, taken at nine different locations that range from 16 to 37 km in radial distance from the impact center. The objective is to relate the Ries observations to ejection, and to emplacement processes of large-scale, planetary crater deposits. The observations regarding the modal-stratigraphic characteristics of the Bunte Breccia may be summarized as follows: only <0.15% (weight) of the total deposit consists of crystalline clasts larger than 1 cm that are derived from depths of >600 m; some 0.7% is composed of Triassic clasts, originating from 300 to 600-m depths; Lower and Middle Jurassic horizons (approximately 300–150 m) constitute some 2.3%, and Upper Jurassic (0–150 m) makes up some 31.5%. In addition, the Bunte Breccia contains Tertiary materials in the form of >1-cm clasts (29.1%) and as highly comminuted, fine-grained "matrix" (<1 cm) accounting for the remaining 36.3%; these Tertiary materials constituted the immediate crater environment, i.e., a substrate, onto which the Ries ejecta were deposited. These substrate materials were thoroughly mixed into the continuous deposits. The ratio of "primary crater ejecta" to local substrate components decreases with increasing radial range. There is, however, no vertical stratification with regard to modal-stratigraphic composition at any specific location; modal-stratigraphic composition is highly variable on meter scales; Bunte Breccia appears to be a chaotic mixture resulting from a highly turbulent depositional environment. Also, the orientation of clasts larger than 1 cm is random. Detailed grain size data reveal progressively decreasing grain sizes with increasing radial range of both primary crater ejecta and local substrate materials. In addition, progressive comminution of primary ejecta related to increasing target depth is observed. Components shocked to >10 GPa constitute <0.1% (weight) of the entire deposit, which indicates that Bunte Breccia was emplaced at essentially ambient temperatures. When possible, the above observations are quantified via linear regressions throughout the text. All of these observations are consistent with, if not predicted by, a ballistic emplacement scenario as postulated by Oberbeck and co-workers: primary crater ejecta are expelled ballistically and will form secondary craters in the local substrate; a mixture of primary and secondary ejecta results and combines into a highly turbulent, ground-hugging debris surge as the final phase of ejecta emplacement. Total emplacement time for the Bunte Breccia ($\geq$200 km^3) is estimated to be of the order of 5 min only. These findings are compared with cratering theory relating to a number of ejecta thickness decay models and with the so-called Z model, addressing material flow during various stages of crater formation. Qualitative to fair agreement of observations and predictions results. An initial crater radius of 6.5 km, an excavation depth of 1650 m, an excavation volume of 136 km^3, and an associated transient cavity volume of aproximately 230 km^3 appear to be reasonable estimates. Approximately 170 km^3 of material was involved in slumping and restoration of the transient cavity for the above radius and Z = 2.7. The modal composition of Ries ejecta with regard to preimpact target stratigraphy indicates that materials contained in the continuous deposits of large, complex planetary craters are predominantly derived from depths as small as one-hundredth the apparent crater diameter. A number of implications are addressed regarding remote sensing of planetary surfaces and investigation of lunar and meteoritic impact breccias.

CONTENTS

Introduction 1668
The problems 1668
The geology of the Ries Crater 1669
Field observations 1675
General comments 1675
Overview 1675
The contact Bunte Breccia/Country Rock 1675
Textural observations 1678
Breccias within breccias 1679
Summary of field observations 1683
Laboratory techniques and definitions 1683
Stratigraphic assignments 1683
Sieve analysis 1685
Heavy minerals 1686
Matrix studies 1686
Grain size analysis 1686
Heavy minerals 1687
Summary of matrix studies 1689
Clast studies 1689
Grain size 1689

This paper is not subject to U.S. copyright. Published in 1983 by the American Geophysical Union.

Paper number 3R1201.

Modal composition 1693
Clast orientation 1699
Shock metamorphic effects 1699
Summary of clast studies 1701
Comparison with cratering theory 1702
Ejecta distribution 1702
Excavation cavity 1704
Transient cavity 1707
Summary 1708
The deposition of Bunte Breccia 1709
The secondary cratering hypothesis 1709
Other emplacement scenarios 1713
Continuous deposits and target stratigraphy 1713
Summary of ejecta emplacement mechanisms 1716
Planetary implications 1716
The Apollo 14 landing site 1717
The Apollo 16 landing site 1717
The lunar megaregolith 1717
Lunar basin chronology 1717
Planetary impact breccias 1718
The formation of lunar light plains 1718
The chemistry of basin-forming projectiles 1718
Flow phenomena and impact melts in distal crater deposits 1718
Continuous deposits on Mars 1719
Concluding remarks 1720
Appendix A: rationale for specific site selection 1720
Appendix B: detailed core descriptions 1721

INTRODUCTION

Most extraterrestrial samples currently available for detailed analysis in the laboratory are derived from impact deposits. Detailed geologic-stratigraphic information on such deposits is generally unknown, and the stratigraphy of the original target site(s), such as the ancient lunar crust or an asteroidal surface, may be destroyed by impact cratering beyond direct observation. Therefore stratigraphic-petrogenetic reconstruction of planetary crusts and surfaces must employ various assumptions regarding impact processes.

Significant progress in our understanding of hypervelocity cratering has been accomplished during the last decade, but a large number of geologically important issues remain poorly understood. The reasons rest on one hand in the exceedingly complex and dynamic nature of the cratering process, which presently escapes comprehensive theoretical treatment from first principles, and on the other hand in our limited ability to extrapolate small-scale laboratory impact experiments with confidence to large, natural impact structures [e.g., *French and Short,* 1968; *Hörz,* 1971; *Roddy et al.,* 1977*a*; *Schultz and Merrill,* 1981]. Phenomenologic studies via photogeologic techniques and detailed investigation of terrestrial impact structures combine therefore with theory and experiment into our present understanding of the cratering process.

This study attempts to contribute specifically to a better understanding of the ejecta deposits of relatively large craters. Emphasis will be placed on synthesis of previous and new observations in the continuous deposits surrounding the Ries Crater, Germany. This structure is the largest terrestrial impact crater (26 km in diameter) where significant amounts of ejecta are preserved, and it thus constitutes the best terrestrial analog of large-scale planetary impact deposits. We will attempt to conceptualize first-order characteristics of the ejection process and its relation to target stratigraphy via detailed field and laboratory observations of the Ries ejecta.

THE PROBLEMS

Because the excavation of a crater cavity entails vertical and lateral redistribution of target materials, impact cratering is an important planetary transport and sedimentation process [*Oberbeck,* 1975; *Head,* 1976], indeed most likely the dominating process for redistributing crustal materials during early planetary evolution. Excavation, transport, and sedimentation processes occur on a wide variety of scales, because impact cratering may range from submicron size structures to big basins measuring hundreds of kilometers in diameter. Thus manifestations of the planetary cratering record will range from submicroscopic indentations on the surfaces of component grains to events of global, catastrophic consequences, resulting in complete destruction of the local stratigraphic record and significant redistribution of deep-seated, crustal materials over lateral distances exceeding 1000 km. Details of the ejection sequence and resulting ejecta transport and emplacement processes are poorly known for large-scale impact events, i.e., structures tens and hundreds of kilometers in diameter.

Numerous photogeologic studies contributed heavily to our understanding of the radial extent of ejecta blankets surrounding large fresh craters of morphological rim radius R (in kilometers). The average radial range r of "continuous" ejecta blankets on the moon is generally accepted as

$$r = 2.348R^{1.006} \quad (1)$$

according to *Moore et al.* [1974] and others. "Discontinuous" deposits beyond this radius are abundantly observed in the form of rays. An important question already arises: how much mass is deposited in the continuous deposits versus the discontinuous ray materials? The question cannot be solved by photogeologic techniques, because mass estimates require knowledge of the third dimension, which cannot be assessed with confidence via such techniques. Generally, one is forced to accept a model calculation (in part extrapolated from small-scale impact or explosion experiments) that describes the ejecta mass decay as a function of radial range, e.g.,

$$t_e = K(r/R_0)^{-x} \quad (2)$$

where t_e is the thickness of ejecta at radial range r and R_0 again is the radius of the parent crater. There is, unfortunately, considerable uncertainty concerning the exponent x as well as the constant K.

Another uncertainty concerns the actual mechanism(s) by which these ejecta are emplaced, i.e., particularly the continuous deposits. A ballistic transport regime was postulated and detailed as early as 1962 by *Shoemaker* [1962], which was more recently expanded by *Oberbeck* [1975] and others. Although considerable differences among various "ballistic" models exist, as detailed below, they principally contrast with "nonballistic" viewpoints. The latter envision depositional mechanisms akin to volcanic base surge processes in which some liberated, gaseous phase provides for adequate flow lubrication [*Heiken et al.,* 1973; *Lindsay,* 1974]. While such base surge processes are probably not operative on atmosphereless, volatile-poor bodies such as the moon [see *Oberbeck,* 1975], gaseous or liquid lubricants may well be important factors for volatile-rich targets, e.g., the earth and Mars [*Carr et al.,* 1977; *Greeley et al.,* 1980; *Kieffer and Simonds,* 1980]. Another nonballistic view entails that the

ejecta emanate from the crater cavity as a massive flow which contains sufficient kinetic energy to drape the crater environs to the observed distances of approximately 2.5 R [*Chao*, 1976, 1977*a*, *b*].

The differences in geological implications between ballistic and nonballistic emplacement mechanisms may be significant. Ballistic ejecta will form secondary craters in the "local" substrate surrounding the crater; secondary crater ejecta will be mixed with those from the parent crater; therefore the ejecta deposits constitute a mixture of primary and local (secondary) ejecta [*Oberbeck*, 1975]. Nonballistic mechanisms do not provide such interaction with the local substrate, and the continuous deposits are therefore predominantly composed of primary ejecta.

Another area of great uncertainty in large-scale cratering is the degree to which initial stratigraphic relationships within the parent crater are preserved in the continuous deposits. Small-scale cratering experiments [*Gault et al.*, 1968; *Stöffler et al.*, 1975; *Stöffler*, 1981], observations at Meteor Crater, Arizona [*Shoemaker*, 1963; *Roddy et al.*, 1975] and theoretical aspects [e.g., *Ahrens and O'Keefe*, 1978; *Schultz et al.*, 1981] indicate relatively orderly flow processes during crater excavation, resulting in an "overturned" flap of inverted target stratigraphy. Deep-seated target horizons are generally deposited on or near the rim, while successively shallower target strata occur predominantly at increasing radial ranges. Accordingly, a radial traverse on a crater's continuous deposits may yield stratigraphic information. Does this concept of inverted target stratigraphy, abundantly verified for relatively small impacts, also hold for large structures?

The Ries Crater is ideally suited to address some of the above questions. Its high degree of preservation is coupled with a fortunate geologic circumstance: the "local" substrate to the south of the crater is of distinctly different lithology than all "primary" crater ejecta, and thus an ideal situation exists for assessing the incorporation of local substrate components, i.e., for testing ballistic versus nonballistic scenarios. In addition, the initial target stratigraphy is well known and consists of a sequence of Triassic and Jurassic sediments. The various stratigraphic members can easily be identified with the naked eye on the basis of lithology and/or color, even as clasts that may be as small as 1 cm. Therefore individual ejecta fragments occurring at various radial ranges can be placed back into their proper vertical target position, and the concept of inverted target stratigraphy may be addressed.

The present paper details field and laboratory observations from nine drill cores totaling 560 m in cumulative length that penetrated the continuous Ries deposits at radial ranges from 16.5 to 37.5 km from the point of impact [*Hörz et al.*, 1977]. Additional field evidence reported by others will be reviewed. After synthesizing these Ries findings, general conclusions concerning cratering theory and planetary impact deposits will be offered.

THE GEOLOGY OF THE RIES CRATER

The Ries Crater was formed 15 m.y. ago [*Gentner and Wagner*, 1969], and it excavated a target of crystalline basement overlain by some 600 m of well-bedded, horizontal, Mesozoic sediments [*Preuss and Schmidt-Kaler*, 1969] as illustrated in Figure 1.

The crystalline rocks are of pre-Permian age (300–320 m.y. [*Jessberger et al.*, 1978; *Staudacher et al.*, 1982]). Both igneous and metamorphic rocks are present, i.e., a variety of granites, gneisses, and some subordinate amphibolites and lamprophyres [*Abadian*, 1972; *Graup*, 1975, 1978]. *Graup* [1978] provides the most detailed attempt to reconstruct the complex structural relationships of the crystalline basement. As best as can be determined, it appears that the basement is formed by a number of granitic intrusions into older gneisses. These late, intrusive granites form slablike, more or less horizontal bodies that thus occupy a relatively large surface area despite their relatively small absolute volume. There are uncertainties in thickness estimates for the lowermost members of the sedimentary column (Buntsandstein, Muschelkalk). Their thickness estimates given in Figure 1 are most likely on the high side. Starting with Keuper, however, the stratigraphy is well behaved and relatively flat lying, and thicknesses are well understood; i.e., >90% of the sedimentary stratigraphy is well known.

The existence of a Tertiary cap rock, however, is again somewhat problematical judging from Tertiary exposed in the vicinity of the Ries. Throughout the Tertiary period the general Ries area was subject to modest tectonic activity that opened or closed access to the Molasse Basin to the south. The Tertiary sediments in the Ries area are thus characterized by a series of marine transgressions and regressions as well as periods of erosion and deposition of freshwater sediments, the latter in part reworked from previous marine deposits; facies changes, and lithologic variability is commonplace over small vertical (5 m) and horizontal (1 km) distances. The actual cap rock at the target site was a Miocene freshwater deposit termed "Obere Süsswasser Molasse" (OSM, Figure 2). However, as schematically illustrated in Figures 1 and 3, the Ries target was cut into mesa-type ridges and deep valleys, some of the latter reaching below the base of Upper Jurassic [e.g., *Gall et al.*, 1975]. It is uncertain whether these mesa tops were capped by erosional remnants of OSM or not. In any case, OSM appears to be a volumetrically insignificant crater component. A few kilometers to the south of the present crater rim, however, OSM may have been more continuous, and thicknesses there may locally have reached some few tens of meters [*Hüttner*, 1969].

These OSM freshwater deposits are underlain by marine deposits termed "Obere Meeresmolasse" (OMM in Figures 2 and 3) to the south of the crater. It is extremely important to note, and in large part the crux of the analyses to follow, that the northernmost extent of these marine OMM deposits is clearly defined by a fossil cliff line. This cliff line, where not covered by Ries ejecta, is still visible in the field today [*Gall*, 1974]. Since the cliff line is located to the south of the present crater rim, it is thus established that the OMM deposits never could have occurred farther to the north (Figures 2 and 3). As a consequence, OMM demonstrably did not extend into the crater cavity and thus did not participate in the primary ejection process.

Therefore a fortunate geologic circumstance exists that allows the ballistic ejection concept to be tested in the field: a "local" substrate (OMM) occurs in the immediate crater environs that can be distinguished with ease on lithologic grounds from most crater-derived, primary ejecta. It cannot be distinguished with ease, however, from OSM (see discussion below).

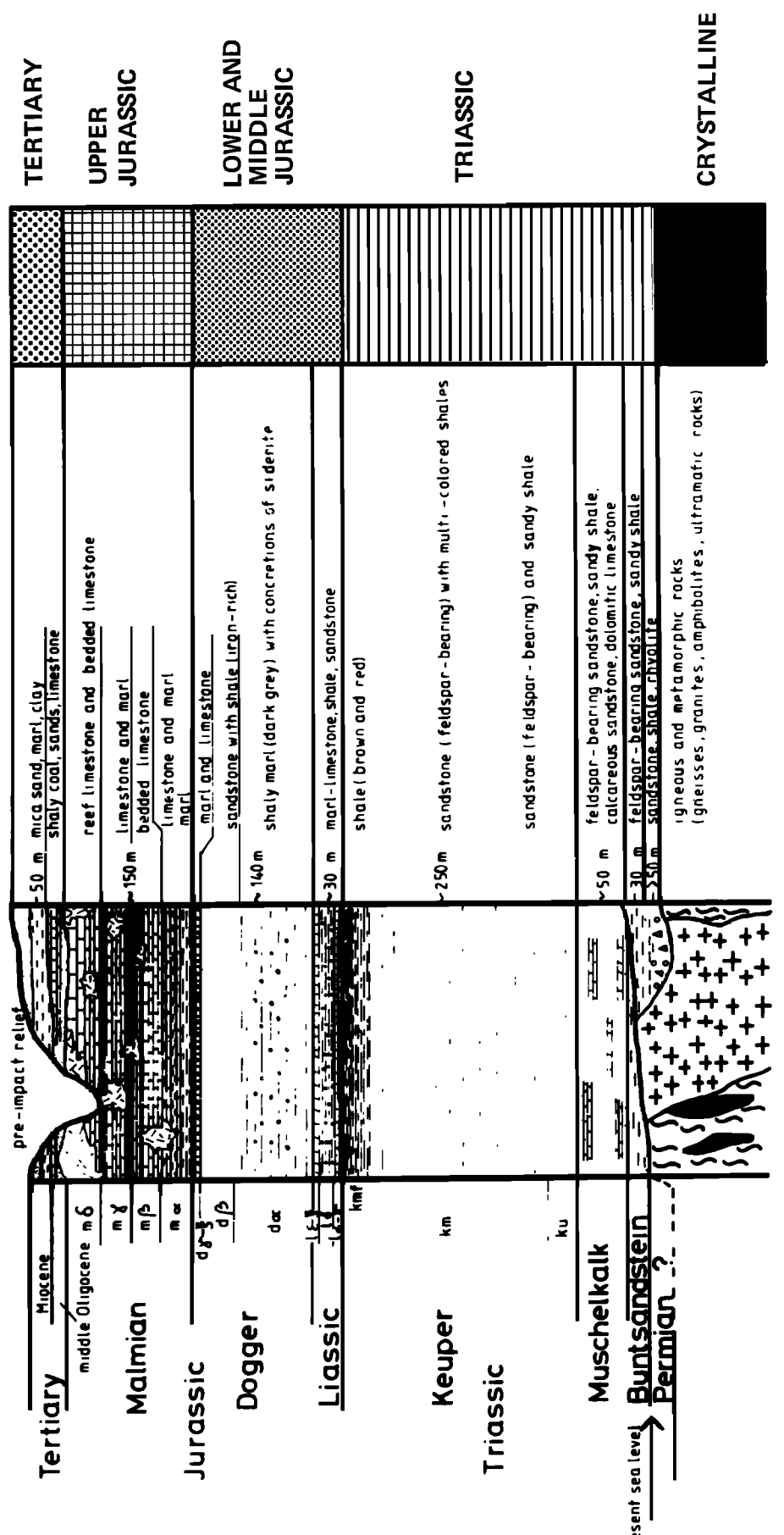

Fig. 1. Detailed stratigraphy of the Ries target [from *Pohl et al.*, 1977] and simplified profile (right) as used throughout this paper.

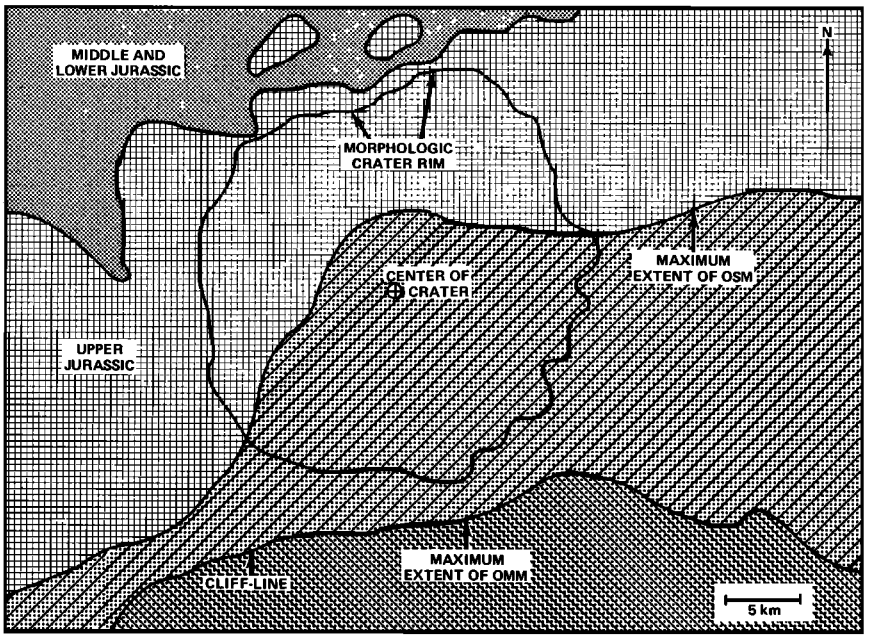

Fig. 2. Approximate reconstruction of the paleogeology of the Ries area depicting maximum extent of OSM and OMM [from *Pohl et al.*, 1977]. Note the northernmost extent of the OMM deposits, i.e., marine sediments, confined by a fossil cliff line; they do not extend into the crater cavity. Also note that OSM principally extended into the crater cavity, although most, if not all, of it was eroded at the target site when the impact occurred. Also at the time of impact, the target area was crossed by steep valleys (not depicted) which rendered Upper Jurassic less continuous as depicted, and an escarpment had developed as illustrated in Figure 3.

Figure 4 presents a simplified map of the present-day ejecta distribution, synthesized by *Hüttner* [1977] from detailed field mapping on 1:25,000 scales by a large number of Ries geologists that was recently summarized on 1:100,000 [*Schmidt-Kaler et al.*, 1970] and on 1:50,000 [*Gall et al.*, 1977*a*] scales. The present-day ejecta are distinctly asymmetric in distribution. This asymmetry may be due to two causes: On one hand, the target had an asymmetric "mass distribution" because it was crossed by an escarpment of 100–150 in relief (see Figures 3 and 4); this may have led to more voluminous deposits in the south and southeast. On the other hand, differential erosion occurred during the past 15 m.y. that almost quantitatively removed all ejecta to the north as detailed by *Hüttner* [1969] and *Gall et al.* [1975]. It

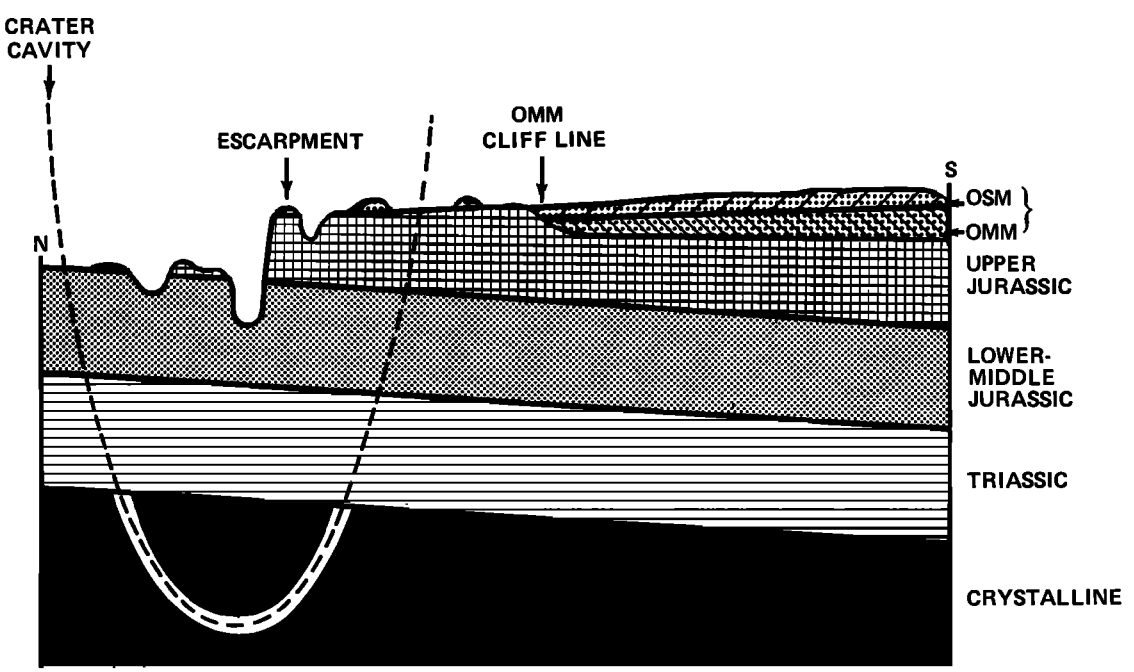

Fig. 3. Schematic cross section through the Ries target at the time of impact. Note (in contrast to Figure 2 which essentially displays only the maximum extent of various Tertiary deposits) how irregular the actual distribution of OSM was. Deeply eroded valleys and mesalike ridges existed, the latter possibly capped by erosional remnants of OSM, if at all [*Hüttner*, 1969, and personal communication, 1982]. Also note the position of the cliff line toward the south and the position of the Upper Jurassic escarpment cutting across the target.

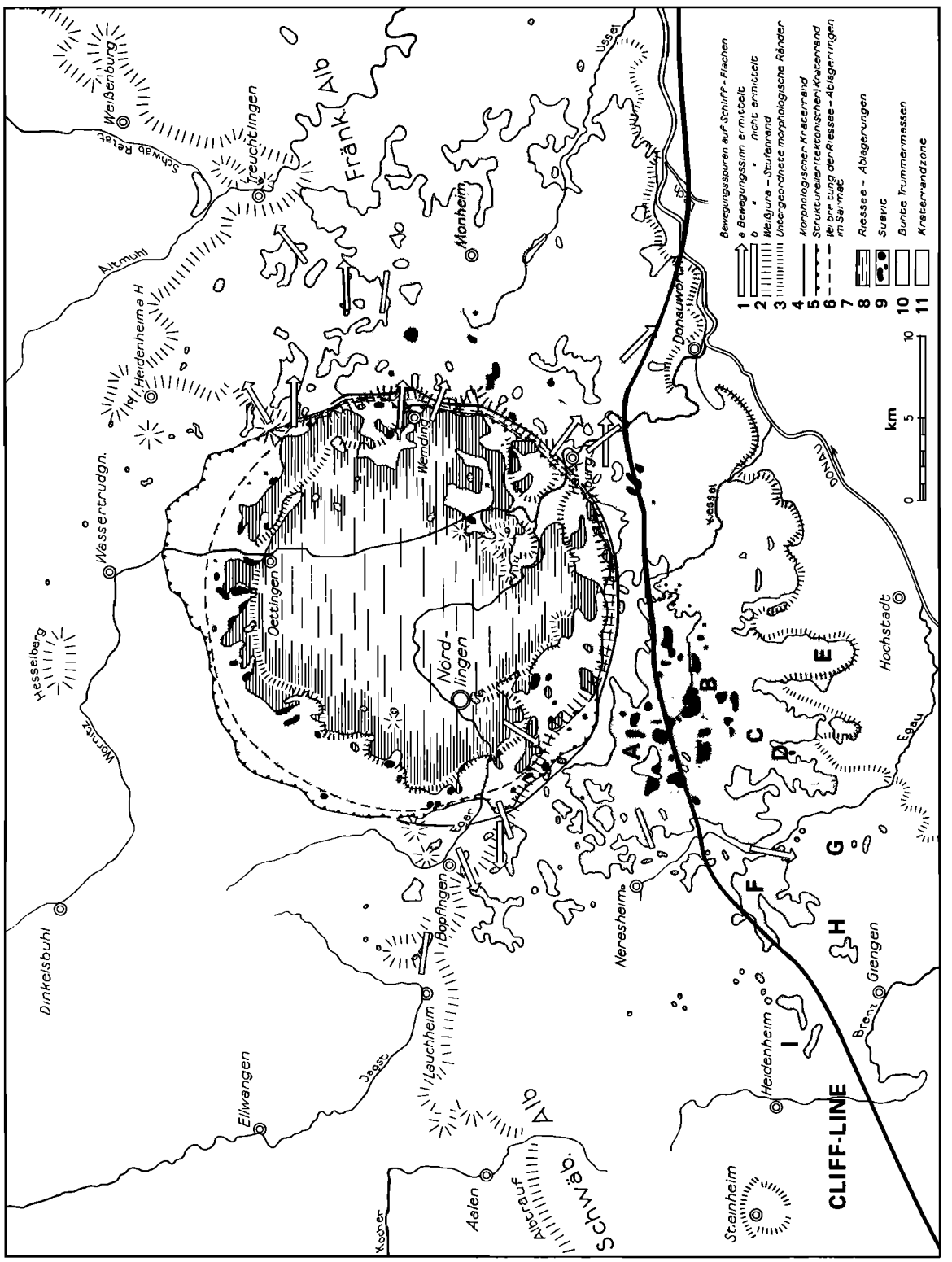

Fig. 4. Distribution of present-day ejecta as summarized by *Hüttner* [1977]. Continuous geologic mapping on 1:25,000 scales exists for the entire crater and its surroundings. The asymmetric ejecta distribution most likely is an erosional effect (see text). Points labeled A–I (with increasing radial range) indicate specific drill locations of our shallow drilling project: (1) direction of motion of ejecta according to striae measurements by *Wagner* [1964], (2) strike of prominent striae, but sense of motion not determined, (3) present-day, major escarpment of Upper Jurassic limestone plateau, (4) subordinate escarpments and terraces inside the Ries, (5) morphologic crater rim, (6) tectonic crater rim, (7) maximum extent of freshwater lake fill, (8) freshwater lake fill, (9) suevite, (10) Bunte Breccia, and (11) zone of big slump blocks and terraces.

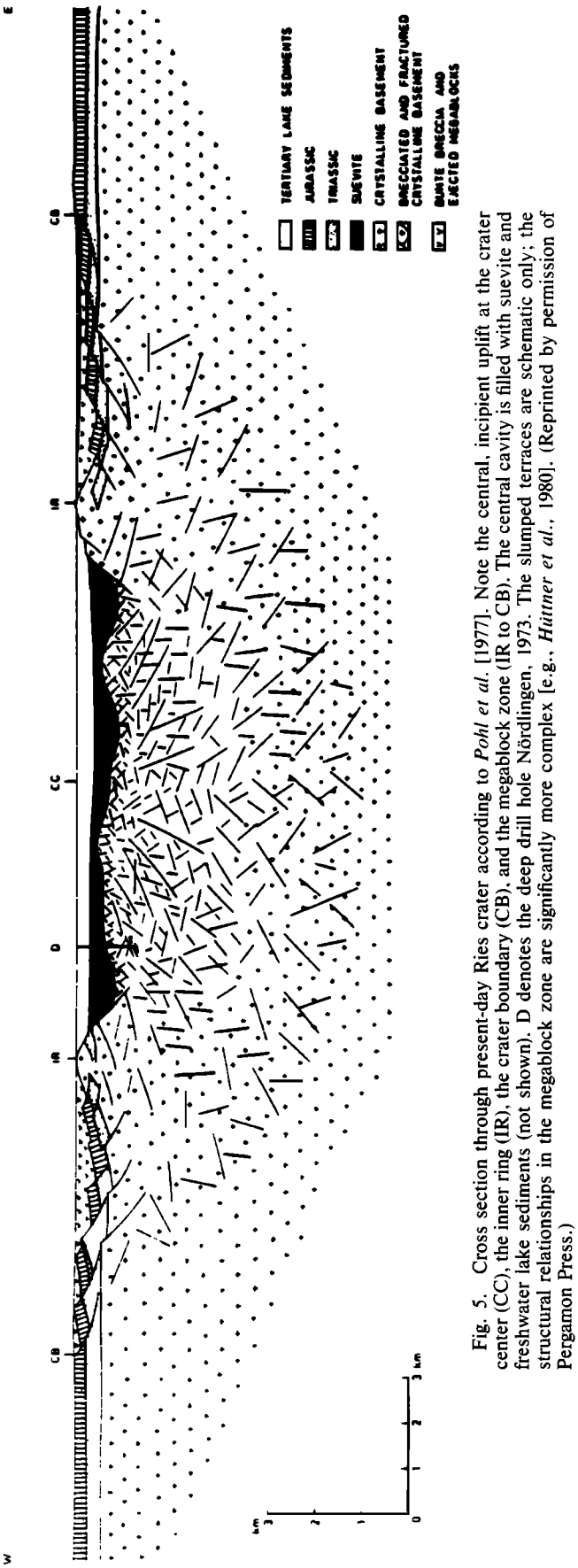

Fig. 5. Cross section through present-day Ries crater according to *Pohl et al.* [1977]. Note the central, incipient uplift at the crater center (CC), the inner ring (IR), the crater boundary (CB), and the megablock zone (IR to CB). The central cavity is filled with suevite and freshwater lake sediments (not shown). D denotes the deep drill hole Nördlingen, 1973. The slumped terraces are schematic only; the structural relationships in the megablock zone are significantly more complex [e.g., *Hüttner et al.*, 1980]. (Reprinted by permission of Pergamon Press.)

is not necessary, and probably incorrect, to postulate oblique impact to explain the observed ejecta asymmetry; indeed, *Gall et al.* [1975] argue against such an inference.

Two principal ejecta units are readily distinguished: (1) the "Bunte Trümmermassen" and (2) the "suevite." The Bunte Trümmermassen are commonly termed "Bunte Breccia" also; the distinction between those two terms is essentially one of grain size and mapping convenience [*Hüttner*, 1969]: one may differentiate and map individual, large clasts (typically >25 m in dimension), and one may contrast these clasts with the undifferentiated "groundmass" (<25 m in maximum grain size). In a strict sense the term Bunte Breccia is a field term that refers to this undifferentiated breccia only, while the Trümmermassen also include gigantic (>25 m), individually mapped clasts [*Hüttner*, 1969]. Since the <25-m components tend to dominate volumetrically, the term Bunte Breccia is commonly used by many workers also for the entire deposit; we will use the term Bunte Breccia throughout this paper in the latter sense, i.e., synonymous with Bunte Trümmermassen. Lithologically, the Bunte Breccia is almost exclusively derived from the sedimentary sequence within the Ries target; crystalline inclusions are rare; impact melts are absent (by definition). Incorporation of locally dislodged, Tertiary sediments is common and was first described by *Ammon* [1905].

The ejecta unit termed suevite (Figure 4) is primarily derived from the crystalline basement, and these deposits do contain impact melts in the form of characteristic bombs (see, for example, *Gall et al.* [1975], *Pohl et al.* [1977], *Hüttner* [1977], and *Stöffler* [1977]). There is considerable question as to the degree to which the typical, present-day occurrence of suevite as relatively isolated patches, of a few hundred meters in lateral extent and <20 m in depth, may reflect an initial, discontinuous distribution of suevite and/or the erosional remnants only of an initially more widespread, more continuous, and thus more voluminous deposit [e.g., *Hüttner*, 1969; *Gall et al.*, 1975; *Stöffler*, 1977].

Indeed, there is considerable question regarding total erosion of the Ries deposits during the past 15 m.y. Clearly, significant erosion has taken place in the north (see Figure 4), and some erosion must have occurred also to the south, despite the substantial thickness of Bunte Breccia observed there. The exact degree of erosion may, however, not be established with any degree of confidence in the south because it is demonstrably variable from location to location. For example, some suevite occurrences still have quenched margins at the top surface, indicating essentially no removal of Ries ejecta at all, while some present-day river valleys, etc., mandate erosion on scales of tens of meters. Thus erosion is variable from place to place.

A cross section of the crater is illustrated in Figure 5 from *Pohl et al.* [1977]. It is based on surface mapping, geophysical data [*Ernstson*, 1974; *Pohl and Angenheister*, 1969], and some drill cores, especially the 1200-m-deep "Forschungsbohrung Nördlingen, 1973" [*Schmidt-Kaler*, 1977]. Accordingly, the Ries is a multiple ring structure with (1) an incipient, poorly organized, central uplift some 4 km in diameter and of approximately 200 m relief, (2) an inner ring (IR) some 12 km in diameter, and (3) an outer ring (crater boundary (CB)) 26 km in diameter. The depressions (1) inside the inner and (2) between the inner and the outer ring are now completely or partially filled with impact breccias or postimpact freshwater lake sediments. The outer ring coin-

TABLE 1. Estimates of Ejecta Volume of the Ries Crater, Germany

	Ejecta Volume, km³				
	Pohl et al. [1977]	*Chao* [1977*b*]	*Söffler* [1977]	*Engelhardt and Graup* [1981]	This work*
Crystalline basement					
Total volume	30–45	8–18	43–67	70	30
Inside tectonic rim			38–60		>25
Outside tectonic rim			5–7		<3
Mesozoic sediments					
Total volume	$70_{(min)}$ to $140_{(max)}$	166–176	113–157	68	110
Inside tectonic rim		<10%			20
Outside tectonic rim		>90%			90
Total ejecta volume	124–200	184	180–200	138	136

*See text and Figure 42.

cides with the present-day morphological crater rim only in a few areas toward the south; in general, the present morphological rim is inside this 26-km-diameter outer rim [*Gall et al.*, 1977*b*; *Hüttner et al.*, 1980]. The outer ring is defined as the boundary beyond which permanent lateral and vertical displacement of autochthonous materials had terminated; it is thus somewhat of a "tectonic" boundary. Giant blocks, cubic kilometers in dimensions, slumped from this boundary toward the crater center, and they may on occasion form the morphological crater rim inside the 26-km perimeter.

The area between inner and outer rings is also known as the "megablock zone," a mixture of gigantic blocks, frequently hundreds of meters in dimensions [*Pohl et al.*, 1977]. Toward the inner ring these blocks appear to be derived preferentially from deep-seated target strata and occur sometimes in inverted stratigraphic position as summarized by *Pohl et al.* [1977] and *Graup* [1978]. In the vicinity of the outer ring the megablocks appear predominantly derived from the crater walls. The megablock zone may thus result from a combination of ejection and slumping processes.

The crater profile (crater bottom) illustrated in Figure 5 appears fairly accurate and includes, of course, short- and long-term modifications of the actual excavation, and transient crater cavities [e.g., *Dence et al.*, 1977; *Pike*, 1977; *Croft*, 1978, 1981; *Settle and Head*, 1979; *Settle*, 1980]. As with most other large impact structures, exact geometry of the transient excavation cavity remains model dependent for the Ries, and therefore various mass balance calculations regarding total crater volume and that of specific target strata exist. Recent estimates by various investigators are summarized in Table 1. Despite the diversity of these estimates, there is, however, unanimous consensus that the ejecta emplaced beyond the 26-km rim are predominantly (>90%) derived from the sedimentary strata [e.g., *Pohl et al.*, 1977; *Stöffler*, 1977; *Chao*, 1977*a*]. Crystalline basement in the form of suevite, as monomict or polymict crystalline breccias [*Graup*, 1978], or as an occasional clast (see discussion below) in the Bunte Breccia constitutes ≪10% of all materials displaced beyond the outer crater rim [*Schneider*, 1971; *Graup*, 1978]. On the basis of these mass estimates the Bunte Breccia therefore corresponds to the photogeologically observable "ejecta blanket" surrounding large planetary craters.

This general description serves to illustrate that it is possible to study the continuous deposits of the Ries with truly exceptional field control: (1) Azimuth and radial range relative to impact center are readily obtained. (2) Observations in vertical profile are possible. (3) Specific breccia components may be assigned to discrete stratigraphic positions within the Ries target. (4) Owing to fortuitious geologic circumstances, the local substrate to the south of the crater cavity is lithologically distinct from all crater-derived material. This outstanding field control appears unique among large terrestrial craters.

We therefore embarked on a shallow drilling program in the continuous deposits of the Ries Crater to provide much needed observations in complete, vertical profile (in contrast to relatively small man-made or natural outcrops) and to investigate the modal composition of Bunte Breccia with regard to target stratigraphy.

The drilling operations concentrated toward the south of the 26-km Ries rim where Bunte Breccia is plentiful (see Figure 4) and thus hopefully least eroded. Further, it is there where the most detailed, modern 1:25,000 maps exist [*Hüttner*, 1958; *Gall*, 1969] and, importantly, where the upper Miocene cliff line halted trangression of the OMM sediments. It was thus natural to concentrate the drilling operations in this area, termed southwest "Vorries."

Additional considerations to drill toward the south of the crater rim were as follows: (1) Suevite is relatively abundant, and because it always overlies Bunte Breccia, one can obtain demonstrably uneroded Bunte Breccia profiles. (2) The most distal Bunte Breccia occurrences are located in the southwest. (3) Total thickness of Bunte Breccia was poorly known in the area south of the cliff line. A relatively thin (10–30 m) deposit is commonly observed north of the cliff line; thus popular inference implied similar thicknesses to the south [e.g., *Hüttner*, 1969; *Gall*, 1969], and it was thought that Bunte Breccia in essence would mimic a preexisting relief. This thin "draping" hypothesis could be tested by locating specific drill sites on local topographic highs and ridges. This test seemed to be important because the ballistic hypothesis entails a certain degree of erosion and degradation of the landscape surrounding a prospective crater due to the excavation of secondary craters. (4) "Type localities" in the form of quarries that led, for example, to the thin ejecta draping hypothesis or that were used by *Oberbeck et al.* [1975] and *Chao* [1974] for or against a secondary cratering regime could be assessed in detail. (5) Importantly, limited resources mandated that the drilling focus on a restricted area that hopefully would yield the most diagnostic and representative information. Thus the specific locations explored

TABLE 2. Location of Drill Sites and First-Order Core Information

Drill Location (Core)	Range,[a] km	Azimuth, °N	Elevation of Drill Point, m		Total Thickness of Bunte Breccia,[d] m	Bottom of Bunte Breccia,[e]	In Situ Material[f]
			Top[b]	Bottom[c]			
A	16.5	207	568	588	>80[g]	<488	?
B	19	195	502	460	34	468	Upper Jurassic
C	23	196	553	469	76	477	OMM
D	25.5	196	534	471	52	482	OSM
E	26.8	184	503	401	84	419	OSM
F	27.5	215	558	486	47	511	OSM
G	32	206	505	482	21	484	OSM
H	35.2	216	560	528	28	532	OSM
I	36.5	225	492	446	17	475	Upper Jurassic

[a]Range from crater center [see *Pohl et al.*, 1977].
[b]Elevation of drill point above sea level (top of profile).
[c]Elevation of final drill depth above sea level (bottom of profile).
[d]Total thickness of Bunte Breccia encountered.
[e]Elevation above sea level of contact between Bunte Breccia and undisturbed country rock.
[f]Undisturbed country rock in contact with Bunte Breccia.
[g]Contact misinterpreted initially; terminated in Upper Jurassic limestone megaclast.

represent trade-offs made in the field between close spacing of neighboring sites, representative areal coverage, exploration of important type localities, and fiscal considerations. A brief rationale for each drill site is outlined in Appendix A.

FIELD OBSERVATIONS

General Comments

The following definitions, established in the field, apply throughout this report, including the laboratory analyses:

Megaclasts. These are monolithic clasts larger than 64 cm; frequently, they measure several meters in length.

Clasts. These comprise all detrital, lithic material between 1 and 64 cm.

Matrix. This comprises all components smaller than 1 cm; the major fraction of matrix, however, is <1 mm. The matrix is highly variable in grain size and dominant lithology, i.e., in the ratios of clay/silt/sand, including variable color shades, and it is also highly variable in the modal composition of very small (<1 cm) detrital material. Changes in the above matrix characteristics are generally abrupt, giving rise to distinct "matrix sections" or "matrix types" in vertical core profile. Such (internally relatively homogeneous) matrix sections may occur on scales as small as 10 cm, but typically they are more than 1 m in core length.

Polymict breccias. This term relates to an entire core section and combines clasts and matrix; it thus defines a discrete "polymict breccia section" in core profile (also occasionally termed "polymict breccia type").

Overview

Table 2 summarizes some geographic, topographic, and geologic data; Figure 6 displays some first-order core observations. Accordingly, a cumulative core length of 560 m was obtained; core recovery was 95%. Since many cores contain megaclasts measuring a few meters in dimension, it was necessary to penetrate potential in situ materials at least some 5–10 m to assure that autochthonous bedrock was encountered. Undeformed, horizontal bedding planes are diagnostic for such in situ materials.

The topographic data presented in Table 2 serve to demonstrate that the Bunte Breccia rests on a terrain with an irregular relief. In general, the absolute elevation of the contact with bedrock and the specific bedrock lithology display some relation to the elevation and lithology of bona fide autochthonous material when exposed somewhere in the vicinity. The isohypses of contacts exposed in nearby quarries, etc., may serve as rough guides for predicting the absolute elevation of the contacts in the drill hole. A first-order field result therefore demonstrates that the Bunte Breccia south of the cliff line does not drape a preexisting, irregular relief akin to that of today as already noted by *Hörz et al.* [1977]. The present-day topography and relief in the area investigated appears largely unrelated to that existing at the time of impact. Geoelectrical sounding results of *Homilius and Schmidt-Kaler* [1979] indicate similar relationships farther to the east. Most of the present-day relief is confined to the Bunte Breccia. Most topographic highs in the Vorries are entirely composed of crater deposits.

The salient features illustrated in Figure 6 are as follows: The Bunte Breccia contains relatively large megaclasts that may readily exceed a few meters in dimension; the largest clast measured 29 m (core A). The megaclasts may be derived from local Tertiary sources as well as from the crater cavity; however, the latter materials are dominated by Upper Jurassic; Lower Jurassic megaclasts are exceedingly rare and occurred only in cores A and B; none were encountered in the more distal drill sites; megaclasts of still more deep-seated target position (e.g., Triassic or crystalline basement) were not observed at all. Thus the megaclast population is totally dominated by shallow-seated target strata and locally derived lithologies. Any of these megaclasts may occur anywhere in vertical profile. Further, the volume ratio of megaclasts to polymict breccias is highly variable; for example, core C contains many fewer megaclasts than core E, just 3 km to the south. In summary, the first-order field impression of Bunte Breccia at any given locality is one of a highly chaotic, poorly sorted deposit.

Brief descriptions of individual cores and their relation to the local geologic setting are presented in Appendix B.

The Contact Bunte Breccia/Country Rock

In general, the contacts of the massive Bunte Breccia and autochthonous horizons are stunningly sharp, as illustrated in Figure 7. In most cases the in situ material lacks any evidence of deformation, even a few centimeters from the

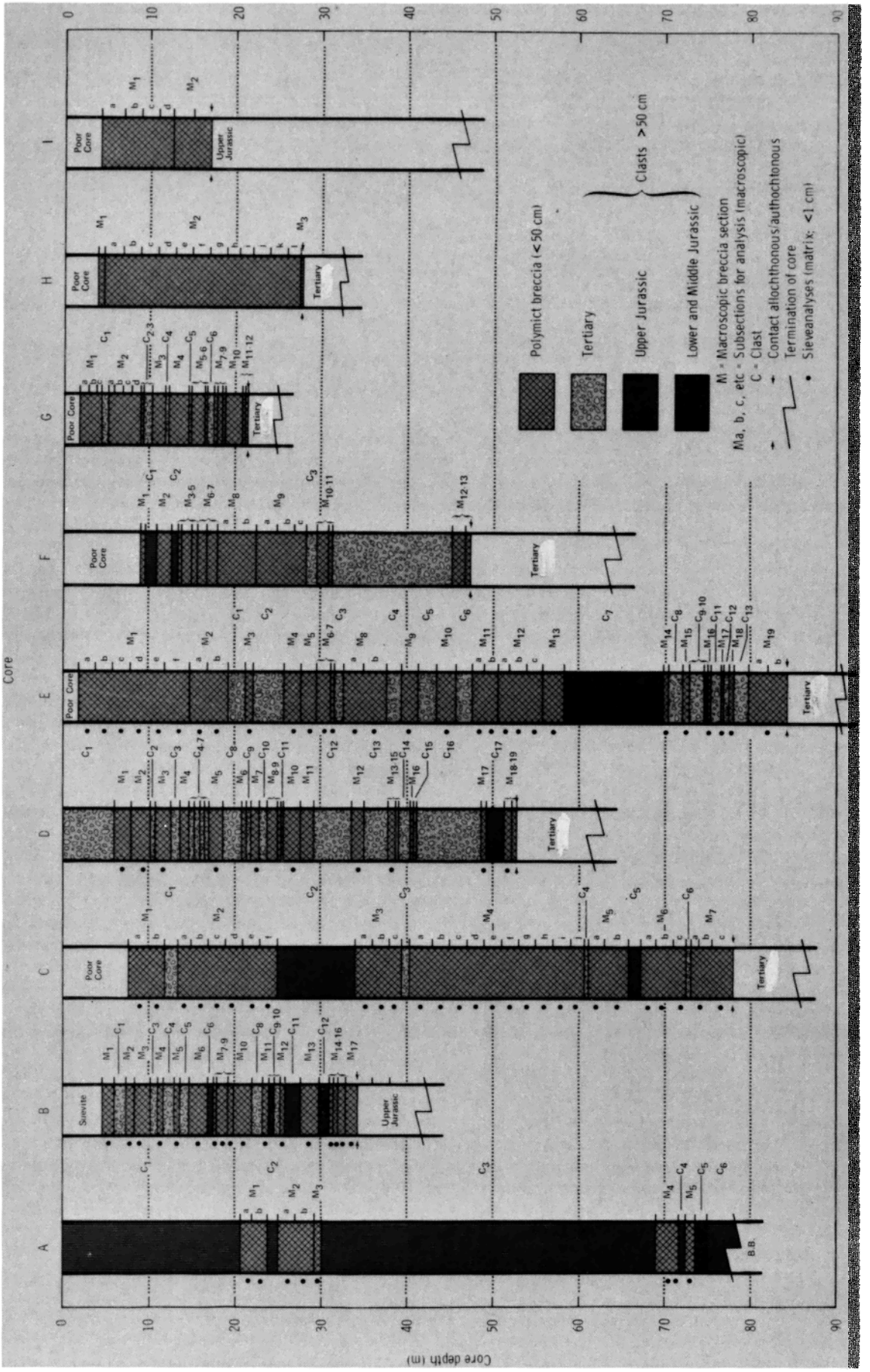

Fig. 6. First-order profiles from nine locations in the Ries continuous deposits. Note the random vertical position of monolithic megaclasts as well as their variable sizes; most megaclasts are predominantly of Upper Jurassic and Tertiary origin. Also note the variable matrix/clast ratios in diverse cores.



Fig. 7. Detailed contact between Bunte Breccia and in situ material for cores E, D, G, C, H, and B. Note the sharp transition. The cores not illustrated either missed the actual contact (core A) or the contacts were disturbed during drilling (cores F and I).

contact [*Hörz et al.*, 1977]. The bedding planes of the autochthonous material, including those of unconsolidated OSM and OMM, are perfectly horizontal and seemingly undisturbed. The only exception to that rule is the autochthonous Upper Jurassic limestone in core C which is highly cataclastic at the immediate contact; the fracture density decreases rapidly with depths, however, and 1 m below the contact the Upper Jurassic displays "normal" fracture densities.

Generally, the breccia sections at or immediately above the contact show no affinity to the in situ substrate; the bottom sections of the Bunte Breccia profile are not formed from the substrate on which they came to rest. Again the lowermost 50-cm section of core H represents an exception to this rule, as it (1) is distinctly different from the entire core and (2) contains OSM sands that are identical to the immediate substrate. A similar situation is observed in outcrop at the Guldesmühle [*Hüttner*, 1969]. *Chao* [1977*a*] used these Guldesmühle observations to postulate a widespread, universal "basal mixing zone." On the basis of the thickness (about 3 m) of this zone at Guldesmühle, he inferred that interaction with the local substrate was not significant. Our core observations demonstrate that these generalizations from one outcrop do not apply to most Bunte Breccia contacts.

Without exception, none of the contacts observed represent the old land surface at the time of impact. All contacts lack any weathering horizon, e.g., lateritic soils rich in limonite. Such weathering products are found, instead, commonly as discrete clasts in the Bunte Breccia deposit. Our observations complement the findings of *Wagner* [1964], who studied predominantly the contacts of Bunte Breccia with competent, Upper Jurassic limestone. Such limestone surfaces may be heavily scarred and striated, implying again that the entire weathering horizon was completely stripped; in isolated cases it is possible to demonstrate stripping even of some few meters of Upper Jurassic limestone itself, such as at Gundelsheim (Figure 8; see also *Hüttner* [1969]). Thus direct evidence of ejecta interacting with the local bedrock is frequently observed in outcrop. The numerous Tertiary megaclasts, commonly totaling tens of meters in core length, indicate removal of tens of meters of local material. The primary crater ejecta did not simply move over the ground but must have interacted significantly with the local bed-



Fig. 8. Bunte Breccia resting on competent, well-bedded Upper Jurassic limestone at the Gundelsheim quarry, some 12 km to the east of the crater rim. Note the substrate surface formed by a bedding plane. It is on such surfaces where *Wagner* [1964] measured the predominantly radial strike of striae as illustrated in Figure 4; the (delicate) striae are not visible in this photograph.

rock. The preexisting relief was destroyed; Bunte Breccia came to rest on a freshly generated substrate surface.

Textural Observations

The textural variety of the Bunte Breccia cores is bewildering. It ranges from matrices of variable grain sizes to polymict breccias of enormously variable clast contents and clast sizes to megaclasts that may or may not display brittle or plastic deformation features.

First, the total amount of matrix differs from locality to locality and ranges from 10% (volume) in core A to 75% in core H. Conversely, this implies highly variable clast and megaclast content (see Figure 6).

Second, even within any given core the matrix is highly variable, as evidenced by different color shades, differing grain sizes (essentially the sand/silt/clay content), and varibale populations of lithic detritus less than 1 cm in size. When the clast population larger than 1 cm is considered, additional variations and differences are introduced. The various polymict breccia sections are typically a few meters in length, although variations on smaller (<20 cm) and larger scales (>10 m, e.g., core H) are also observed. The various types of polymict breccias are generally in knife-edge sharp contact with each other (Figure 9). On occasion, however, a transition zone of a few centimeters thickness occurs, in which the two neighboring matrices appear to be mixed. Nevertheless, sharp contacts are the rule. Similarly, the contacts of polymict breccia sections with megaclasts, even those made up of unconsolidated sands, are generally very sharp. Typically, distinctly different breccia types are encountered on either side of a megaclast, although exceptions to this rule exist.

Next to these essentially modal differences there is a bewildering array of deformational features of individual clasts, including megaclasts. Primary sedimentary structures such as bedding planes of clasts of clay, silt, sand, and shale range from completely preserved to modestly wavy, possibly folded, to highly contorted, twisted, and otherwise completely deformed, irregular structures (Figures 10 and 11). Similarly, the overall shape and plan view of individual clasts may range from relatively equant and subrounded to dramatically distorted, highly irregular shapes. The smaller clast populations (e.g., <5 cm) generally display fewer deformation features than those larger than 20 cm, as most of the small clasts are probably fragments of initially larger clasts. Nevertheless, even large megaclasts of unconsolidated materials are on occasion only modestly deformed, if at all. The competent Upper Jurassic limestone clasts display similar variability in deformational states: megaclasts as long as 29 m (in core A) may be completely shattered with typical fragment sizes less than 1 cm, while other clasts in the same core (e.g., from 76 to 82 m) are free of fractures and

seemingly unaffected. Frequently, one even encounters totally cataclastic limestone clasts of 5–10 cm in dimension floating in the matrix.

As evidenced in Figures 7–11, a crucial point regarding variable degrees of deformation is the fact that they may occur in close juxtaposition, i.e., on scales of centimeters. Neighboring clasts may have experienced dramatically different strains and stresses. Similarly, the bottom sections of the core profiles are not more (or less) deformed than any other section. Style and degree of deformation are independent of vertical position.

On the whole, then, the Bunte Breccia is a massive deposit to the naked eye. Individual clasts show no preferred orientation. Even those clasts that are demonstrably smeared and sheared (with length to width ratios as large as 10) appear of irregular dip. The modestly deformed megaclasts also display random dip angles of initial bedding planes (see Figure 10). Similarly, the contacts between variable polymict breccia sections or between polymict breccias and megaclasts display a large variety of dip angles. Also, the actual fine-grained matrix has no lineation. Thus the typical Bunte Breccia deposit displays no evidence of lineation to the naked eye. Again, however, one observes rare exceptions to these rules in the form of well-lineated matrix textures of approximately horizontal dip and occasionally in the form of some preferred orientation of a group of clasts. The well-lineated matrix type tends to occur especially at contacts, either with megaclasts or between different polymict breccia sections. Such features, however, occur infrequently and generally do not exceed some 20 cm in core length. They are volumetrically insignificant (<1%).

Breccias Within Breccias

A large number of situations occur that indicate multiple mixing and processing of diverse materials before ultimate deposition at any particular site. Starting from large scales

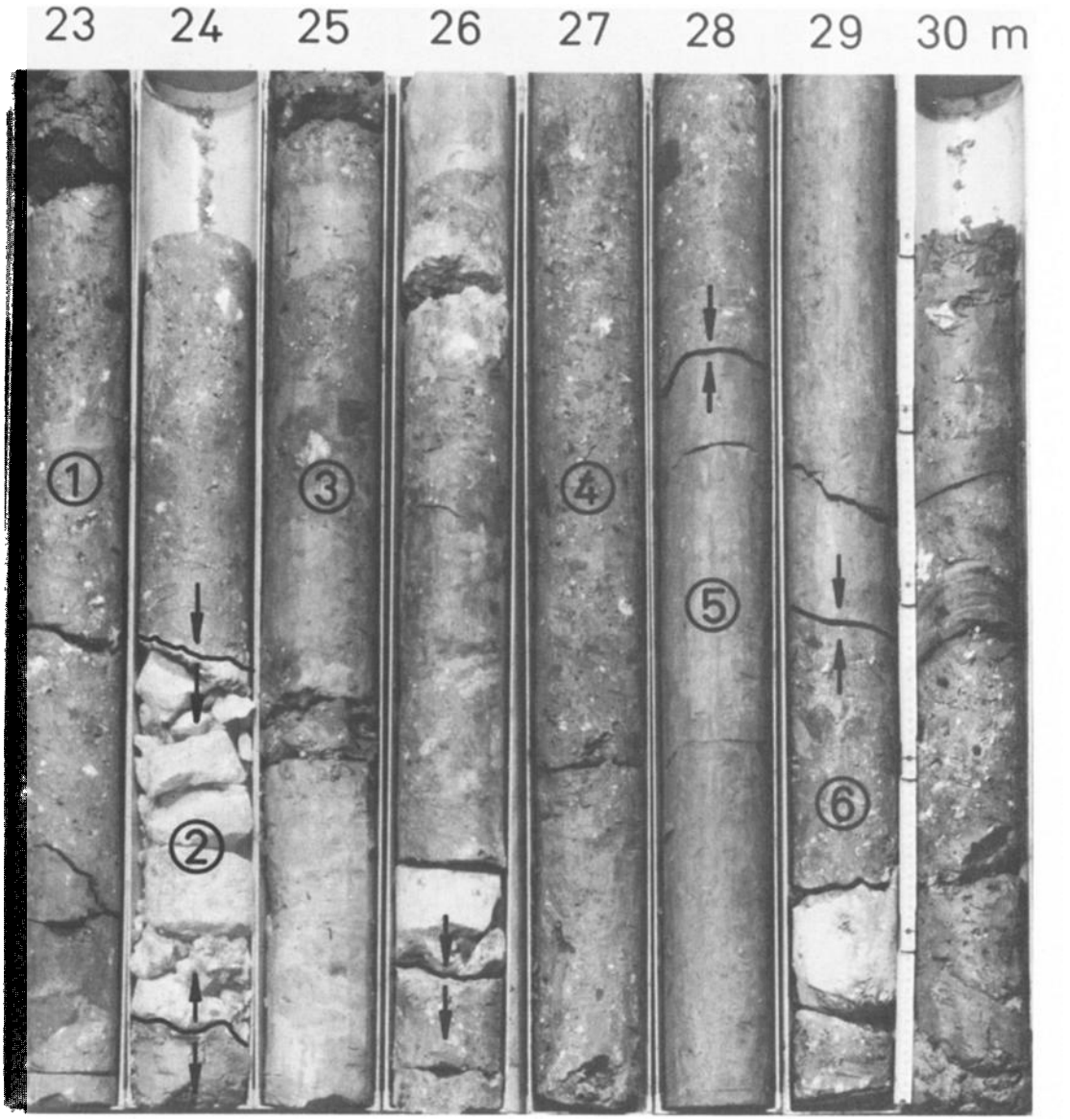

Fig. 9. Different breccia types in continuous core sections (23.00–31.00 m) of core F: (1) relatively homogeneous matrix with fair amount of Triassic clay clasts, (2) cataclastic clast of Upper Jurassic limetsone, (3) Bunte Breccia section with unusually high percentage of decimeter-sized Tertiary clasts, (4) comparatively homogeneous, fine-grained, polymict breccia section, (5) Tertiary clay clast, and (6) highly heterogeneous polymict breccia section. Each "matrix" of a specific section is of a different color shade, caused by different sands, silts, or clays and/or variable mixtures thereof.



Fig. 10. Details of deformation features in Tertiary megaclasts, all from a single core (core E). (*a*) Moderately deformed clast as evidenced by the intercalating sand/silt layers. Note that initially "horizontal" bedding planes are dipping very steeply. (*b*) Essentially identical lithology to that of the clast in Figure 10*a*, significantly deformed, however, by plastic flow. Note the highly distorted, folded, twisted, and irregular deformation features in a single clast. (*c*) Example of "brittle failure," i.e., small-scale fault (bottom section) of a relatively coarse grained, unconsolidated sand containing some interbedded clay layers which are highly distorted.

(more than meters), one may observe a specific polymict breccia section either being bounded by two additional breccia types or being surrounded by the same breccia type, being in contact with (or sandwiched by) diverse megaclasts, etc. Thus "breccia within breccia" relationships on meter scales are the rule rather than the exception for Bunte Breccia. Further, each specific breccia section itself may contain, for example, cataclastic limestone clasts or bona

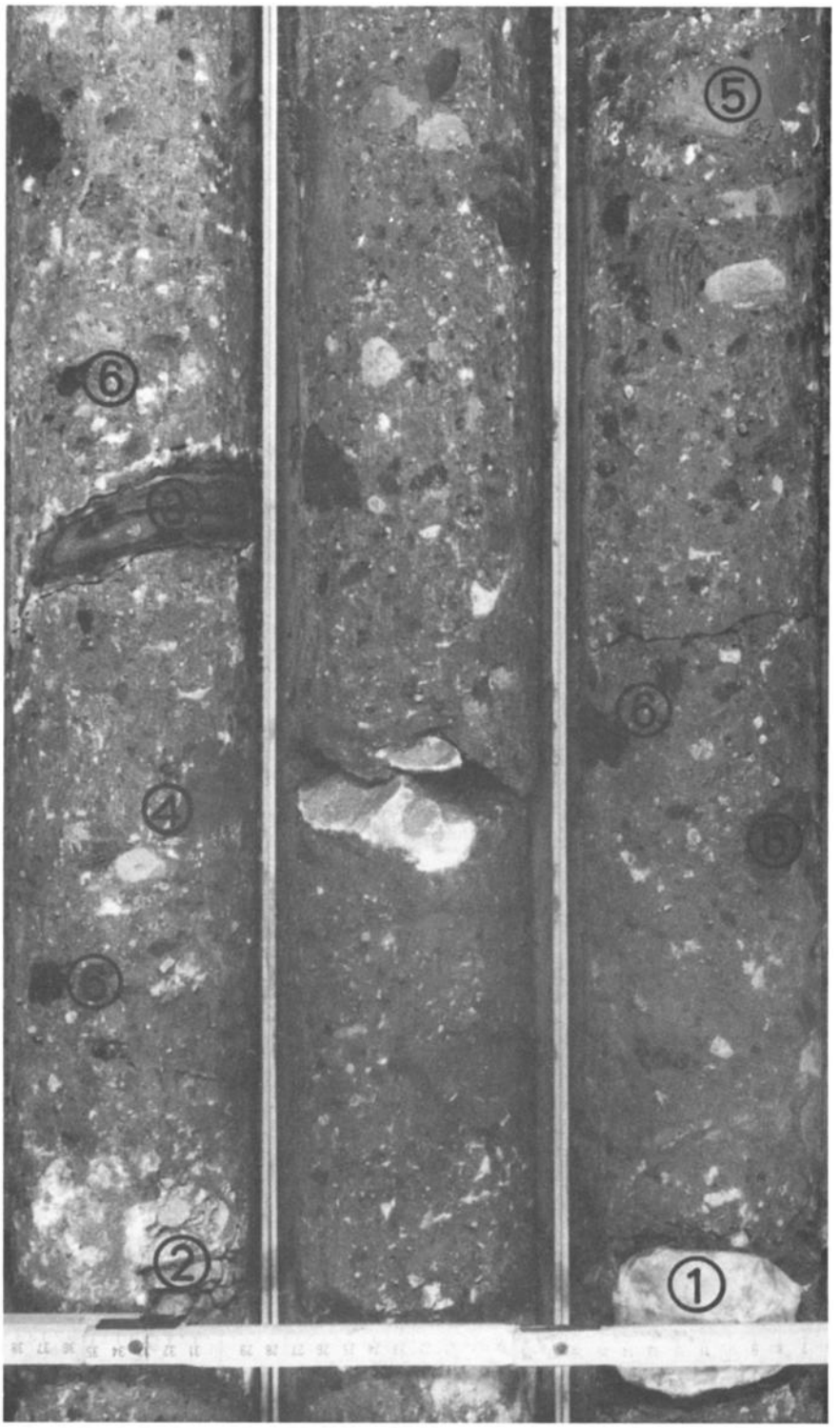

Fig. 11. Detailed textural phenomena in a relatively homogeneous, fine-grained polymict breccia section (core H). Note the different degree and style of deformation, for example, (1) competent limestone clast, (2) highly cataclastic clast of same limestone material, (3) plastically deformed, Tertiary clay, (4) and (5) relatively undeformed Tertiary clay clasts, (6) compare shapes of relatively undeformed Lower Jurassic and Tertiary clay clasts, ranging from rounded to highly angular. Clast 5 is a mixture of two distinctly different clays (breccia within breccia). Also note the massive nature of the polymict breccia and the random orientation of the clasts.

fide polymict clasts composed of two (or more) intimately mixed and smeared out lithologies (Figure 12). In the latter case one lithology itself may be loaded with clastic debris, either monomict or polymict; on occasion the polymict clastic material itself may have genuine polymict matrices that differ from that of the host matrix. Thus breccia within breccia relationships occur on a wide variety of scales, and up to four breccia generations were observed. As a consequence the entire Bunte Breccia deposit attests to discrete mixing events that must occur on a wide variety of scales. The lithologic diversity indicates mixing of a restricted set of possible lithologies and thus mandates mixing events at



Fig. 12. Breccias within breccias. (*a*) Core H, about 24 m: (1) highly polymict clast of diverse Tertiary clays and Upper Jurassic limestone fragments residing in polymict matrix. (*b*) Core E, 54 m: highly disjointed Lower Jurassic shales intruded by fine-grained "matrix" material that differs from the host rock matrix. (1) Note the jagged and angular shapes of the black shales in the lower section versus the more plastically deformed material in the middle section. Further, a Tertiary clay clast (2) hosts a small, mixed clast (about 0.8 cm) of finely crushed Upper Jurassic limestone (the white portion) and some Lower Jurassic shale (the dark portion). Clast 3 is a mixture of various Triassic clays. (*c*) Core F, about 19 m: a highly fragmented Upper Jurassic marl clast (1) in a state of almost complete disaggregation and prominently invaded by fine-grained matrix. Also, a relatively small (about 1 cm) dark shale clast (2) is invaded by polymict material that differs from the main matrix. (*d*) Core B, about 23 m: (1) highly deformed, "mixed" clast of Lower Jurassic and Triassic clay, in part, invaded by host matrix; (2) Tertiary clay clast deformed by faulting and invaded by host matrix (h) and "foreign" matrix (4), the latter unrelated to the host matrix; and (3) one of the few examples of highly lineated Bunte Breccia sections (note the extremely sharp contact to the massive matrix above; actually the failure of the core may have been aided by this contact). (*e*) Core B, about 24 m: (1) a large clast (>50 cm) of Lower Jurassic clay, utterly deformed and containing schlieren of polymict matrix as well as fine limestone detritus and (2) a large, monolithic Tertiary clay clast with relatively well preserved bedding planes (dashed lines) hosting a few limestone clasts. Compare the deformational styles of these two large clay clasts in close juxtaposition.

distinctly different locations and, on textural grounds, at distinctly different times.

Summary of Field Observations

1. The first-order field impression of Bunte Breccia is that of a highly chaotic, poorly sorted, massive deposit. Large, monomict megaclasts are generally in knife-edge sharp contact with polymict breccias. A large diversity of polymict breccias exist on the basis of subtle to dramatic color differences of the matrix and/or as evidenced by variable populations of >1-cm clasts; such clast variability relates to both grain size and modal-stratigraphic composition. Because the dimensions of discrete polymict breccia sections and those of monomict megaclasts are more or less identical, typically measuring 1–5 m in core length, the entire deposit may be viewed as a chaotic mixture of monomict and polymict "clasts." We will refine this statement via detailed laboratory analyses below.

2. The Bunte Breccia deposit is much thicker than was thought previously. It does not mimic a preexisting relief. In contrast, the lack of any preexisting weathering horizon at the contact between Bunte Breccia and bedrock indicates that the preimpact relief was modified. Bunte Breccia rests on a freshly generated substrate-surface and relief. The present contacts of Bunte Breccia and local bedrock may be tens of meters below the initial land surface, judging from the content of Tertiary megaclasts.

3. The variety of textural relationships of component clasts as well as the variable styles of deformation, all in close juxtaposition on centimeter scales, attest to a highly variable deformation environment (stress? strain?) of individual components which were subsequently mixed and transported to a final resting place. These textural observations, and the apparent lack of any systematic relationship regarding the occurrence of polymict breccia sections and megaclasts in vertical profile, indicate highly turbulent conditions during ejecta emplacement. Thorough and multiple mixing of diverse monomict and polymict components is omnipresent.

4. Breccia within breccia relationships are commonplace; up to four "generations" of breccias were observed. These breccia within breccia textures again attest to highly efficient mixing and turbulence during ejecta emplacement. Considering the totally different nature of suevite and the diverse monomict and polymict crystalline breccias in the Ries [e.g., *Abadian*, 1972; *Pohl et al.*, 1977; *Graup*, 1978], the number of breccia "types" generated during this single cratering event are indeed bewildering.

In conclusion, the emplacement mechanisms of large-scale, continuous crater deposits, such as the Bunte Breccia, must be able to produce turbulent flow and highly efficient mixing. Furthermore, they must transport these mixed materials together with monomict megaclasts from their respective source areas to a common, final resting place.

The differentiation into "matrix," "clasts," and "megaclasts" as used throughout this review is clearly a descriptive convenience of what, in fact, represents a continuum in grain size from <1 mm to >10 m. Similarly, the distinction of discrete polymict matrix sections is in part a descriptive convenience also. The matrix sections identified in this report reflect systematic differences in one or more parameters on such an obvious scale that they are easily recognized with the naked eye by a number of observers. Color changes and generally abrupt contacts are the most common field criteria for the distinction of such breccia types. It must be clearly understood, however, that small-scale heterogeneities are also observed within any specific polymict breccia "section." Such heterogeneities are, however, significantly more gradual in a textural sense (i.e., no sharp contacts) and almost arbitrarily subtle in a modal, compositional sense and associated color hues. Thus the "homogeneity" or "heterogeneity" of polymict breccias, and especially the fine-grained matrix, depends heavily on observational scale and rapidly becomes a matter of degree and descriptive convenience also, invoked to describe a continuum of diverse and not necessarily related matrix properties and/or clast populations.

LABORATORY TECHNIQUES AND DEFINITIONS

Stratigraphic Assignments

All polymict core sections were shipped to the Johnson Space Center in Houston and analyzed in the following way: a clear acetate foil was spread over the cleaned core surfaces and taped onto the plastic core tray. Each core surface was then mapped on 1:1 scales by tracing each individual clast larger than 1 cm and noting exact positions of diverse contacts, etc. Each individually mapped clast was assigned a numerical code representing its proper stratigraphic source (Figure 13).

Assignment of individual clasts to specific target horizons was in most cases readily accomplished, although some ambiguities remained on occasion as described below. Category 1, the crystalline inclusions, was no problem whatsoever; they were not differentiated into granites, gneisses, amphibolites, etc., during the mapping phase. Category 2, the Triassic sediments, was dominated by purple and violet clays; subordinate amounts of sandstones and arkoses occurred. Some greenish Triassic clays could be confused with Tertiary clays; however, the green Triassic clays are a minor component of the total Triassic profile, and thus potential misassignment of such Triassic materials to Tertiary sources may introduce a minor error at best. Category 3, the Lower and Middle Jurassic, is dominated by dark brown, dark gray, and almost black clays and shales; subordinate components include brown, ferruginous, oolitic sandstones. Category 4, the Upper Jurassic, is represented by a variety of limestones ranging from massive to well bedded and including marly limestones and genuine marls, a subordinate, yet characteristic component. The Tertiary materials were assigned to category 5. Initially, we attempted to distinguish between the marine OMM and the freshwater OSM. This, however, is successfully done only on the basis of accessory minerals (muscovite and glauconite) for large megaclasts. Sampling and hand lens inspection, however, become increasingly more difficult and ultimately impractical for ever decreasing clast sizes, especially clasts less than 5 cm. As a consequence, reliable assignment to OMM and OSM is not possible in most cases, and therefore they were lumped into one "Tertiary" category.

Accordingly, category 1, 3, and 4 stratigraphies are diagnosed macroscopically with extreme ease and confidence and are readily reproduced by different observers. Potential misassignment of rare green Triassic clays (category 2) is of no consequence to the major mass balance. Our inability to differentiate rigorously between OMM and OSM, however, may be of significance, because OSM could represent some

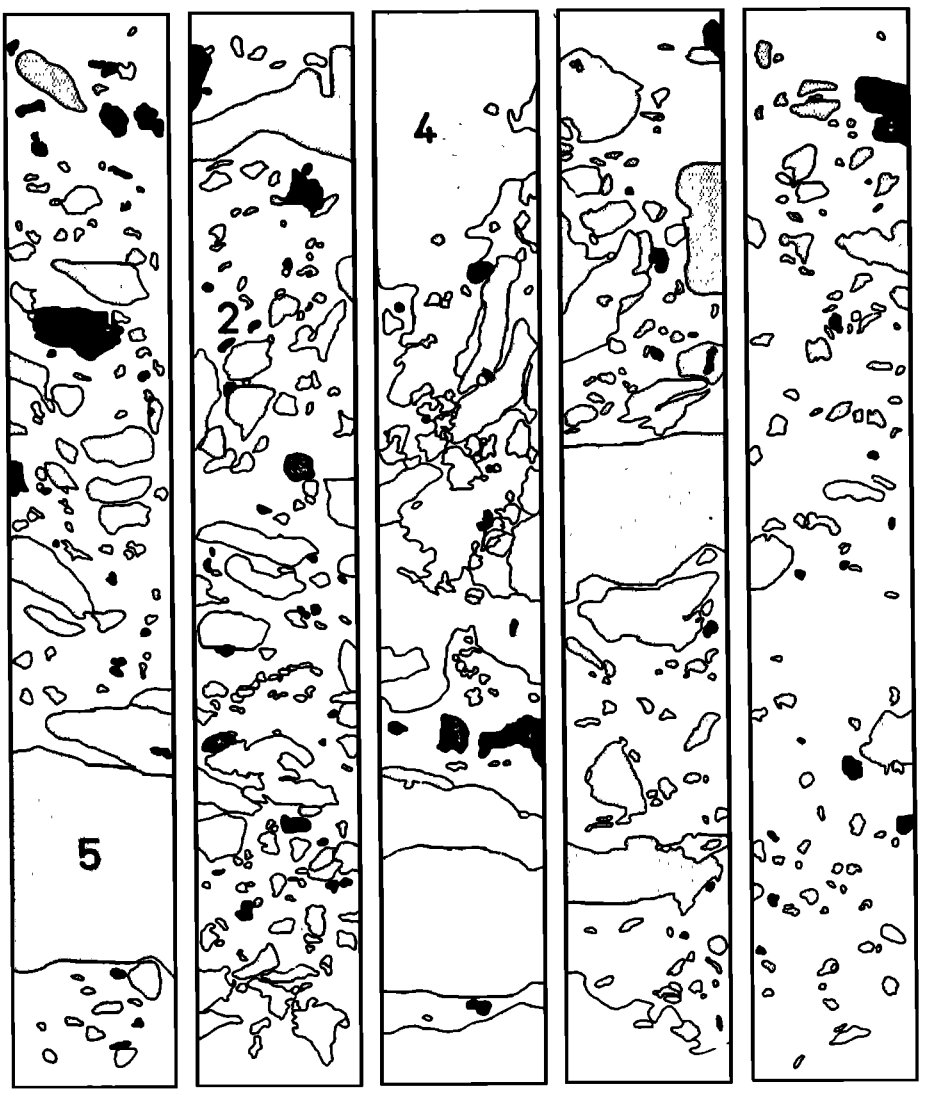

Fig. 13. Example of an acetate foil mapping product from core C: (1) crystalline (not present), (2) Triassic, (3) Lower and Middle Jurassic, (4) Upper Jurassic, and (5) Tertiary.

crater-derived materials next to the local substrate (see Figures 2 and 3); OMM only is of unambiguous "local" derivation. We therefore must resort to a variety of general Ries observations to justify the ultimate assignment of all Tertiary as being derived from local sources.

These additional field arguments entail paleogeographic considerations (see Figures 2 and 3) and the occurrence of diverse facies of OSM. First, detailed field studies [*Hüttner*, 1969, 1977, personal communication, 1982] indicate severe erosion of OSM prior to the Ries impact, and it is questionable whether OSM was even present at the target site. Second, the particular OSM facies encountered in the general drilling area does not occur as a component of the Bunte Breccia anywhere else. This observation also severely limits thickness and spatial distribution of crater-derived OSM, because any major target stratum generally is deposited in a centrosymmetric fashion [e.g., *Shoemaker*, 1963; *Gault et al.*, 1968; *Stöffler et al.*, 1975]. Indeed, considering all Bunte Breccia occurrences, there is no cosmopolitan OSM facies (or other Tertiary) observed. All OSM (Tertiary) that participates in the formation of Bunte Breccia has strong affinities to, or is mostly identical with, the OSM (Tertiary) that is exposed in the general region. This distinctly regional character of most Tertiary breccia components was already vividly described by *Ammon* [1905] and was recently reviewed by *Hüttner* [1969, 1977]. In brief, all OSM (Tertiary) observed in diverse Bunte Breccia localities has affinities to the undisturbed, regional, Tertiary bedrock.

In stark contrast to Tertiary the Upper Jurassic indeed contributes cosmopolitan breccia components; diverse facies may be found everywhere in the Bunte Breccia, indicating that Upper Jurassic is indeed the uppermost target stratum of volumetric significance. Interestingly, *Hüttner* [1958, 1969], *Gall* [1969], and *Gall and Müller* [1974] describe Upper Jurassic components in the Bunte Breccia that appear to be also dislodged locally. The best examples are (1) the "Wellheimer Scholle," a clast some 30 m in dimension [*Gall and Müller*, 1974] and (2) materials dislodged from the Miocene cliff line, i.e., clasts characterized by numerous pholade (mollusc) boreholes, akin to modern cliff rocks. Such borehole-studded materials are now found on occasion as Bunte Breccia components, and because the cliff line clearly never extended into the crater cavity, they were dislodged from the local substrate. Furthermore, one frequently observes Upper Jurassic limestone clasts that contain crevasses and pockets filled with lateritic soil; such

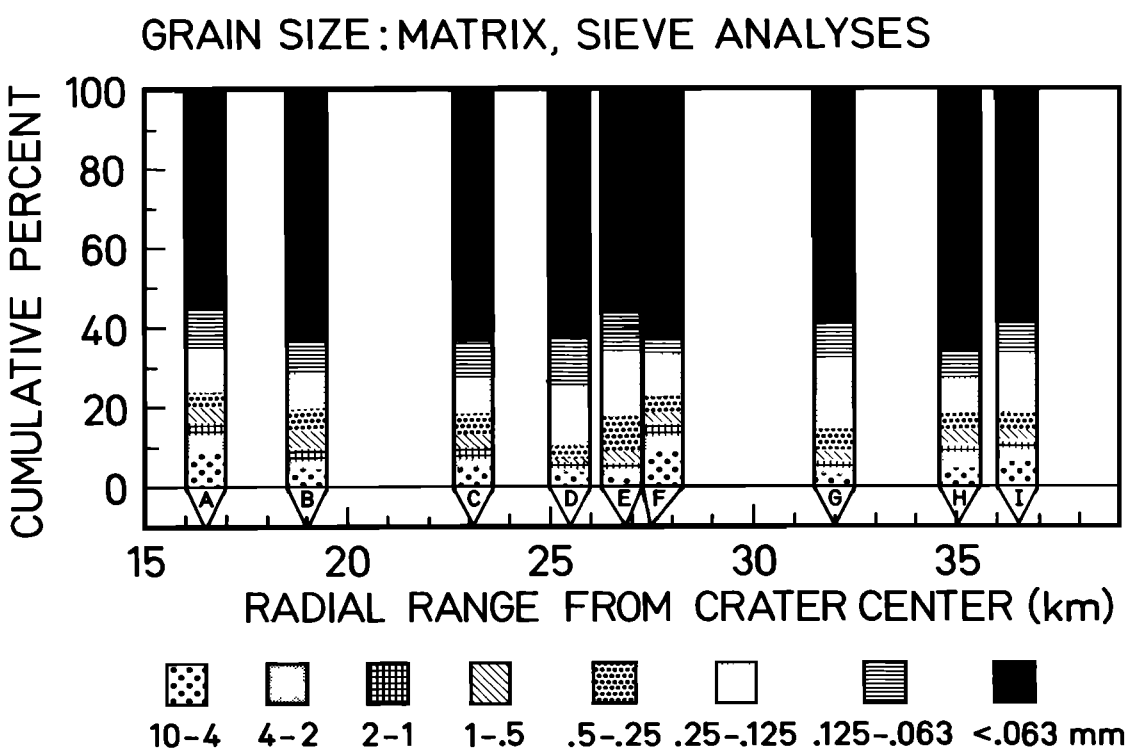

Fig. 14. Core averaged grain size distribution of Bunte Breccia matrix (<1-cm components) as a function of radial range. Note the grossly similar character of Bunte Breccia at all locations, spanning a substantial radial range of the Ries continuous deposit.

weathering products are also observed as discrete breccia clasts. Clearly, these clasts derive from the land surface exposed at the time of the Ries event. Further, as stated above, the local Upper Jurassic limestone surface is frequently stripped to a specific bedding plane (see Figure 8). Thus some Upper Jurassic components in the Bunte Breccia are demonstrably of local derivation, i.e., dislodged from the land surface outside the crater cavity.

In summary, the lumping of OSM and OMM into one stratigraphic category is a matter of practicality. The assignment of this category to a local source area, however, is an interpretation, albeit justifiable on the basis of various field evidence. The converse situation applies to Upper Jurassic clasts: a local source can be demonstrated in favorable cases, but it is impossible to differentiate systematically between these and the crater-derived components.

Thus for the purposes of our analysis all Upper Jurassic clasts were assigned to "primary" crater ejecta, and all Tertiary materials were considered "locally" derived. Therefore both local Tertiary contributions may be modestly overestimated as well as the crater-derived Upper Jurassic. On balance, both effects tend to cancel, and we estimate conservatively that the overall ratios of local versus crater-derived materials (to be presented later) are accurate to better than 10%.

After assigning each clast one of the above stratigraphic categories the clear acetate foils were reproduced with a blueprint machine; these blueprint copies were then tediously clipped with an x-acto knife, yielding a total of approximately 17,000 individual clasts. For each polymict breccia section the clast content was first grouped into specific stratigraphic horizons and then, for each horizon, sorted according to size: (1) 1–2 cm, (2) 2–4 cm, (3) 4–8 cm, . . . , (8) >128 cm. Each of these paper clippings (or piles of clippings) were then weighed on a microbalance, giving an accurate representation of the planimetric frequency.

Data reduction and management were then performed via computer techniques. The microbalance weights were converted via measured densities (pyknometer techniques) of the respective lithologies into weight percent. At this stage the cores were also reconstituted with regard to the large megaclasts left in the field, thereby restoring complete mass balance of megaclasts, "mapped" clasts, and "mapped" matrix per core. A flexible software program and various plotting routines allowed various parameters and combinations thereof to be isolated and plotted.

Sieve Analysis

It appears that the enormous diversity of matrix types is best documented via grain size characteristics. Detailed grain size data may also yield, hopefully, some clues regarding the relative contributions of OSM and OMM in the matrix. Thus conventional wet sieving techniques were employed on matrix samples as well as pure megaclasts. A number of small subsamples, spaced approximately 20–30 cm apart, were collected and combined in such a fashion that approximately 350–400 g of material represented a specific, macroscopic polymict breccia matrix. Homogeneous breccia sections that were more than 2 m long were also sampled in this fashion, and a sieve analysis was performed at least once every 2 m. A total of 240 samples were sieved.

Unfortunately, the grain size data obtained do not adequately reflect the true grain size distributions in the polymict matrix, because all noncohesive clasts disaggregated into their component grains during wet sieving. The data, nevertheless, should be useful in documenting the great variability of individual matrix types.

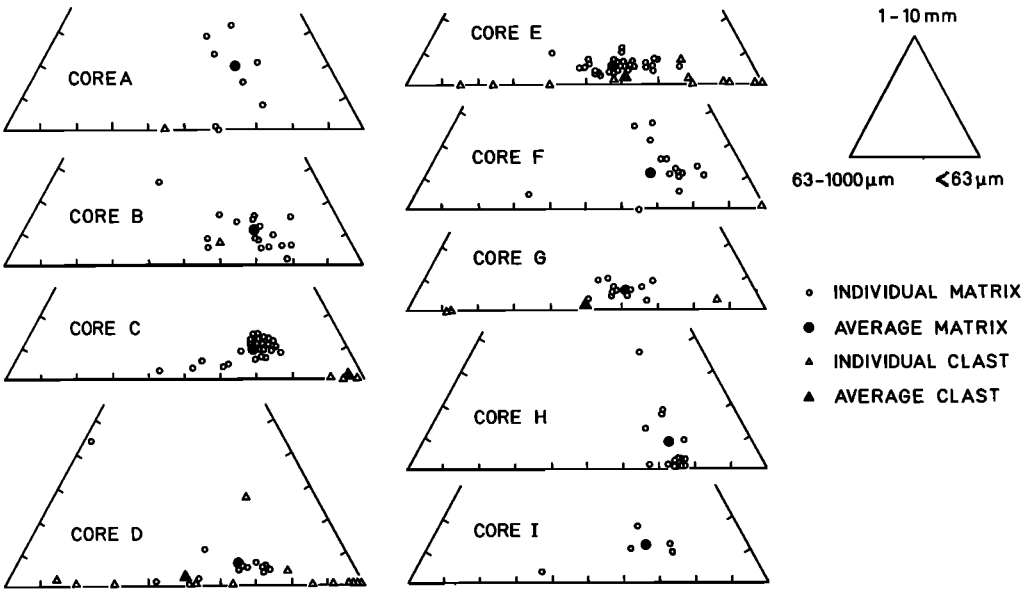

Fig. 15. Grain size distributions of individual matrix sections, discrete megaclasts, and averages thereof. Note the distinctly different mixing trends of cores A and F, for example, as opposed to those of cores D and E. Also note the tight clustering in core C, compared to the wide scatter in cores A, B, F, and H. Clearly, a diversity of end-members and various mixtures thereof are implied. Also note that the averages of matrix differ from the average of pure megaclasts.

The 4- to 10-mm fraction not destroyed by the wet sieving procedure was predominantly composed of limestone fragments or other competent lithologies; generally, >80% of this 4- to 10-mm fraction was crater-derived detritus. For the 1- to 4-mm fraction the ratio of local to crater-derived materials was approximately 50:50. Stratigraphic assignment of the <1-mm "clasts" was not practical; however, limestone detritus is very rare, as revealed by a few powder mount thin sections. The <1-mm fraction contains essentially no identifiable crater detritus (see also *Ostertag* [1978] and *Gasse* [1981]).

Heavy Minerals

Approximately 3 g of the 63- to 125-μm grain size fraction was subjected to standard heavy mineral separation using bromoform/benzol mixtures of density 2.85–2.88 g/cm^3. The heavy mineral yield was typically in the 0.5–1% range. Inasmuch as garnet, epidote, and limonite vastly dominated the heavy mineral spectrum (>90%), other minerals (zircon, staurolite, rutile, hornblende, tourmaline, and apatite) were counted in detail only initially; at a later stage they were lumped (see also *Ostertag* [1978]).

MATRIX STUDIES

Grain Size Analysis

Figures 14 and 15 compare the grain size distributions of polymict breccia matrices with those of monolithic, Tertiary megaclasts. Figure 14 presents individual core averages plotted as a function of radial range. The major observations may be summarized as follows: In general, the grain size distribution of the matrix appears relatively homogeneous in core average. The major constituents are relatively fine grained, and the <63-μm fraction composes between 56 and 67% (by weight, core A, core H) of the total matrix; the 2- to 10-mm components vary between 12% (core A) and 4% (cores E and G). In contrast, the grain size distribution of the unconsolidated Tertiary megaclasts (Figure 18) appears more variable, especially in the <63-μm fraction, which varies from 58% (core D) to 94% (core C). Such average values, however, are not necessarily representative, because some cores contained only one megaclast; for example, the megaclast analyzed in core F was clearly a clay clast, while the megaclasts in cores A and B were fine grained and relatively coarse grained sands, respectively.

The variability of Tertiary megaclasts and individual polymict breccia matrices is illustrated in detail in Figure 15 by plotting each sieve analysis. Note the general scatter of data points. Nevertheless, the Tertiary megaclasts scatter more widely than do the matrices. Even where many megaclasts were analyzed, such as in cores D and E, the matrix averages tend to differ from the average for the megaclasts. Without exception, however, the >1-mm fraction in the matrix exceeds that of the megaclasts. This increase in larger grain sizes is due to crater-derived detritus, i.e., mostly Upper Jurassic limestone, as described above. As illustrated in Figure 16, there is no systematic trend in vertical profile regarding a potential, systematic increase or decrease of coarse (fine) matrix components.

The data contained in Figures 14–16 do not lead to simple, much less quantitative, mixing relationships of diverse Tertiary components during matrix formation. This may in part be due to experimental error, i.e., limited sampling, as some cores contained only very few, if any, megaclasts for reference. More important, however, both OMM and OSM display pronounced facies changes over small lateral (<1 km) and vertical scales (<10 m), and grain size distributions may vary accordingly. Exact end-members for mixing calculations cannot readily be established. Despite these uncertainties, it nevertheless appears that the matrix materials for any given core are not a direct mix of the spatially associated megaclasts. Matrix and megaclasts may have derived from distinctly or subtly different, small-scale geologic environments.

Identical arguments apply to individual matrix sections:

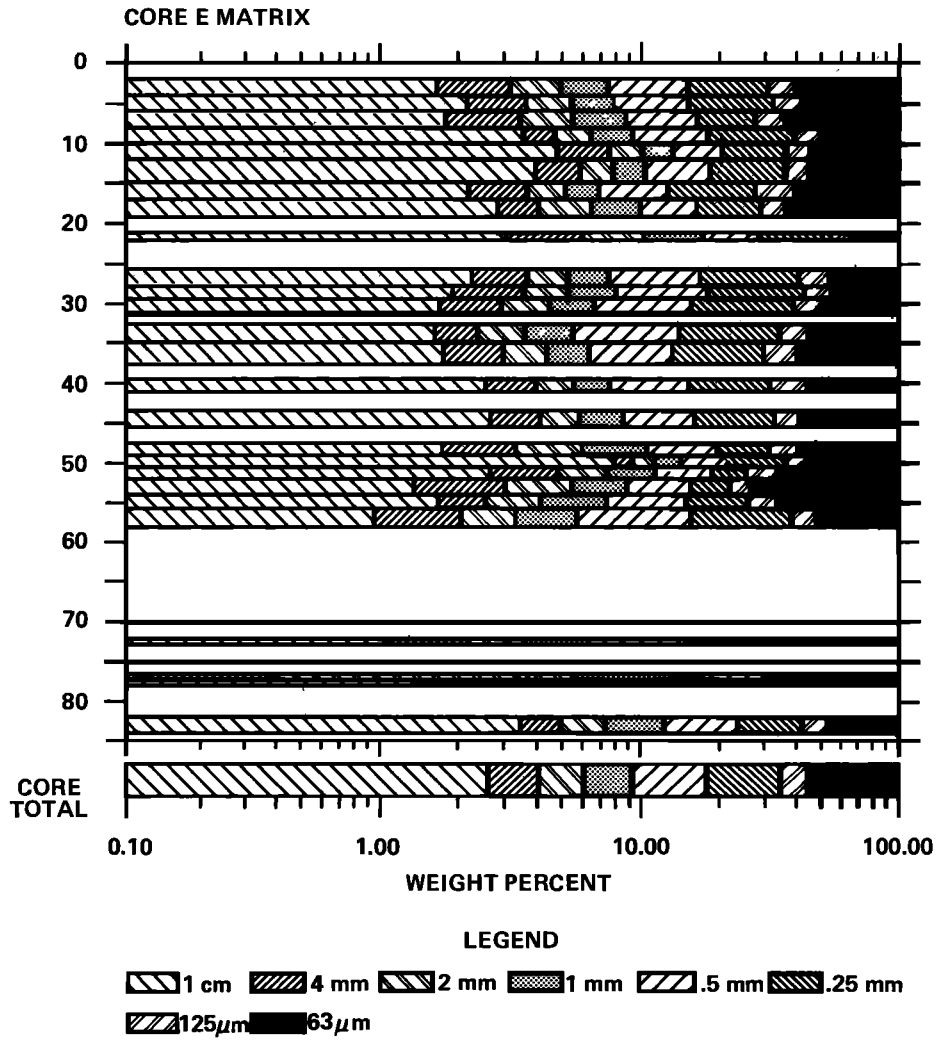

Fig. 16. Grain size distribution of Bunte Breccia matrix in vertical profile as exemplified by core E.

the considerable scatter in their grain size properties clearly indicates formation from various source materials. In detail, however, each individual core may be dominated by a specific local mix as evidenced by variable mixing trends. For example, core E (Figure 15) appears to be derived from a mixture of relatively fine grained components, in contrast to cores A, F, and H, which clearly also incorporated variable proportions of coarse components. Further, core C appears to be made up of a more restricted mix of end-members because of the close cluster of data points in Figure 15, or it may be unusually well homogenized.

While we highlighted in the above section the variability of Bunte Breccia matrix and its implications, we also must emphasize that the diverse matrices are indeed mixtures of various Tertiary sources. Unfortunately, this cannot be diagnostically extracted from the grain size data alone but rests largely on field and other macroscopic evidence. There simply is no significant stratum in the Ries target to yield the observed clay-, silt-, and sand-rich matrices of the characteristic brown, olive, and greenish hues; Tertiary components dominate the matrix.

Heavy Minerals

The principal purpose of the heavy mineral studies was to obtain additional criteria to differentiate between crater-derived and local components in the fine-grained matrix. A secondary objective was hopefully to define the relative contributions of OSM and OMM.

The crater-derived materials are dominated by zircon, tourmaline, and rutile, i.e., by a "stable" heavy mineral paragenesis [e.g., *Schnitzer*, 1954; *Füchtbauer*, 1955; *Schmidt-Kaler*, 1969; *Dressler et al.*, 1969]. In contrast, the Tertiary sediments are characteristically dominated by garnet and epidote [e.g., *Lemcke et al.*, 1953; *Füchtbauer*, 1955, 1964]. Thus the heavy mineral assemblages of potential crater components differ significantly from the Tertiary materials. Among the Tertiary lithologies one may differentiate between OMM and OSM via the dominance of garnet over epidote. The garnet/epidote ratios are typically <1 for OMM, while OSM typically displays ratios of >2 and higher; frequently, the garnet/epidote quotient is >10, and values as high as 58 were reported for OSM [*Lemcke et al.*, 1953; *Füchtbauer*, 1964; *Ostertag*, 1978]. As a consequence the heavy mineral spectra are certainly suitable for differentiating between crater-derived and local materials, and furthermore, it appeared possible to determine the relative contributions of OMM and OSM.

Our heavy mineral analyses, based on 240 individual samples, are summarized in Figure 17. The dominant species are "limonite" (actually limonite + pyrite, i.e., secondary

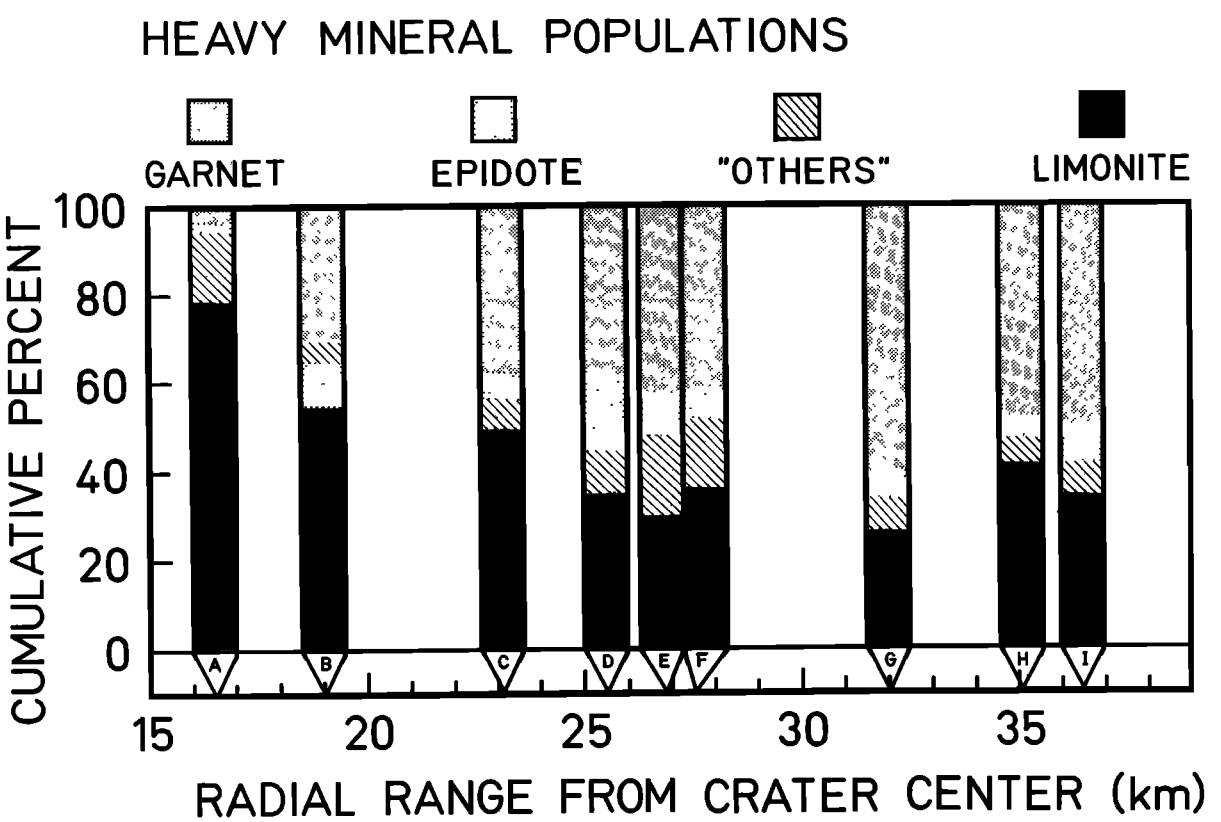

Fig. 17. Total core averages for heavy minerals as a function of radial range.

products), garnet, and epidote, together typically accounting for about 90% of all heavy minerals. The remainder is made up of apatite, rutile, tourmaline, zircon, staurolite, zoisite, and hornblende, none of them individually exceeding 5% of the total population in all samples.

The heavy mineral populations illustrated in Figure 17 provide an additional, strong argument for the predominantly local derivation of the Bunte Breccia matrix: within the sensitivity of the data the matrix could be totally derived from local, Tertiary sources. The mineral spectra of the matrix are identical to those of Tertiary megaclasts and/or genuine autochthonous Tertiary. Total heavy mineral yields are also identical. This similarity further includes identical habits and morphologies of individual mineral species. Since the potentially dominant supplier of crater-derived materials would have to be the crystalline basement, its heavy minerals should be freshly comminuted, angular detritus; such freshly broken fragments are generally rare, and their (low) frequency in the matrix is identical to that in pure Tertiary materials, i.e., megaclasts and autochthonous bedrock.

We now turn to the garnet/epidote ratios (Figure 18) to explore their usefulness in establishing the relative contributions of OMM and OSM. We also observed systematic differences between OSM and OMM materials that are entirely compatible with previous heavy mineral studies [*Lemcke et al.*, 1953; *Füchtbauer*, 1955, 1964]. OMM sediments are characterized by abundant epidote, yielding garnet/epidote quotients ranging from 0.07 to 1.0. In contrast, all OSM yielded garnet/epidote ratios of >1, with typical values between 3 and 5, although values above 10 occurred on occasion and the highest ratio found was 27 for a pure OSM clast (core B). The wide range of garnet/epidote in pure OSM may be ascribed to the greater susceptibility of garnet (relative to epidote) to weathering and ultimate disappearance, which is observed outside the Ries for such OSM strata that at some time resided near the surface [e.g., *Schmeer*, 1955; *Schnitzer*, 1953]. In detail, however, even OMM has garnet/epidote ratios that can also vary by an order of magnitude. Because of this variability in OSM as well as OMM it is very difficult to define reasonable "end-member" compositions for quantitative OMM/OSM mixing calculations. The problem is compounded by poor sample statistics, i.e., by the small number of megaclasts in each individual core (many cores have <3 megaclasts). Ultimately, however, mixing calculations could not be performed, because the garnet/epidote quotient of the breccia matrix (see Figure 18) is occasionally higher than that of associated megaclasts (end-members?); even the garnet/epidote average for an entire core may be higher than the most garnet-rich, Tertiary megaclast contained in such a core. It is obvious that the garnet-rich component present in the matrix is not represented by the megaclasts. Clearly, this component must be OSM. *Lemcke et al.* [1953] report particularly high garnet contents (up to a garnet/epidote ratio of 58) for fine-grained silts. Silts are represented in our megaclast population, but we have not encountered the ones with exceedingly high garnet contents. There is no ready explanation why such materials are not present as megaclasts or, conversely, why they seem to participate preferentially in matrix formation. Being part of the OSM and therefore stratigraphically above OMM, it seems plausible that the uppermost strata of the local environment are particularly prone to comminution during emplacement of Bunte Breccia.

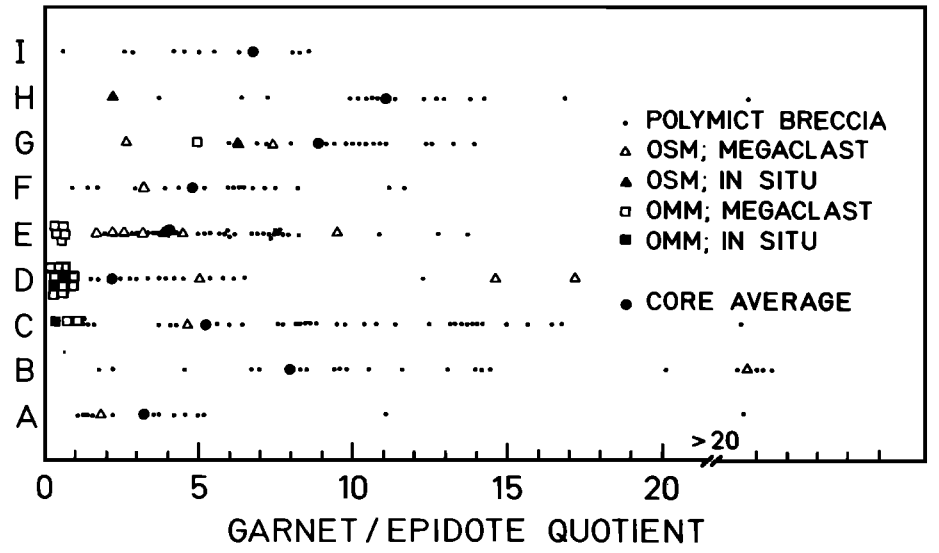

Fig. 18. Individual analyses of the garnet/epidote ratio of polymict matrices and pure Tertiary materials for cores A–I.

Although quantitative mixing calculations were unsuccessful, Figure 18 nevertheless illustrates other important matrix characteristics, in part substantiating and corroborating some conclusions offered above. (1) The matrices of individual cores are subtly or significantly different from each other; individual cores seem to be derived from a restricted set of lithologies. Note that there is hardly any overlap between cores H and I or between cores A and B. (2) The megaclasts present in any given core have only limited resemblance to the materials incorporated into the matrix; matrix and megaclasts appear to come from different, small-scale environments. (3) The local bedrock which the cores penetrated is not necessarily an overwhelming matrix component. Much of the matrix (and megaclasts) may come from sources unrelated to the local bedrock upon which the Bunte Breccia came to rest. (4) Last, some extremely garnet-poor or garnet-rich matrices demonstrate their almost exclusive derivation from either pure OSM or OMM. These samples attest particularly to the utterly "local" derivation of the Bunte Breccia matrix.

Summary of Matrix Studies

The above sieve analyses, heavy mineral populations, and other matrix observations may be summarized as follows:

1. The 4- to 10-mm grain size fraction that survived wet sieving is predominantly crater derived; a substantial fraction of the 1- to 4-mm fraction is also primary crater ejecta. The polymict matrix, however, is dominated by <1-mm components, and >50% (weight) is <63 μm. The observed grain size distributions of <1 mm are consistent with pure Tertiary sands, silts, and clays and do not require admixture of crater-derived components. On the basis of these grain size distributions the total content of crater-derived materials in the <1-cm fraction of the Bunte Breccia is <5% (weight).

2. Similar relationships are obtained from the heavy mineral studies. Absolute heavy mineral content and relative frequency of specific minerals are totally consistent with 100% Tertiary source materials. The garnet/epidote ratio strongly supports this view. Further, identical habits of heavy minerals in pure Tertiary materials (monolithic megaclasts and in situ Tertiary) and polymict matrices exclude significant contributions of freshly comminuted, heavy minerals from the crater cavity.

3. Importantly, both grain size analyses and especially the heavy mineral populations indicate the occasional presence of matrices that are derived exclusively from either pure OSM or pure OMM. Such matrix sections illustrate conclusively the utter dominance of locally derived matrix components.

4. Both grain size analyses and heavy mineral populations support the view that the matrix is not necessarily derived exactly from the spatially associated megaclasts. Therefore megaclasts and matrix derive from different source areas, the spatial separations of which, however, do not necessarily have to be very large. Exact distances cannot be obtained with confidence from the present data.

5. Unfortunately, it was not possible to derive quantitative mixing ratios of OSM and OMM via grain size data or heavy mineral populations.

In conclusion, the above matrix studies quantify our first-order field observations: the variability observed in pure OSM and OMM end-members reflects itself in highly variable matrix properties. Some ≥95% of all matrix materials are derived from the local substrate. The matrix variability requires mixing and processing at distinctly different locations prior to ultimate deposition at the drill site.

CLAST STUDIES

We now return to those Bunte Breccia components that are larger than 1 cm in diameter and that represent fragments of specific lithologies and therefore of discrete stratigraphic horizons. We will first describe their grain size properties and then discuss their modal composition regarding stratigraphic position in the initial Ries target. In most cases we will not distinguish between clasts (<64 cm) and megaclasts (>64 cm) in this section.

Grain Size

Figure 19 displays a variety of grain size data; individual core averages are plotted. Figure 19*a* is an overview concerning all grain sizes and specifically illustrates the ratio of matrix (<1 cm) to total clast plus megaclast content. Note that total clast content (1–64 cm) is somewhat variable; a

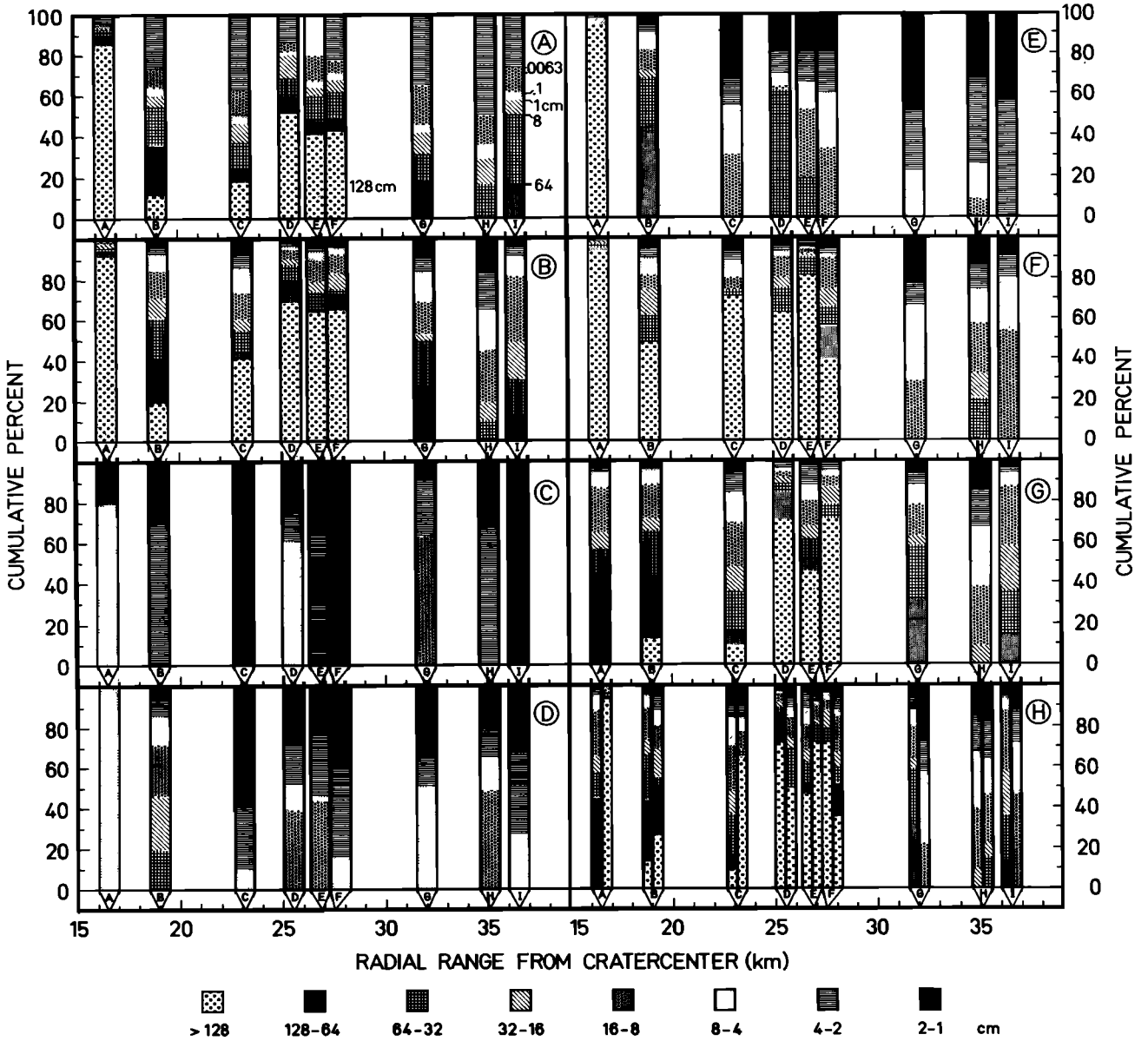

Fig. 19. Grain size distribution of >1-cm clasts derived from specific stratigraphic units as a function of radial range. Exact core locations A–I are indicated on the horizontal axis; subfigures refer to the letters A–H in the upper right-hand corner; and percentages are in weight percent. (*a*) Total clast (>1 cm) versus matrix (<1 cm) content (note special legend). (*b*) Grain size distribution of all clasts >1 cm. (*c*) Grain size distribution of crystalline clasts (>600-m target depth). (*d*) Grain size distribution of Triassic sediments (600–300 m deep). (*e*) Grain size distribution of Lower and Middle Jurassic sediments (300–150 m deep). (*f*) Grain size distribution of Upper Jurassic sediments (150–0 m deep). (*g*) Grain size distribution of "local" Tertiary clast (outside the crater cavity). (*h*) Comparison of all "crater-derived" clasts (left column) versus those of local derivation (right column).

gross trend toward decreasing grain size with increasing radial range may be inferred, however.

Figure 19*b* illustrates the measured size distributions of all clasts from all stratigraphic horizons. Inclusions larger than 128 cm in size constitute substantial amounts up to radial ranges of 30 km; clasts in the more distal cores are of distinctly smaller maximum as well as mean diameters. Combining Figures 19*a* and 19*b*, it is readily seen that the entire grain size distribution tends toward decreasing sizes with increasing radial range. As evidenced by the scatter contained in Figures 19*a* and 19*b*, significant deviations from this general trend may occur locally, thus attesting anew to the highly variable nature of continuous crater deposits.

Detailed clast size data referring to specific stratigraphic target horizons are illustrated in Figures 19*c*–19*f*. The most deep-seated, crystalline materials (Figure 19*c*) are typically only a few centimeters across; the largest inclusion measured 7 cm. The Triassic (Figure 19*d*), Lower and Middle Jurassic (Figure 19*e*), and Upper Jurassic (Figure 19*f*) clasts show a continuous progression toward larger grain sizes; the largest clast, an Upper Jurassic limestone boulder, measured 29 m in length (core A). The data contain a systematic trend in maximum as well as mean grain size with regard to specific target strata. Increasing comminution with increasing target depth is indicated. Finally, Figure 19*g* depicts the clast sizes of locally derived Tertiary components. They are,

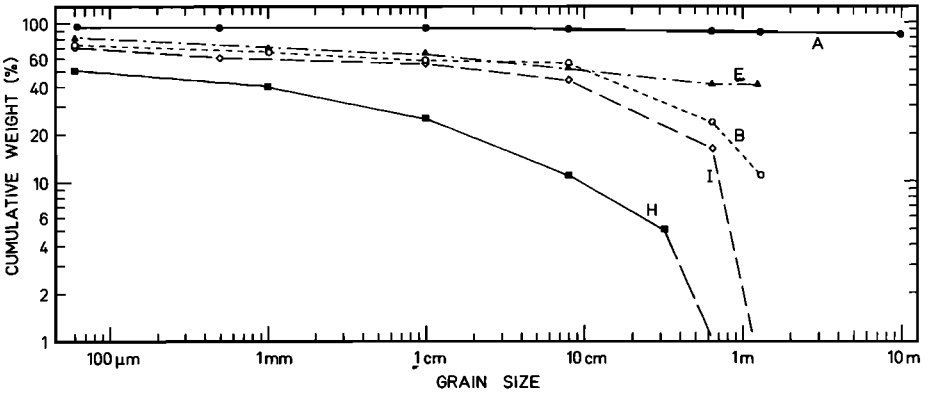

Fig. 20. Cumulative grain size distribution of Bunte Breccia. For clarity, not all cores are depicted.

on average, somewhat smaller than those of Upper Jurassic. Nevertheless, Tertiary clasts larger than 128 cm still constitute a substantial volume fraction; the largest Tertiary clast measured about 12 m (core F). Again the most distal cores (G, H, and I) seem to be more fine-grained than those of smaller radial ranges. Thus there is a systematic trend also in the degree of comminution with increasing range for locally derived breccia components, a conclusion in principle already evident from the increased fraction of fine-grained matrix (Figure 19*a*) in the distal deposits.

Another important result emerges when "primary" crater ejecta as a group are compared with the "local" clasts (Figure 19*h*). As we will see later, the crater materials are totally dominated (volume percent, mass percent) by Upper Jurassic clasts, and thus the "crater" clast sizes depicted in Figure 19*h* largely reflect those of Upper Jurassic. The crater and local clasts display qualitatively similar size distributions, although variability again is prominent. In some cores the local components are of coarser grain size than the crater materials, and vice versa. We also see that grain size parameters of clasts alone cannot be used to discriminate between primary and local breccia components. The absolute volumetric abundances, however, are dominated by Tertiary components (as discussed below), which therefore strongly influence the total clast size distribution of Bunte Breccia as illustrated in Figure 19*b*.

After considering core averages regarding clasts larger than 1 cm in Figure 19, we now display in Figure 20 the total grain size distribution, including matrix, in traditional cumulative fashion for a few cores only (for reasons of clarity). Note the enormous variability among cores. Most important, note the extremely poor sorting displayed by nearly every core; indeed, the grain size distribution is so heterogeneous that many parameters traditionally used to characterize sediments (e.g., curtosis and skewness) may not even be calculated from the present data set: some of the cores are dominated entirely by extremely large megaclasts (e.g., core A) in such a fashion that the total weight percent of a single clast amounts already to >30% of the total; conversely, the <63-μm fraction constitutes also typically >20%. We did not see any great scientific benefit to engaging in the time-consuming detailed grain size analysis of the <63-μm fraction via Atterberg settling, or any other grain size technique.

An example of the grain size distribution in vertical profile is illustrated in Figure 21 for Upper Jurassic of core E; numerous other plots could be presented. Figure 21 serves merely as an example (1) that clast size distributions of specific polymict breccia sections are indeed variable and (2) that there is no systematic trend in vertical profile. These conclusions hold for each single core and every specific target stratum. There are no systematic trends in vertical profile regarding grain size distribution. Extremely large clasts of, for example, Upper Jurassic (>50 m) are, however, observed in the field to reside preferentially toward the basal sections, if not at the base of Bunte Breccia, as noted by *Hüttner* [1958, 1969]. In principle, even such gigantic clasts may, nevertheless, occur anywhere in vertical profile [*Hüttner*, 1958, 1969].

We have plotted the grain size distributions in traditional cumulative fashion (not illustrated) to determine graphically the mean grain size of a specific lithology either for each individual core or for the total Bunte Breccia deposit. Linear regression analyses of the form $\log y = A \log x + \log B$ were performed to quantify potential trends in radial range ($r = x$). The mean grain sizes for the entire Bunte Breccia deposit (S_{MBB}), including the matrix, may be described as follows:

$$S_{MBB} = 3.3 \times 10^3 (r/R_D)^{-8.9 \pm 4.2} \quad (3)$$

where grain size S is in centimeters, absolute radial range r is in kilometers, and morphologic crater radius R_D is in kilometers (R_D = 13 km for the Ries). The ±4.2 values above correspond to standard errors. The correlation coefficient for equation (3) is −0.626; thus the quality of fit is fair at best. Nevertheless, mean grain sizes of 100 m result for $r <$ 10 km, consistent with field observations in the megablock zone.

In this equation, and similar ones to follow, it must be emphasized that the exponent x, i.e., the slope of the resulting best fit, is highly forced by the values of core A, which is unusual in many properties and which occupies the site closest to the crater center. As seen by the poor correlation coefficient and large standard deviations, equation (3) represents at best an order of magnitude estimate.

A linear regression through the mean grain size of primary crater ejecta alone (S_{MP}) as a function of radial range yields

$$S_{MP} = 2.6 \times 10^3 (r/R_D)^{-5.6 \pm 1.3} \quad (4)$$

The correlation coefficient for (4) is 0.843.

These grain size observations complement many field studies by, for example, *Hüttner* [1958, 1969], *Gall* [1969], and *Gall et al.* [1975]. They, and other field geologists, observed qualitatively a systematic decrease in the dimensions of gigantic clasts with increasing radial range; their observations refer to clasts larger than 25 m that were

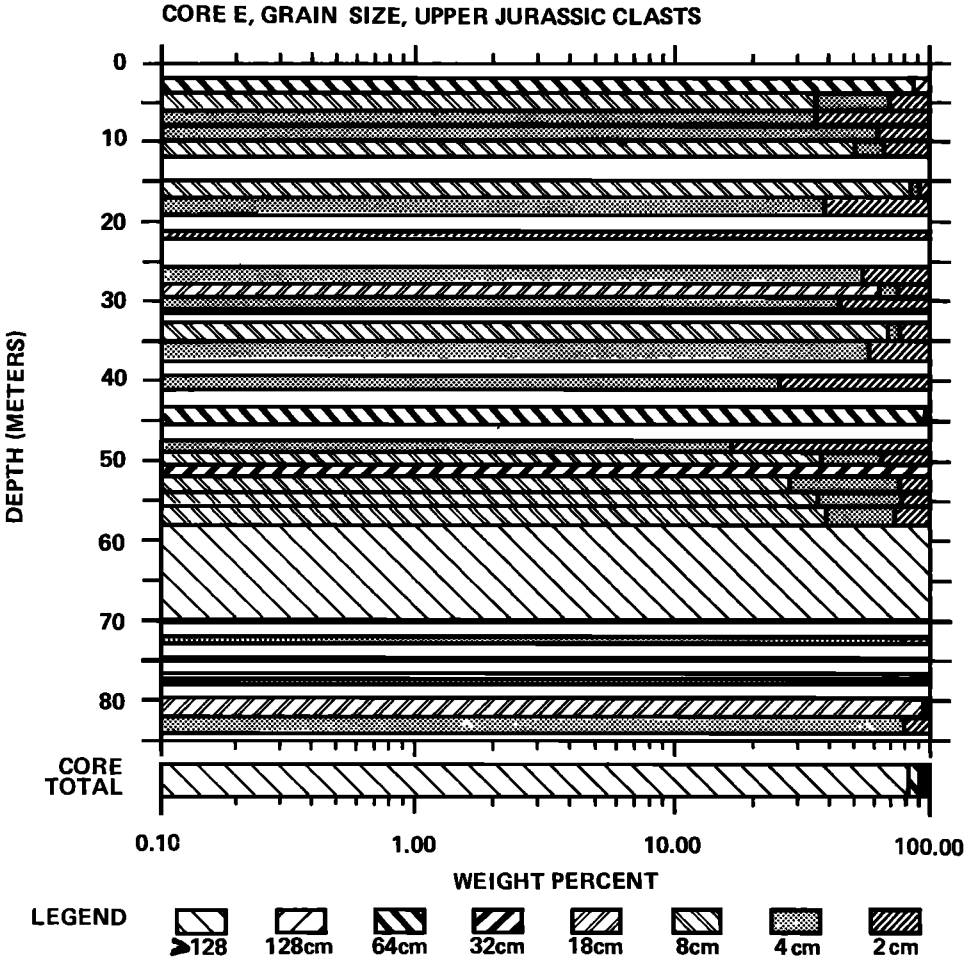

Fig. 21. Detailed grain size distributions in vertical profile for >1-cm clasts of Upper Jurassic (core E). Note the highly variable grain size distribution between neighboring polymict breccia sections and the lack of any systematic trend with increasing depth.

mapped individually on 1:25,000 scale maps. The only quantitative data were collected by *Gall* [1969], who finds these block sizes to decrease with $r/R_D^{-3.4}$; this exponent is slightly smaller than the one in (4). Our somewhat steeper comminution gradient either implies additional fragmentation and fracturing of predominantly small components during ejecta emplacement or reflects a possible mapping bias, because "small" clasts (e.g., 25–30 m in dimension) are more difficult to field-map quantitatively relative to the bigger ones (e.g., >50 m); some clasts (25–30 m) may have gone undetected during field mapping.

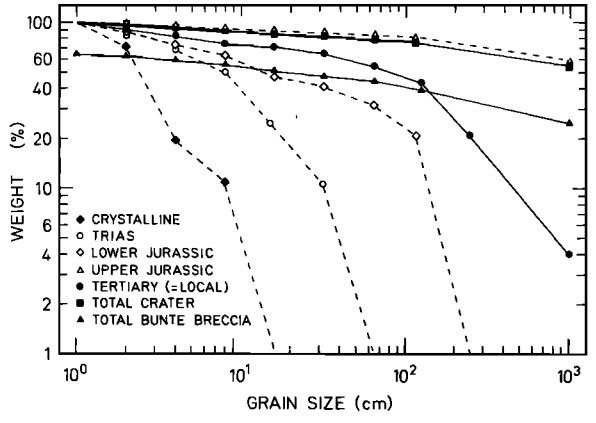

Fig. 22. Cumulative grain size distribution of all clasts from specific target strata for all crater materials and for the entire Bunte Breccia.

Further, *Gall* [1969] and *Gall et al.* [1975; Figure 4 and Table 1] systematically measured the surface area occupied by such gigantic megaclasts (>25 m) relative to the more fine-grained, typical Bunte Breccia, i.e., the <25-m-diameter components. The ratio of <25/>25 m varies typically between 1 and 5 for radial ranges of approximately 19–22 km and increases to ratios of ≈40 at radial ranges of ≥ 30 km.

Thus there is also macroscopic field evidence for decreasing block size and decreasing frequency of such blocks with increasing radial range. These field studies together with our laboratory data therefore demonstrate that the grain sizes of large-scale continuous deposits decrease in a systematic fashion with increasing radial range. *Shoemaker* [1963] reports similar findings from Meteor Crater, Arizona, and *Stöffler et al.* [1975] also observe such trends in small-scale laboratory impact experiments. The Ries data, however, are the only ones available for a large crater. The relatively steep comminution gradients are most likely caused by increased comminution within a large-scale excavation cavity and additional fragmentation due to secondary cratering as suggested by *Schultz and Mendell* [1978].

We now return to the apparently systematic trends in degree of comminution as a function of target depth, as

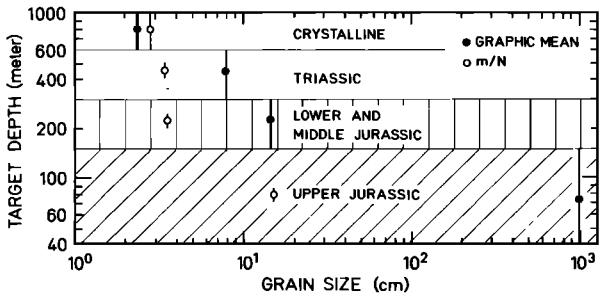

Fig. 23. Mean grain size of specific target strata versus mean residence depth in the target column, illustrating increasing comminution with increasing target depth.

already pointed out in Figure 19. Figure 22 illustrates the grain size distribution of all clasts from a specific stratigraphic horizon, averaged for the entire Bunte Breccia (all cores). Clearly, crystalline is more comminuted than Triassic, etc; Upper Jurassic is the most coarse-grained component; approximately 50% (weight) alone are contained in clasts over 10 m in length. Primary crater ejecta, because of the dominance of Upper Jurassic, are more coarse-grained than local, Tertiary clasts. Also depicted is the grand average grain size of >1 cm of all cores. The mean grain size for the entire Bunte Breccia deposit is 19.5 cm.

The mean grain sizes of specific stratigraphic horizons, graphically extrapolated from Figure 22, are plotted in Figure 23 as a function of absolute target depth. The vertical position of each point is plotted at the mean depth (from the target surface) for a given stratum; the vertical position of crystalline is ill defined, and placement at approximately 800 m is somewhat arbitrary. A linear regression fit through these graphic mean data points (S_{MG}) yields

$$S_{MG} = 1.6 \times 10^{-3}(d/R_D)^{-2.5\pm0.5} \quad (5)$$

where absolute target depth d is in kilometers and S_{MG} is in centimeters. The correlation coefficient for (5) is −0.906.

By definition, the above mean grain size S_{MG} relates to total mass; that is, 50% of the mass is contained in smaller (or larger) clasts. Another approach to characterize an average clast size may be attempted by taking the total mass m observed per stratigraphic member and to divide it by total number N of the respective clasts encountered; that is, m/N yields an average clast mass. Accounting for appropriate densities, one then may calculate a spherical body of diameter S_{MD}. The average grain sizes derived by this method are also plotted in Figure 23. They generally yield substantially smaller diameters than the graphic mean, because the latter approach is heavily weighted toward the very frequent, small grain sizes which dominate N. A linear regression through the m/N data points in Figure 23 yields

$$S_{MD} = 3 \times 10^{-1}(d/R_D)^{-0.7\pm0.2} \quad (6)$$

The correlation coefficient for (6) is −0.904.

Thus there appears to be a truly systematic increase in comminution with increasing target depth. The data may be expanded to include suevite, possibly derived from still greater depths than the crystalline clasts in the Bunte Breccia. Consistent with this view, mean grain size of suevite is in the millimeter size range [*Förstner*, 1967]. Surprisingly, these trends exist despite dramatic differences in physical properties (e.g., compressibility) of the diverse clays, shales, limestones, marl, sandstones, and crystalline rocks making up the Ries target.

Modal Composition

As described above, the planimetric frequencies of specific lithologies were converted via appropriate densities into absolute and relative mass fractions. This procedure corresponds to a quantitative modal analysis regarding the geologic stratigraphic makeup of the Ries' continuous deposits.

We will first address the modal composition of individual cores in vertical profile; Figure 24 presents the results for most cores. The detail of the data, although possibly confusing, nevertheless illustrates two important points:

1. There is no systematic trend in vertical core profile regarding enrichment/depletion of any given lithology. There also is no preferred concentration of crater-derived components, local clasts, and/or matrix. All components are highly variable in their frequency over vertical distances measured in meters. Note again that "megaclasts" may occur anywhere in vertical profile, regardless of whether they are primary crater materials or locally derived.

2. If we now concentrate only on the polymict breccia sections, identified by the presence of a "matrix," we can see that neighboring sections may or may not have dramatically different clast populations and/or total clast and matrix content.

The data displayed in Figure 24 quantify what is already quite obvious from first-order field inspections, and they verify the conclusions offered in that section: the Bunte Breccia is a highly chaotic deposit, and no parameter measured yields any systematic trend in vertical profile.

For reasons of clarity, Figure 25 introduces, in vertical profile, the ratio of all crater-derived lithologies and the combined contributions of Tertiary plus matrix (as demonstrated above, the matrix is >95% of local origin). Note the lack of any systematic vertical trend. The data illustrated in Figures 24 and 25 argue very strongly against a "basal mixing zone" as proposed by *Chao* [1977*a*]. Isolated, randomly positioned pockets and zones of crater-rich or crater-poor materials may be observed anywhere in vertical section.

Figures 26 and 27 document the enormous variability of individual polymict breccias. Figure 26 displays the clast populations derived from the crater, while Figure 27 compares total primary ejecta to Tertiary clasts and the locally derived matrix. Large scatter characterizes all plots and again verifies the first-order field observations: there is indeed an enormous variability in breccia "types" generated during one single impact. This variability includes a wide range of crater-derived clast populations as well as variable ratios of crater clasts, local clasts, and fine-grained matrix; numerous additional plots could be generated illustrating similar variability for essentially every single parameter measured in these polymict breccias.

So far we have elaborated on the properties of individual, polymict breccia sections. We now present modal data averaged for individual cores and, furthermore, plot the core position(s) again as a function of radial range. The modal composition of primary crater ejecta is illustrated in Figure 28. Figure 28*a* illustrates the relative frequency of crystalline materials derived from depths of >600 m and those from Triassic strata, the latter representing target depths from 600 to 300 m. Note that the Triassic components vastly dominate

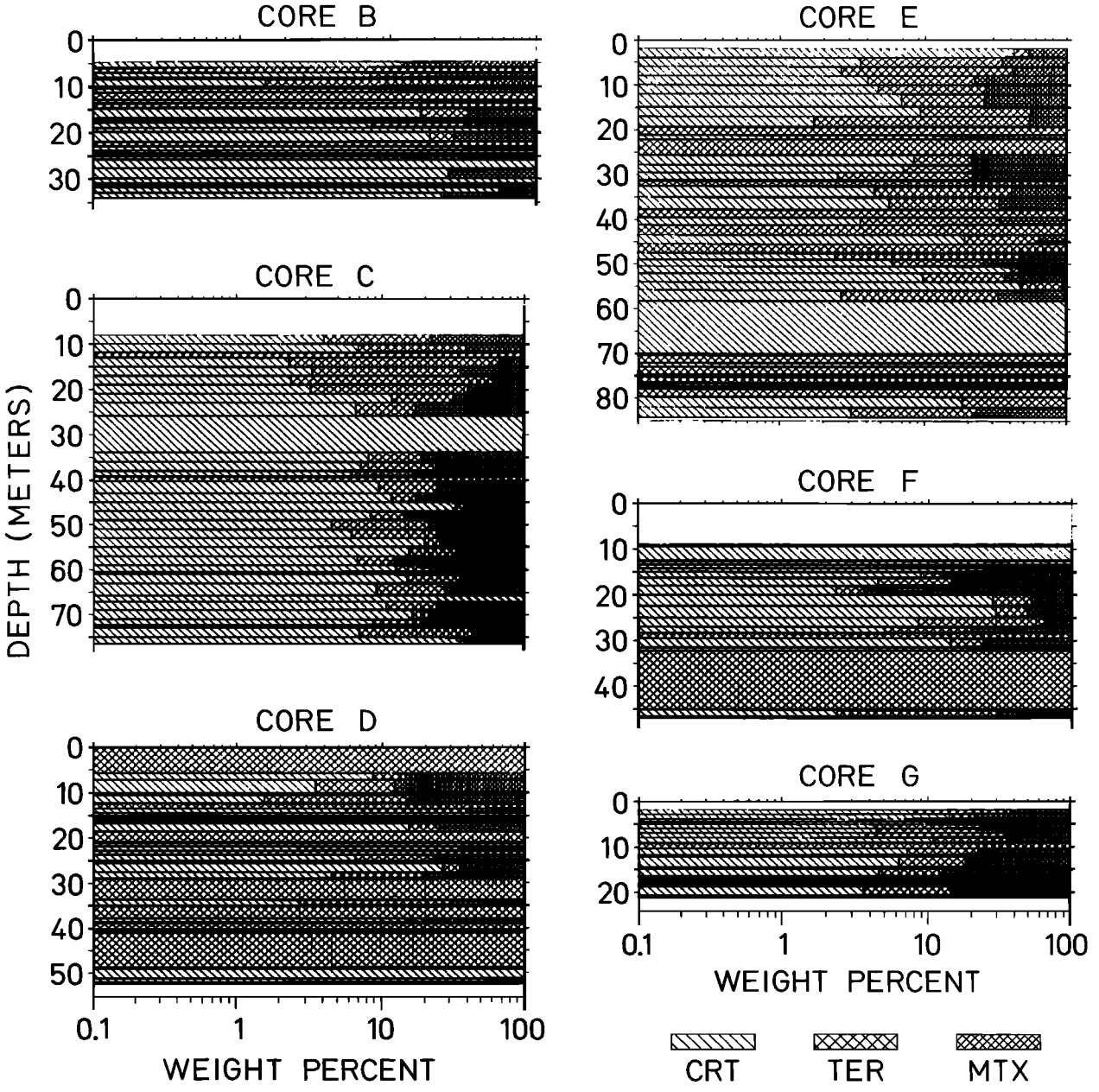

Fig. 24. Modal stratigraphic analysis of cores B–G in vertical profile (cores A, H and I, although not illustrated display the same degree of variability). CRT: primary crater ejecta; TER: local, Tertiary clasts; MTX: (local) matrix.

the crystalline basement, although the exact ratios are variable locally. In Figure 28*b* we added to the previous strata those representing target depths of 300–150 m, i.e., the Lower and Middle Jurassic clasts. Note that these new horizons again vastly dominate the combined contributions of all deeper-seated strata. Finally, in Figure 28*c* we have added the Upper Jurassic limestones, 0–150 m deep, and once again it is obvious that they exceed the combined contributions of all other crater materials by approximately a factor of 4; local deviations from these trends are again, however, commonplace.

The most important findings displayed in Figure 28 are as follows:

1. The sedimentary strata composing the Ries target (see Figure 1) can be subdivided into three identifiable, major horizons, each fortuitously of approximately 200 m thickness. Each successive, new horizon dominates the combined effects of all strata below in contributing materials to the Bunte Breccia deposits at all radial ranges investigated. The average (weight percent) for all core materials recovered is as follows: crystalline, 0.15%; Triassic, 2.15%; Lower and Middle Jurassic, 6.69%; and Upper Jurassic, 91.01%.

2. All target horizons may be found anywhere in the continuous deposits, even in relatively distal locations. Importantly, this statement includes the presence of deep-seated crystalline basement, which was encountered in every single core, albeit in small concentrations generally, i.e., <0.5% and frequently even <0.1% of all primary ejecta. Conversely, the Upper Jurassic limestones, i.e., the shallowest target strata, vastly dominate all crater materials over the entire radial range represented by the core locations.

Linear regression analyses (as a function of radial range) for any individual stratigraphic members (illustrated in Fig-

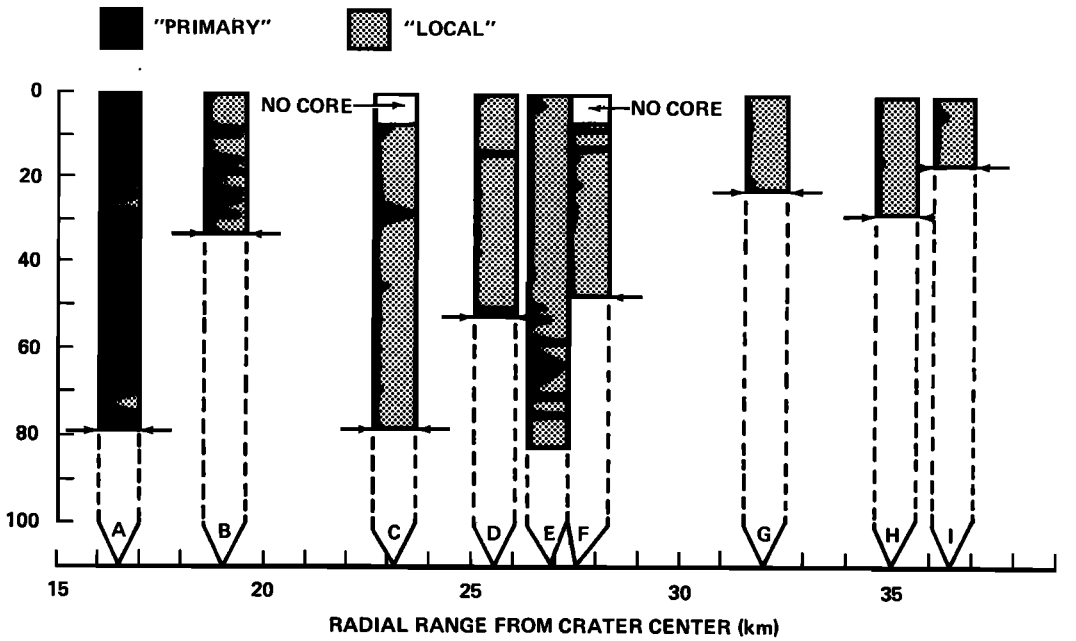

Fig. 25. Ratios of crater-derived and local materials in vertical profile for all cores.

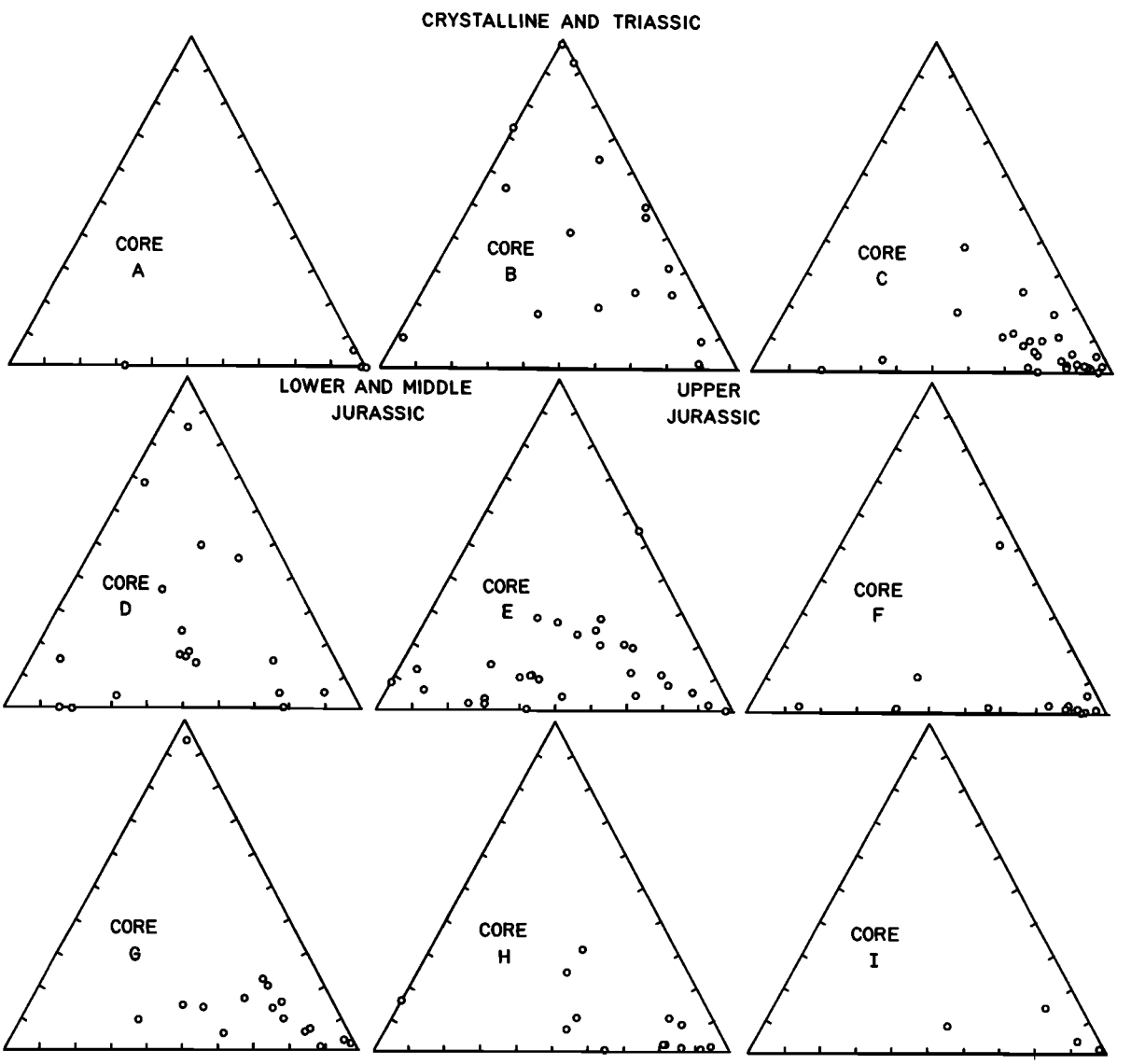

Fig. 26. Three component plots illustrating the variability in modal stratigraphic makeup of individual polymict breccia sections. The figure, specifically, illustrates the variability of primary ejecta.

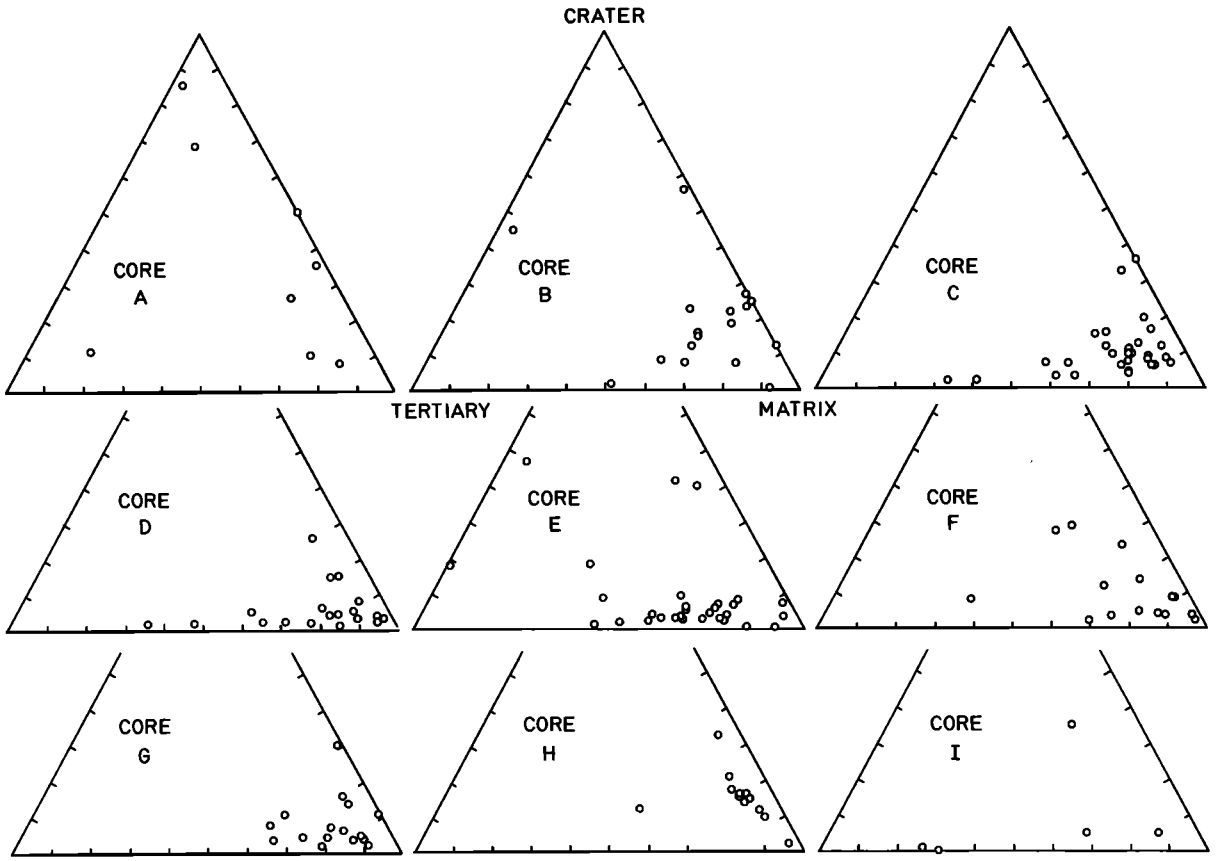

Fig. 27. Modal stratigraphic composition of individual polymict breccia sections with respect to crater-derived components and locally excavated materials, the latter differentiated into Tertiary clasts larger than 1 cm and matrix (<1 cm).

ure 28) are not very illustrative and display little sensitivity with respect to r.

Thus there is little change in the modal stratigraphic makeup of primary ejecta clasts in the Bunte Breccia as a function of radial range. These observations appear at odds with the popular concept of "inverted" target stratigraphy, so abundantly observed and documented in small-scale cratering experiments [e.g., *Gault et al.*, 1968; *Stöffler et al.*, 1975]. While we will address this seeming discrepancy later, it may nevertheless be of interest to use the total Bunte Breccia mode (average of all cores) and its relation to initial target depth. We calculate the cumulative fraction of ejecta, f_E, derived from depths $\geq d$ to be

$$f_E = 1.8 \times 10^{-6}(d/R_D)^{-2.6\pm0.4} \quad (7)$$

This equation simply describes an average modal stratigraphic composition of primary crater ejecta in continuous crater deposits between radial ranges of approximately 1.5–3 R_D; the equation yields nonsensical results for very shallow target depths (e.g., $r < 0.005\ R_D$), because $f_E > 1.0$.

The relative proportions of crater-derived clasts to those of local origin are illustrated in Figure 29*a*. Generally, Tertiary clasts outweight primary crater ejecta, although large deviations may occur locally. The grand weight average of all core materials larger than 1 cm, however, amounts to 54.4% (weight) crater-derived materials because of the two gigantic Upper Jurassic megaclasts encountered in core A (these two clasts alone amount to about 45% (weight) of all crater materials observed in the entire drilling project). Subtracting the somewhat anomalous core A, total crater-derived components amount to approximately 34% of all clasts. Averaging the normalized data illustrated in Figure 29*a*, which essentially eliminates absolute core length and which therefore treats each location equally, results in 43% crater clasts including the anomalous core A and 31% without core A. On average, the more distal cores tend to have higher concentrations of local clasts than those at close radial ranges, although core H clearly represents an (local?) exception to this rule. It is, however, clear that locally derived clasts tend to dominate primary crater ejecta in mass as well as number frequency over substantial radial ranges.

Linear regressions through the clast data (>1 cm) illustrated in Figure 29*a* yield the following relationship for the fraction of primary ejecta materials, f_{PE} (weight percent relative to entire deposit), as a function of radial range:

$$f_{PE} = 9.4 \times 10^{-1}(r/R_D)^{-1.5\pm0.8} \quad (8)$$

The correlation coefficient for (8) is −0.556; thus the fit is not very good, as is already obvious by the scatter in Figure 29*a*.

Similarly, the fraction of "local" ejecta clasts larger than 1 cm, f_{LE}, is given by

$$f_{LE} = 7.4 \times 10^{-2}(r/R_D)^{2.6\pm1.2} \quad (9)$$

The correlation factor is, of course, similarly poor (0.639) as that of equation (8).

Equations (7) and (8) refer to the populations of clasts larger than 1.0 cm. If one adds the fine-grained "matrix," one obtains the results illustrated in Figure 29*b*. Because >95% of this matrix consists of locally derived materials, Figure 29*b* essentially corresponds to a geologic-stratigraphic modal analysis of the entire Bunte Breccia deposit. The locally derived components vary from 10% (core A) to as much as 94% (core G). Again there is large local variability, but local materials in general make up >70% of the entire deposit. The grand average for all cores is 65.3% local materials; if one excludes the somewhat anomalous core A, one obtains 82% locally derived constituents for all cores. The incorporation of local materials is indeed significant. Local materials vastly dominate the actual primary crater ejecta.

Again, linear regressions were performed through the data illustrated in Figure 29*b* to quantify radial trends regarding the fractions of primary crater clasts (f_{PC}), local clast (f_{LC}), and matrix content (f_{MC}) relative to the total Bunte Breccia deposit. The following expressions were obtained:

$$f_{PC} = 1.01(r/R_D)^{-2.5\pm0.7} \quad (10a)$$

$$f_{LC} = 1.9 \times 10^{-1}(r/R_D)^{1.8\pm0.7} \quad (10b)$$

$$f_{MC} = 1.05 \times 10^{-1}(r/R_D)^{1.8\pm0.7} \quad (10c)$$

Correlation factors are 0.808, 0.701, and 0.692, respectively.

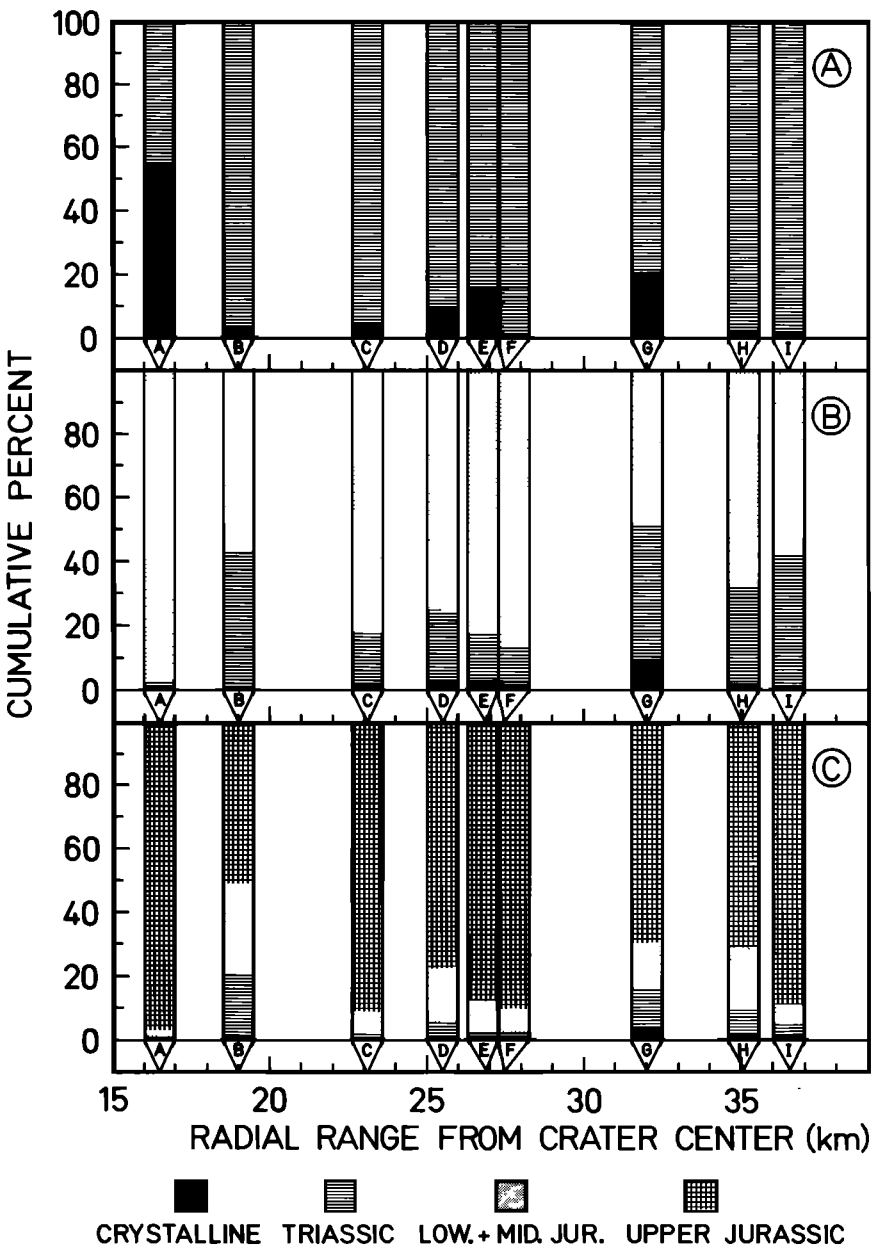

Fig. 28. Relative frequency (weight percent) of major target stratigraphic members within the Bunte Breccia. (*a*) Comparison of all strata more than 300 m deep. (*b*) Comparison of all strata more than 150 m deep. (*c*) Comparison of all target strata. Note (1) the systematic increase of successively higher stratigraphic horizons, (2) that each single horizon is found at all radial ranges, and (3) that the uppermost stratum is by far the dominant component at all radial ranges.

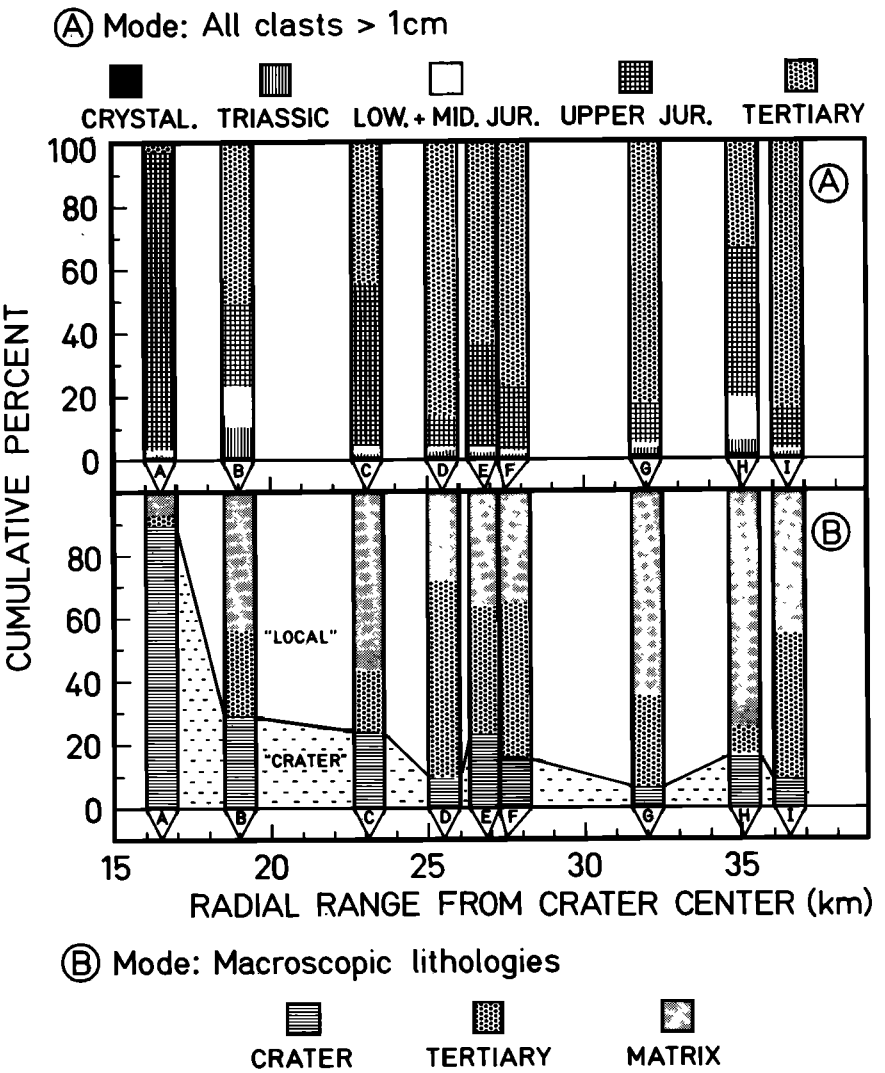

Fig. 29. Modal-stratigraphic composition of Bunte Breccia as a function of radial range. (*a*) Relative frequency (weight percent) of all clasts larger than 1 cm in diameter. Note that the locally derived, Tertiary clasts are a significant component and mostly more abundant than the crater-derived clasts. There is, however, significant local scatter, even in the average for entire cores. (*b*) Absolute stratigraphic lithologic mode (weight percent) of the Bunte Breccia deposit. Note that locally derived materials (after addition of the matrix) vastly dominate the makeup of the Ries continuous deposits at any radial range >20 km from the crater center, or >5 km from the crater rim.

Oberbeck et al. [1974] introduced the term μ as the mass ratio of materials displaced by secondary craters (local components) to primary crater ejecta:

$$\mu = (f_{LC} + f_{MC})/f_{PC} \tag{11}$$

A linear regression through the observed μ values (μ_{ob}) observed in this core-drilling program yields for the Ries

$$\mu_{ob} = 3.82 \times 10^{-6} r^{4.2 \pm 1.2} \tag{12a}$$

or, in normalized fashion,

$$\mu_{ob} = 2.02 \times 10^{-1} (r/R_D)^{4.2 \pm 1.2} \tag{12b}$$

The correlation factor is 0.790 for (12).

Equation (12*b*) corresponds directly to the equations calculated (μ_c) by *Morrison and Oberbeck* [1978, Figure 5] on the basis of experimental and photogeologic studies:

$$\mu_c = 7.16 \times 10^{-4} r^{2.54} \tag{13a}$$

$$\mu_c = 4.79 \times 10^{-4} r^{2.54} \tag{13b}$$

assuming ejection angles of 45° (equation (13*a*)) and 15° (equation (13*b*)) from the local horizontal.

We compare the Ries observations with the predictions of *Morrison and Oberbeck* [1978] in Figure 30. There is obvious discrepancy between observations and predictions, but we must emphasize that most planetary investigations and implications refer to continuous deposits beyond the morphological crater rim and thus apply typically to radial ranges between 1.0 and 2.5 R_D. For such radial ranges there is at most a discrepancy of a factor of 4 for the most distal deposits and assuming the worst case (equation (13*a*)). In general, agreement is within a factor of 2 or better, and we therefore consider predictions and observations to be in good agreement. We will return to these considerations and conclusions later. (Along similar lines it must be emphasized that all linear regressions presented throughout this paper are valid only for scaled radial ranges greater than R_D, with r measured from the crater center; the regressions apply to deposits between radial ranges of approximately 1.3 and 3

R_D, and some of them may yield nonsensical results for much smaller or larger scaled radial ranges.)

Clast Orientation

Macroscopic inspection with the naked eye, and as illustrated in Figures 7–13, indicates a seemingly random orientation of clasts. Dip angles of, for example, elongated clasts or initial bedding planes in well-preserved megaclasts appear to be irregular. The deposit appears to be "massive" in texture. Quantitative measurements of clast orientation were performed according to the following procedures.

The blueprint mapping products were overlain with transparent tracing paper that had 1/10-in. gridlines, suitable for accurate length determination of horizontal and vertical intercepts of any specific clast along a point counting grid spaced 1 in. apart (see Figure 31). The horizontal (H) and vertical (V) grid intercept lengths were added separately, and division of their cumulative intercept lengths yielded the ratio of horizontal to vertical orientation vectors; if $H/V = 1$, the orientation is perfectly random; for $H/V < 1$ there is a vertical trend, and conversely, $H/V > 1$ quantifies the degree of preferred horizontal orientation.

Figure 32 illustrates these measurements for cores D, B, and G; measurements were not performed on all cores, as macroscopic inspection indicated these unmeasured cores to be essentially identical to the ones subjected to the very time-consuming analysis. The numerical values obtained for all clasts are 1.04 (core D), 1.03 (core B) and 0.99 (core G). These results verify the macroscopic evidence for random orientation of Bunte Breccia clasts. Note also that there is no

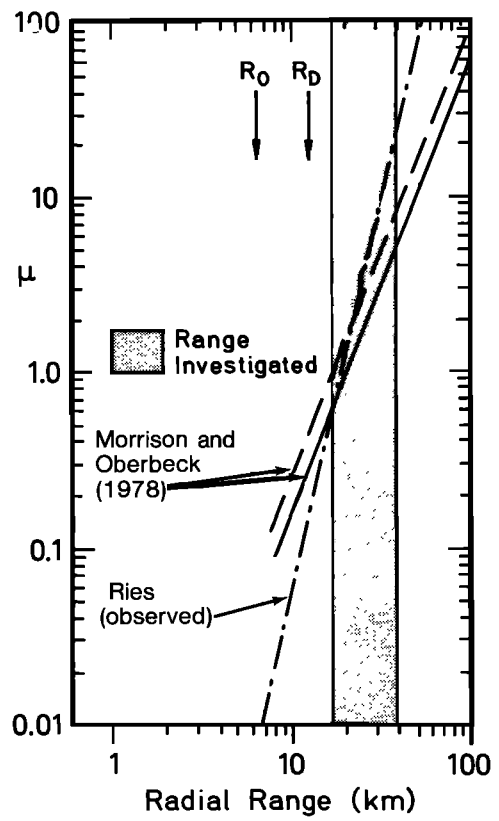

Fig. 30. Comparison of predicted [*Morrison and Oberbeck*, 1978] and observed μ values for the Ries; μ is the mass ratio of locally derived materials versus primary crater ejecta (for details, see text).

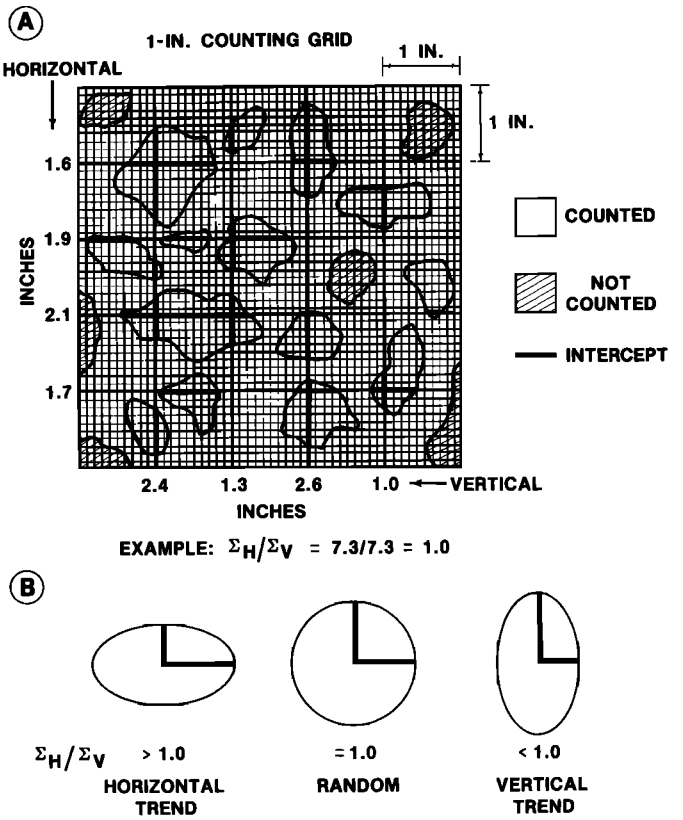

Fig. 31. Graphic point-counting technique employed to determine orientation parameters for Bunte Breccia clasts. Only the solidly drawn intercepts were counted. Note that nonintersecting (small) clasts were deleted if they did not intersect the master grid; also, all fractional clasts (at the periphery) were deleted entirely.

significant difference between local and crater-derived clasts. Also, it can be seen in Figure 32 that some rare polymict breccia sections may have pronounced horizontal or vertical lineation trends.

Shock Metamorphic Effects

As already detailed previously [*Hörz and Banholzer*, 1980], the only materials containing discernable shock effects in the Bunte Breccia cores are the crystalline inclusions. In accordance with *Schneider* [1971], none of the Triassic and Lower Jurassic clasts investigated in thin section displayed planar shock elements in component quartz or feldspar grains, i.e., shock indicators for peak pressures in excess of 10 GPa. Also in accordance with *Graup* [1978], the highest shock pressures recognized in our Bunte Breccia samples were <40 GPa. Therefore the pressure regimes during Bunte Breccia formation were modest and certainly not sufficient to generate any impact melts. These observations lead *Hörz and Banholzer* [1980] to the conclusion that Bunte Breccia was deposited at ambient temperatures. Such a conclusion was anything but new to Ries geologists. Even the earliest workers (for example, as summarized by *Löffler* [1926]) recognized the dichotomy between "hot" suevite and the "cold" Bunte Breccia, although the genetic relationships, such as we now know, were recognized only recently. This obvious dichotomy in thermal regimes was also used by *Chao* [1973] as a major argument to postulate the deposition of relatively cold Mare Imbrium ejecta at the Apollo 14 site in the form of the Fra Mauro formation. Therefore the

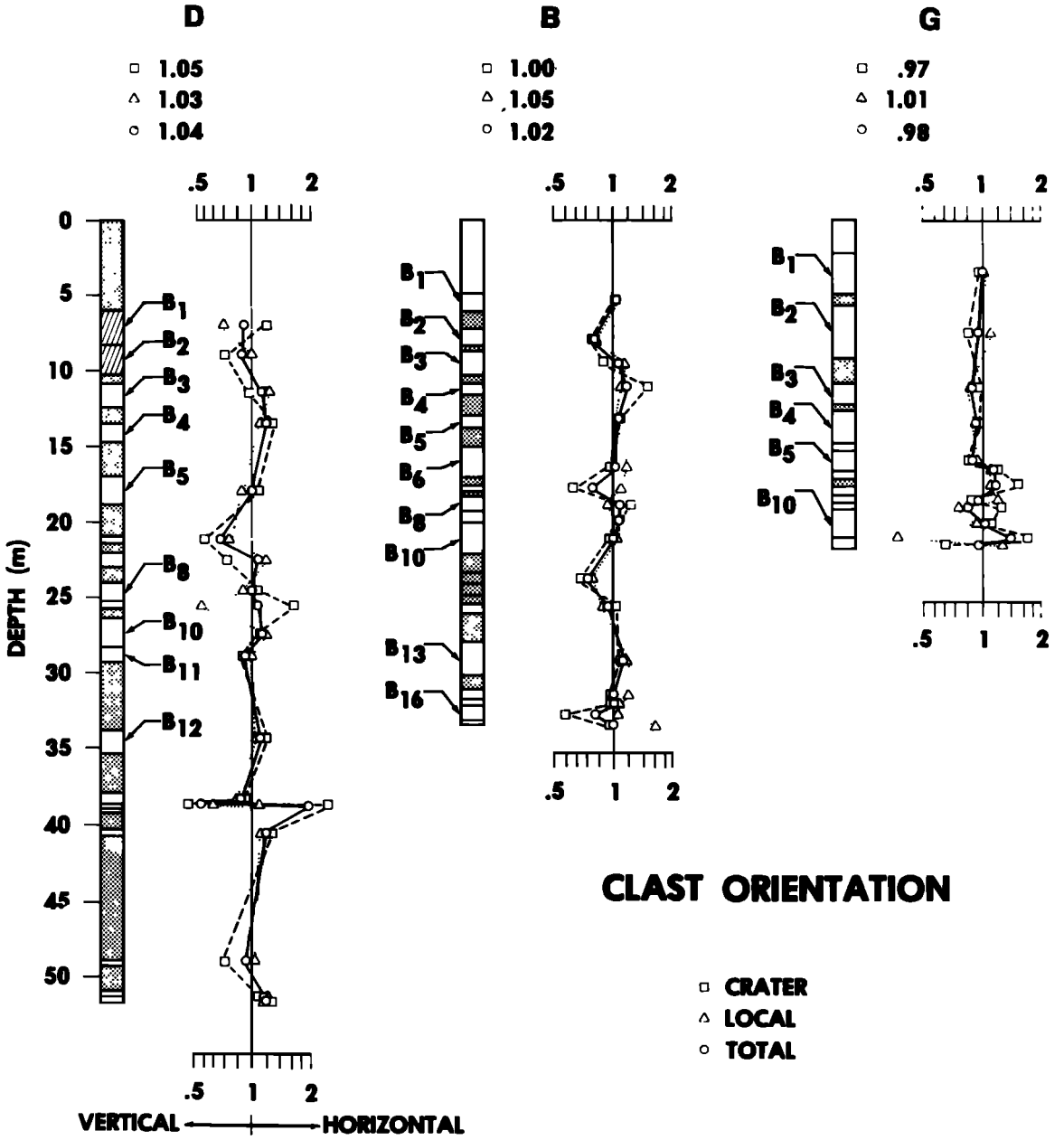

Fig. 32. Clast orientation in vertical profile of cores D, B, and G. (B_1, B_2, etc., denote discrete polymict breccia sections).

conclusions of *Hörz and Banholzer* [1980] were, in principle, not new, but one of strong reemphasis.

For completeness our detailed data leading to this reemphasis are illustrated in Figures 33 and 34. Figure 33 displays the types of crystalline rocks encountered in the cores (70% granites, 22% gneisses, 8% amphibolites and lamprophyres), their approximate position in vertical profile (±0.5 m), and their associated degree of shock. The shock classification used is that of *Stöffler* [1972], which is largely based on deformation features in quartz and feldspar; tectosilicates are particularly sensitive to peak pressures of <40 GPa [*Stöffler*, 1972]. Shock stage 0 (0–10 GPa) is characterized by abundant, irregular, intragranular fractures, reflecting essentially brittle failure of the component mineral grains. Shock stage I (10–25 GPa) is principally defined by single or multiple sets of planar features, patchy extinction, and possibly decreased birefringence. Finally, shock stage II (25–40 GPa) is characterized by complete solid-state vitrification resulting in diaplectic quartz and feldspar glasses, the latter commonly termed "maskelynite." At shock pressures above 45 GPa the tectosilicates begin to melt (shock stage III); no such melting was observed in any of the samples investigated. Returning to Figures 33 and 34, one can see that about 40 GPa is the maximum pressure experienced by the most severely shocked Bunte Breccia clasts. Note also that samples shocked to maskelynite grade (stage II) generally compose <20% of all crystalline samples investigated.

Importantly, the degree of shock is independent of vertical position within the Bunte Breccia deposit (see Figure 33). All shock levels may occur anywhere in vertical profile. Also, shock grades 0, I, and II may in principle occur anywhere in radial traverse (Figure 34). Very importantly, one always has

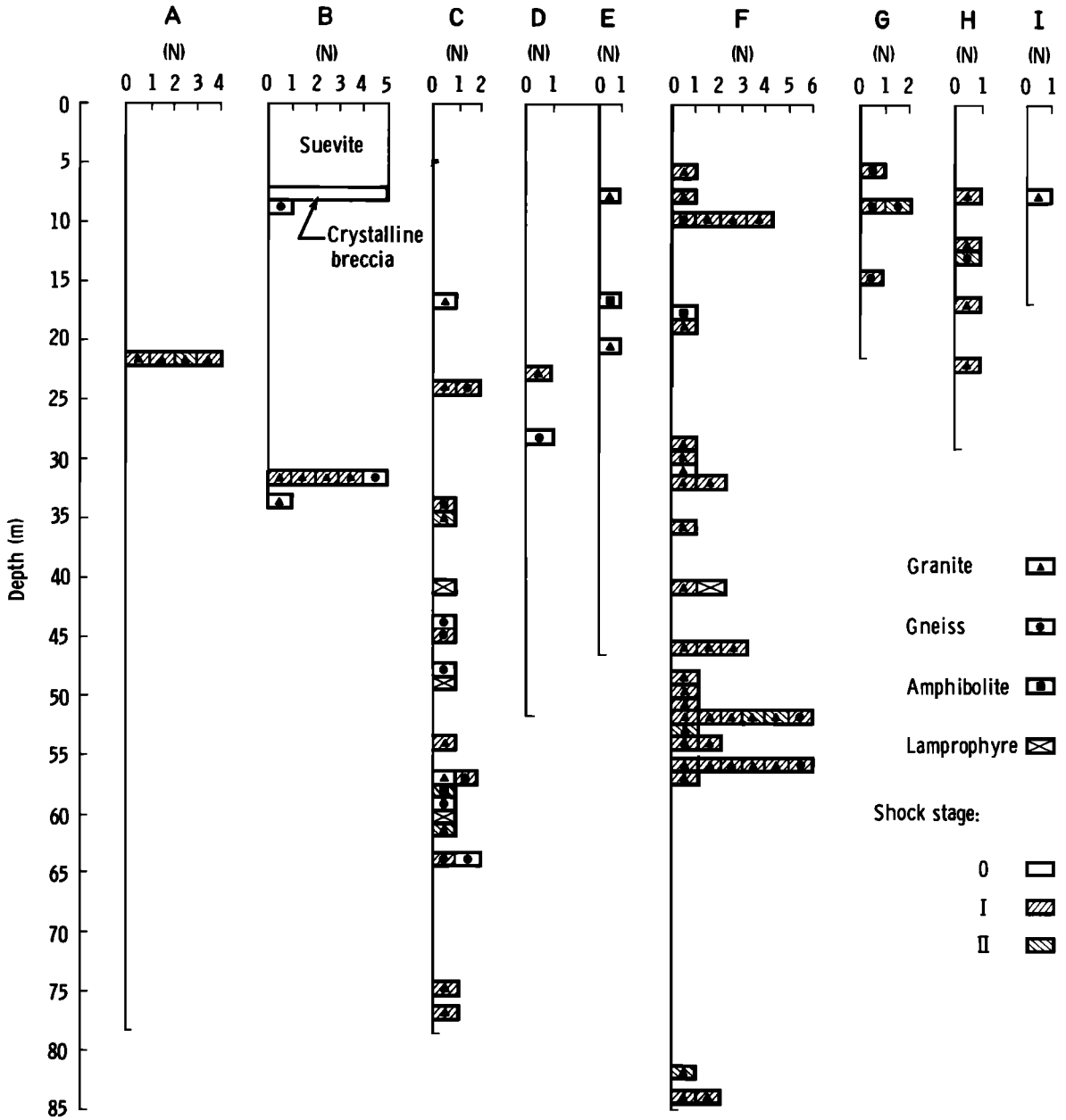

Fig. 33. The shock history of crystalline clasts in nine Bunte Breccia cores. The prominent lithologies and their associated degree of shock metamorphism are illustrated together with the actual position (±0.5 m) at which these clasts occurred in vertical profile. Note that (1) crystalline clasts may occur anywhere in vertical profile, (2) the degree of shock is independent of vertical position, and (3) the crystalline clasts tend to occur frequently in "clusters," although variable lithologies and degrees of shock may make up specific cluster populations.

to keep in mind that the total amount of all crystalline materials is $\ll 1\%$ and thus that $\gg 99\%$ of all Bunte Breccia components do not display any evidence of shock discernable with the optical microscope.

The distribution of shock metamorphic effects in continuous crater deposits may be used as clues to estimate prevalent temperatures during ejecta deposition, as each shock level may be associated with a certain peak temperature [e.g., *Raikes and Ahrens*, 1979]. Accordingly, our 40-GPa maximum peak pressure corresponds to approximately 600°C. At most some 0.1% of the entire Bunte Breccia deposit may have experienced this temperature. The majority (>99.9%) of the Bunte Breccia, i.e., in essence the entire deposit, was emplaced at ambient temperatures. This conclusion has important planetary implications as discussed below and as already summarized, in part, by *Hörz and Banholzer* [1980].

Summary of Clast Studies

In a number of ways the above clast studies yielded phenomenologic insight into large-scale continuous impact deposits:

1. From a grain size point of view, continuous crater deposits are among the most poorly sorted materials known; absolute grain size in the Bunte Breccia varies over 8 orders of magnitude.

2. Because locally derived components larger than 1 cm dominate volumetrically those derived from the parent cra-

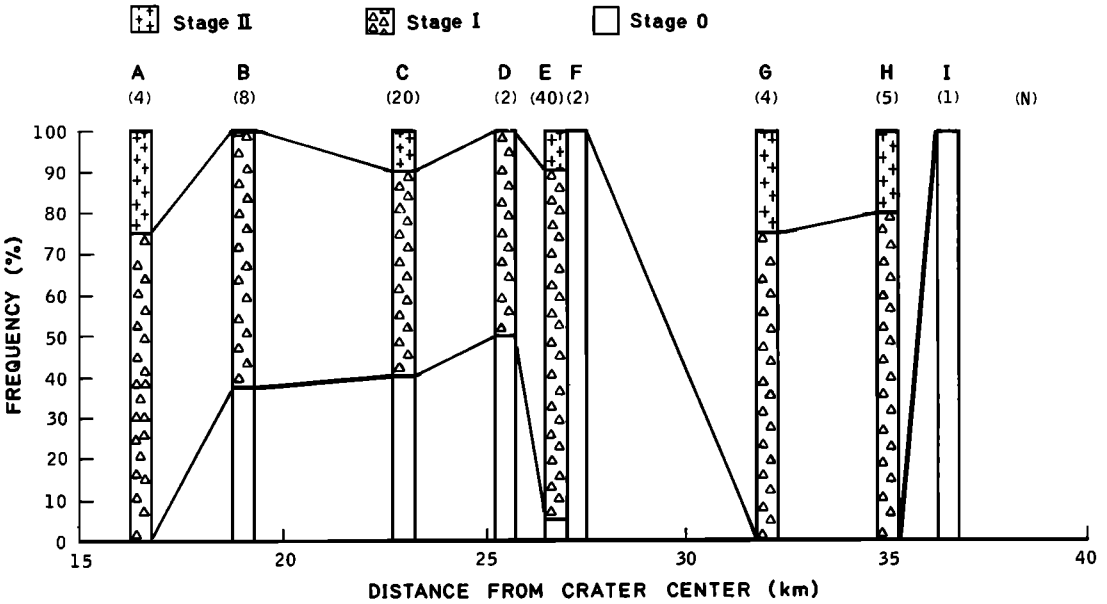

Fig. 34. Radial distribution of the degree of shock in crystalline inclusions from nine Bunte Breccia cores. Note that (1) generally <80% of all crystalline clasts are shocked to levels below 25 GPa (the remainder may have experienced peak pressures as high as 40 GPa) and (2) all shock stages may occur anywhere in radial traverse.

ter, overall grain sizes of Bunte Breccia clasts are dominated by local materials. If one includes the locally derived matrix, grain size distribution of the entire deposit is entirely controlled by local components.

3. There is a systematic decrease in grain size with increasing radial range (equations (3) and (4)).

4. Materials from successively deeper target strata are progressively more comminuted (equations (5) and (6)).

5. The modal stratigraphic composition of primary ejecta is essentially the same over the entire radial range investigated. Upper Jurassic, i.e., the shallowest target horizons, vastly dominate successively more deep-seated strata.

6. The average modal stratigraphic composition with regard to initial target position for the entire Bunte Breccia may be described by equation (7).

7. The total amount of primary crater material decreases with radial range according to equation (10*a*). Conversely, the fraction of locally excavated materials increases (equations (10*b*) and (10*c*)). The observed μ values, i.e., mass ratio of local/primary materials, are described by equations (13). The compositional trends described by these equations are in good agreement with the predicted relationships of *Morrison and Oberbeck* [1978]. They are in exceedingly strong support of a ballistic emplacement scenario as detailed in a later section.

8. The orientation of >1-cm clasts is random.

9. More than 99% of the Bunte Breccia components appear unshocked ($\ll$10 GPa). The only materials visibly shocked (>10 GPa) are those from the most deep-seated target strata. These findings lead to the important conclusion that large-scale continuous crater deposits are emplaced at essentially ambient temperatures.

10. None of the parameters measured (grain size, modal stratigraphic composition, clast orientation, shock metamorphism) displays systematic trends in vertical Bunte Breccia profile. These findings, together with the textural observations described above, attest to a highly turbulent depositional regime in which components derived from different source locations are randomly mixed and distributed.

COMPARISON WITH CRATERING THEORY

In the following discussion we will compare the above Ries observations with a variety of current models concerning cratering mechanics. Specifically, we are concerned with the distribution and nature of the continuous deposits surrounding large impact structures and the geometry of their excavation cavity. We will first address the continuous ejecta deposits.

Ejecta Distribution

The ejecta thickness t_e at any radial range r from the crater rim of radius R_0 may be expressed as

$$t_e = K(r/R_0)^{-x} \tag{14}$$

McGetchin et al. [1973] suggest an exponent of $x = 3$, based on field studies around large explosion craters and photogeologic studies (see also *Moore et al.* [1974]). *Stöffler et al.* [1975] find $x = 3.2$ on the basis of small-scale cratering experiments; *Schultz et al.* [1981] calculate $x = 4$ for $r/R_0 < 2.5$ and $x = 2.5$ for large radial ranges ($r/R_0 > 2.5$). Thus there remains substantial uncertainty concerning details of the absolute mass distribution of crater ejecta as a function of range.

In order to utilize our field and laboratory observations it is necessary to define the diameter R_0 and specific geometry of the Ries' excavation cavity, thereby defining the total volume of primary Ries ejecta. As justified below, an excavation cavity diameter of 13 km (R_0 = 6.5 km) and an excavation volume of 136 km^3 were assumed for all Ries calculations presented in Figure 35. Figure 35 also illustrates the predicted values for total thickness of the Ries' continuous deposits, accounting for secondary cratering [*Morrison and Oberbeck*, 1978], albeit for the above (preferred) values for R_0 and crater volume. Superposed on these calculations are the results of cores A–I, differentiated into "crater" materials and those of local origin. Locations A and B were essentially covered by suevite; thus a few meters of crater components should be added. Importantly, each core re-

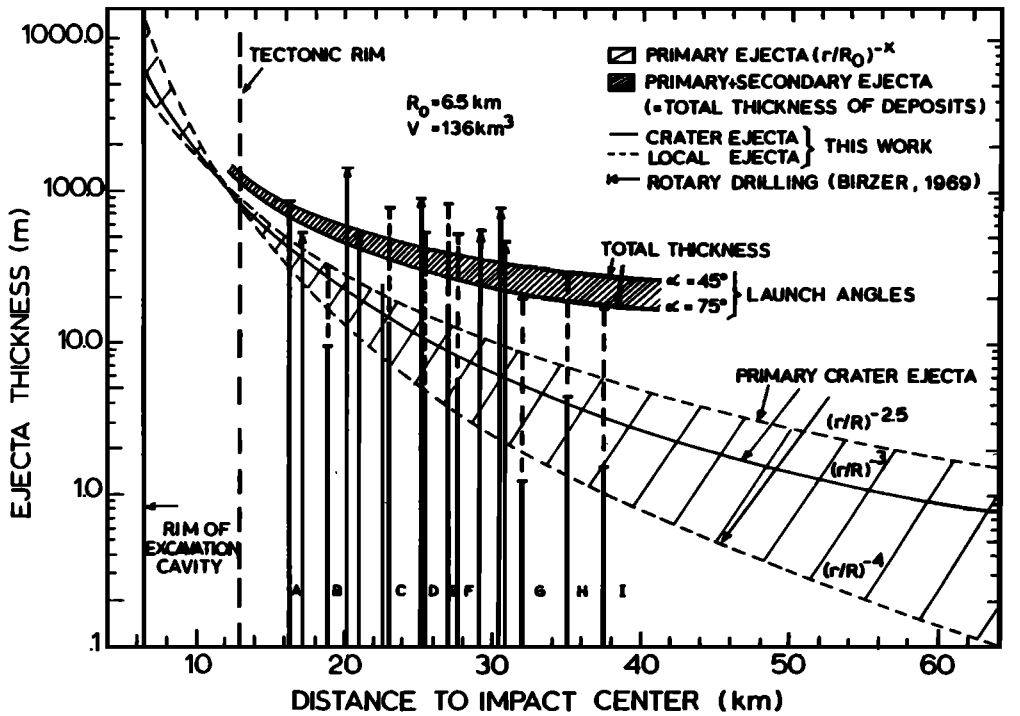

Fig. 35. Predicted ejecta thicknesses in the Ries crater according to various ejecta decay models and comparison with observations. The field of predicted primary ejecta (wide hatching) is contrasted with that of predicted total ejecta thickness including locally excavated substrate materials (narrow hatching). These distributions assume an excavation cavity of radius R_0 = 6.5 km and a total primary ejecta volume of 136 km^3. Vertical lines capped by a bar only represent our cores, subdivided into total primary ejecta (solid lines) and local materials (dashed lines); these thicknesses were calculated from relative volume percent of clasts and matrix for each core. Thin vertical lines with arrows indicate depth of total Bunte Breccia according to rotary drilling by *Birzer* [1969].

flects the present-day situation; considering that some poorly defined erosion took place during the past 15 m.y., the field values may be considered minimum numbers, but then they were frequently obtained from local topographic highs (see appendices A and B) where initial depth may have been unusually deep. Also plotted in Figure 35 are total thickness of Bunte Breccia revealed by other drilling operations, mostly by *Birzer* [1969]. *Homilius and Schmidt-Kaler* [1979] find typical Bunte Breccia thicknesses of 50–100 m at ranges of 15–30 km (not plotted) via geoelectrical sounding techniques.

Provided that R_0 = 6.5 km and V = 136 km^3 are reasonable estimates for the Ries crater, the absolute thickness of Bunte Breccia appears incompatible with any of the above decay models for primary crater ejecta alone; the measured, great thicknesses mandate addition of (locally derived) materials as predicted by the ballistic emplacement scenario of Oberbeck and co-workers. The total Bunte Breccia thickness alone is therefore already in strong support of significant secondary cratering action and excavation.

Figure 36 illustrates the normalized distribution of the total primary ejecta mass in cumulative fashion; it thus

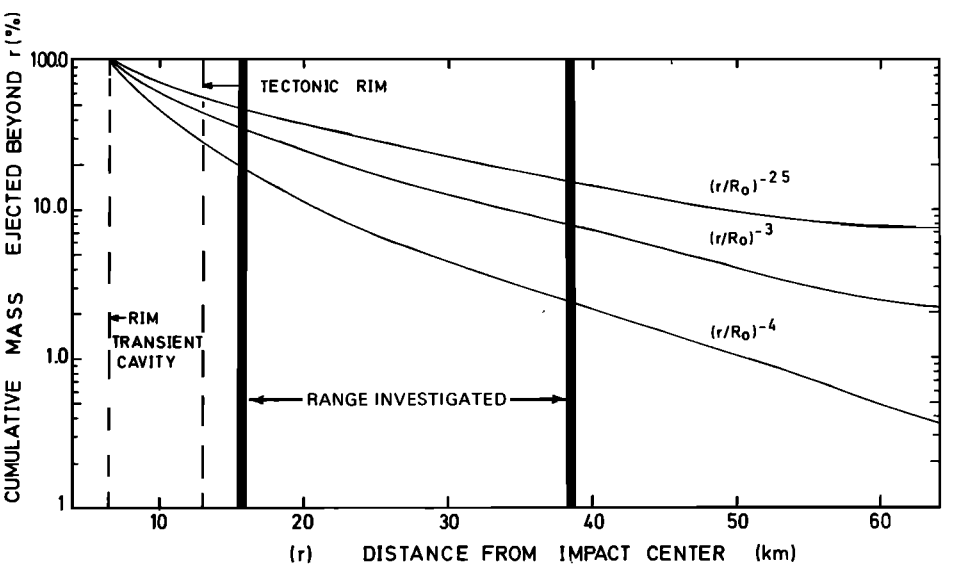

Fig. 36. Cumulative mass distribution for primary Ries ejecta as a function of radial range and according to different ejecta decay models.

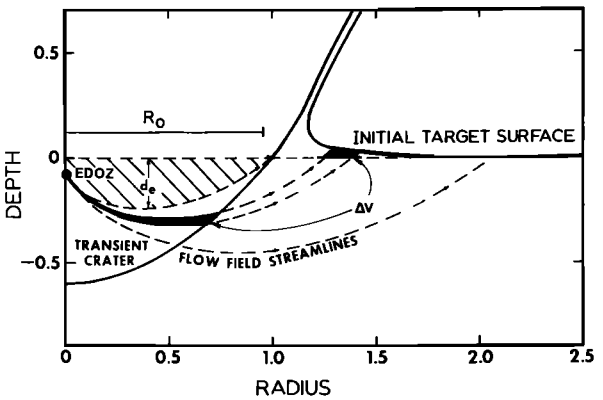

Fig. 37. Principal features of the Z model according to *Maxwell* [1977], *Orphal* [1977], and *Croft* [1980] (modified after *Croft* [1980]).

reflects the fraction of ejecta deposited beyond any range r according to various exponents x in the $(r/R_0)^{-x}$ formulation. Since our core observations are considered to be representative from r = 16.5 to r = 37.5 km, it is possible (1) to calculate the fractional mass of crater ejecta deposited within this well-defined annulus relative to total ejecta mass and (2) to compare this predicted mass with the observed ejecta mass. Using equation (10*a*), one obtains a total of 52 km^3 primary crater ejecta deposited between 16 and 38 km radial range. This volume may be considered an "observed" value. From Figure 36 we obtain that approximately 45% (x = 2.5), 33% (x = 3), and 17% (x = 4) of all crater ejecta were deposited at ranges of >16.0 km; furthermore, 16%, 8.5%, and 2.8%, respectively, were deposited at distances of >38 km. The fractions of primary ejecta residing within the range investigated thus correspond to 29% (x = 2.5), 24.5% (x = 3), and 14.2% (x = 4) of the total primary ejecta. Equating 52 km^3 to these mass fractions, one obtains total primary ejecta volumes of 179 km^3, 212 km^3, and 366 km^3, respectively. All of these values appear, as we will see, in conflict with geophysical investigations and the mass estimates presented in Table 1.

The above estimates critically depend on the somewhat anomalous core A, which alone yielded approximately 46% of all crater materials. Exclusion of core A would reduce the above volume estimates by as much as a factor of 2. Further, these calculations also assume centrosymmetric ejecta distribution, while in fact the ejecta to the south (i.e., where drilled) may have been more massive than ejecta to the north according to *Gall et al.* [1975]. Gall et al. observe that the highest stratigraphic members of Upper Jurassic (i.e., Malm zeta) are found only in the southern ejecta but not in the (few) northerly occurrences of Bunte Breccia. As noted earlier, absolute ejecta mass most likely was affected by a prominent escarpment of Upper Jurassic cutting through the Ries target (see Figures 2–4); it is almost certain that this mass asymmetry of the initial target caused more voluminous ejecta to be deposited to the south. Last, the cores were located such that long profiles could be expected, i.e., on top of topographic highs. It is uncertain whether these ridges introduce bias toward seemingly thick deposits (see also Figure 35).

We had hoped to use the "observed" total volume of crater ejecta deposited within a specific radial range as a new parameter to constrain the estimates of total ejecta volume. This approach, although valid in principle, failed, owing to the nature of the data (core A? topographic highs?) as well as a number of poorly constrained model assumptions (exponent x; centrosymmetry). Thus the total volume of primary Ries ejecta, and therefore the Ries excavation cavity, remains poorly defined via this new approach; more reliable volume estimates continue to rest, predominantly, on geophysical exploration.

Excavation Cavity

We will now consider the excavation cavity of the Ries on the basis of geophysical evidence. Following *Pohl et al.* [1977], the minimum volume excavated is 120 km^3, the maximum is 200 km^3, and the most probable value is 150 km^3. These estimates are derived as follows: the present morphological cavity constitutes 84 km^3; to this, one has to add the volume of the present freshwater lake sediments (28 km^3), i.e., crater fill (which is known from geophysical exploration), and the volume of suevite (7 km^3) inside the inner ring (also known from geophysical studies). These considerations yield a minimum volume of 120 km^3. The most reasonable estimates based on geophysical constraints are 120 km^3 of sediments and 30–45 km^3 of crystalline basement (see *Pohl et al.* [1977] and Table 1); thus a total volume of about 150 km^3 results. Although some of these estimates are modestly model-dependent, we consider them more reliable than our estimates presented above via Figure 36; our "best estimates" presented in Table 1 are heavily influenced by these geophysical constraints. We will now apply these estimates to define, hopefully, the geometry of the Ries excavation cavity.

Detailed understanding of the physical processes during large-scale cratering is still fragmentary. The so-called "Z model" [*Maxwell*, 1973, 1977] has recently become popular in describing specific aspects of mass movement during large-scale cratering [e.g., *Orphal*, 1977; *Croft*, 1980, 1981; *Grieve*, 1980; *Grieve et al.*, 1981; *Stöffler*, 1981]. *Pohl et al.* [1977] and *Pohl and Gall* [1977] applied this model to the Ries with emphasis on chronologic sequences of crater growth and ejection dynamics; the Z model appears to give reasonable insight into these processes and yielded results that appear to be consistent with field evidence, where testable.

The salient features of Maxwell's Z model are as follows: the mass movement during impact and explosive cratering may be described by streamlines of the general form

$$1 - \cos \alpha = (1 - \cos \alpha_0)(R/R_0)^{Z-2} \qquad (15)$$

where α_0 and R_0 are the unit radial direction and distance, respectively, from the geometric center of flow and α and R are the radial direction and distance at any given point within this flow field. When plotted in spherical coordinates, the entire cratering flow field may be described. *Croft* [1980] applied these principles and suggested the following processes schematically illustrated in Figure 37: there is one streamline that cuts through the original target surface with velocity V_e, sufficient to cause ballistic ejection. All materials above this streamline will leave the crater with $V > V_e$, that is, will become genuine, ballistic ejecta; all materials below this critical streamline have $V < V_e$ and will be displaced only, without becoming airborne. Therefore this critical streamline separates an "excavation" cavity (ballistic regime) from those materials that suffer horizontal and vertical displace-

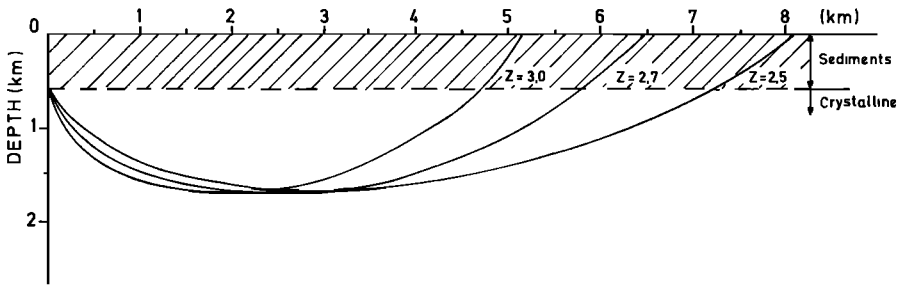

Fig. 38. Principal geometries of potential Ries excavation cavities for constant EDOZ (600 m), various Z values, and constant depth of excavation, d_c = 1650 m.

ment only. This displacement is accommodated by significant uplift of the rim area; for example, the volume contained between a discrete pair of streamlines corresponds to some uplifted volume in the rim region. Following this displacement a temporary "transient" cavity is formed which differs significantly in geometry from that of the excavation cavity. The significant volume contained in the uplifted rim region is gravitationally unstable and will slide back into the cavity, thereby forming a final crater morphology typical for large, fresh impact structures.

In detail there is uncertainty in this formalism regarding the exponent Z; it is assumed to change with time [*Austin et al.*, 1981] from values as small as 2 in the very early stages of cratering to values of >3 in the very late stages. Inasmuch as the exponent Z entirely controls the curvature of the streamlines (see, for example, *Maxwell* [1977] and *Orphal* [1977]), variable Z also implies variable take off angles for ballistic ejecta. *Croft* [1980] and others suggest an average Z = 2.7 that adequately appears to describe the major mass movement in an explosion crater, an experimental impact crater, and at Meteor Crater, Arizona.

Another uncertainty is the exact vertical position of the flow center (EDOZ in Figure 37). In its pure form the formalism proposed by *Maxwell* [1973, 1977] places EDOZ at the very target surface, appropriate for some explosive cratering. Theoretical investigations [e.g., *Croft*, 1980, 1981; *Austin et al.*, 1981] suggest for impact cratering a burial depth of EDOZ approximately of the order of one projectile diameter.

Following *Croft* [1980, 1981], one of the particularly appealing features of the Z model is the fact that it results in a rather shallow excavation cavity within which all of the ejecta originate as opposed to a much deeper transient cavity that is generated by vertical (downward) and lateral displacement of target materials. Also, the clear distinction between "excavation" and "transient" cavity seems to accommodate some important aspects of large-scale cratering, for example, the well-known size-dependent dichotomy be-

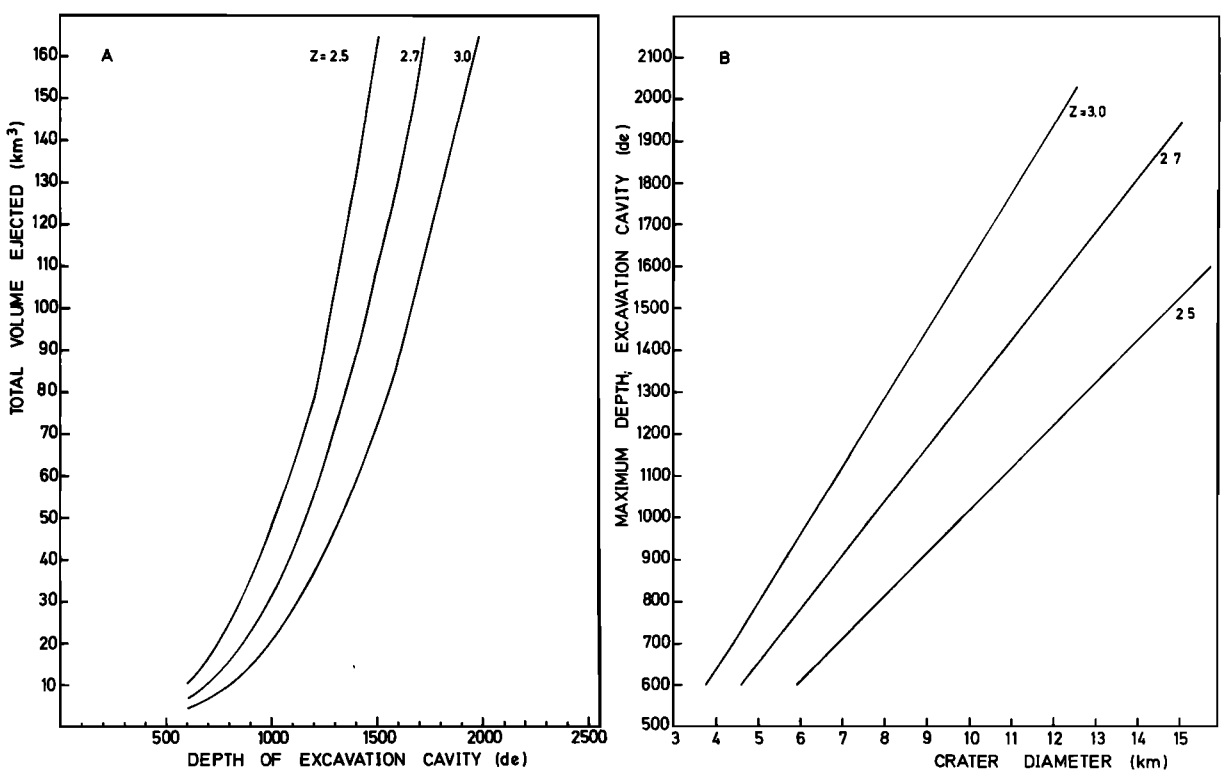

Fig. 39. Consequences of various Z values on total crater volume, maximum excavation depth, and associated crater diameters. (*a*) The relationship of total excavation volume and depth of excavation cavity. (*b*) The relationship of crater diameter and excavation depth.

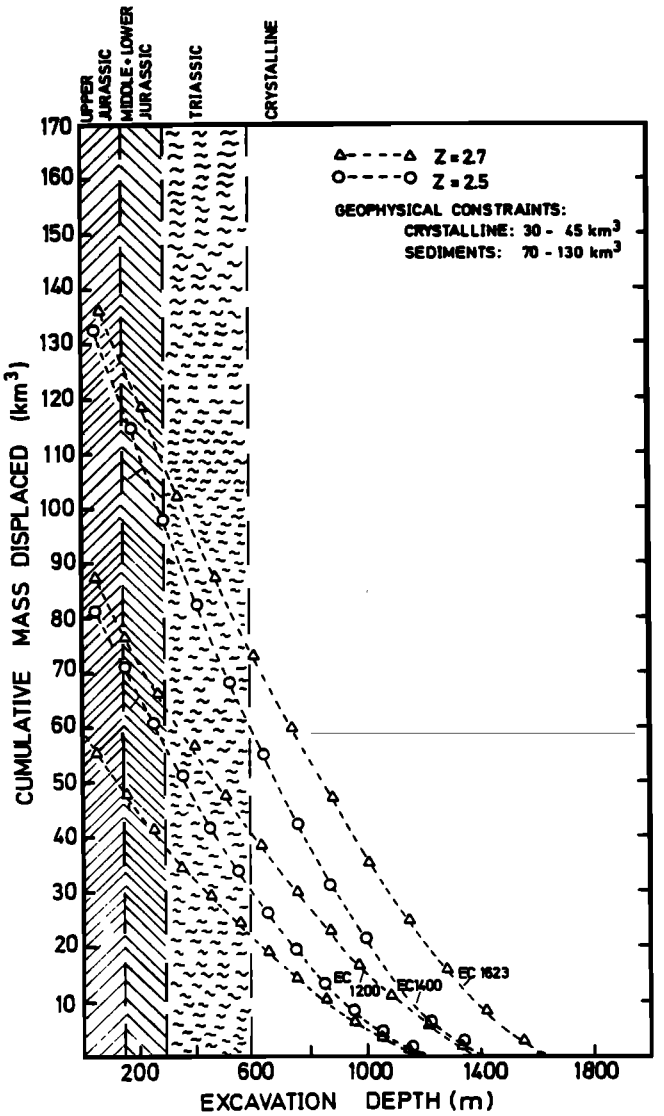

Fig. 40. Potential consequences for modal stratigraphic makeup of ejecta and total excavation volume of the Ries using various model excavation cavities.

tween bowl-shaped, small craters and relatively flat, complex structures [e.g., *Dence et al.*, 1977; *Pike*, 1977], the latter being formed in response to the dynamic and gravitational adjustment of the transient cavity. The Z model also readily explains the sizable vertical uplift of target strata contained in some central peaks [e.g., *Grieve et al.*, 1981].

In the following discussion we will consult Maxwell's Z model with particular emphasis on the possible geometry of the Ries excavation cavity . The idea here is to refine the geometry of this cavity by a unique constraint: the relative proportions of crystalline basement (20–30%) and sedimentary ejecta (70–80%) are fairly well known, and the contact of crystalline basement and sedimentary sequence was approximately 600 m below the original target surface. Thus a horizontal datum of known target depth exists, and it is known approximately how much ejecta originated from above and below this plane. Although our Bunte Breccia studies do not directly relate to the "modal" composition of an excavation cavity, the exceedingly rare crystalline clasts encountered in the continuous deposits also seem to argue that the crystalline basement was not an overwhelming member of the excavation cavity. Thus the new ejecta analyses are consistent with and substantiate the fact that the crystalline basement can only be but a small fraction of the excavation cavity.

Figure 38 illustrates the principal geometry of three model excavation cavities for the Ries based on an average Z of 2.5, 2.7, and 3.0. The cavities use a constant EDOZ at −600 m from the original target surface and are normalized to a constant maximum depth of excavation of 1650 m. It is readily apparent that the proper choice of Z will have a sizable effect on total excavation volume as well as on the ratio of crystalline and sedimentary ejecta.

The principal streamlines illustrated in Figure 38 may be geometrically scaled with regard to excavation depth d_e, crater radius R_0, or volume V_0. Some consequences are illustrated in Figure 39*a*, where we varied excavation depth d_e and then solved for total ejecta volume using Z = 2.5, 2.7, and 3.0. Correspondingly, Figure 39*b* illustrates excavation depths and associated crater diameters (2 R_0).

By combining Figures 38 and 39 we constructed Figure 40: it depicts the cumulative mass ejected during the Ries event from below any absolute depth for a select number of model excavation cavities. We will now take Figures 38–40 to explore which excavation cavity appears to fit the observational constraints best. The following constraints apply:

1. The total volume of ejecta, V_E, is between 125 and 200 km^3; the preferred value is 150 km^3 [from *Pohl et al.*, 1977].
2. The radius of the excavation cavity has to be >6 km, the radius of the present-day inner ring (see Figure 5).
3. The material excavated from the crystalline basement (i.e., from below the −600-m line) is 20–30% of the total ejecta [from *Pohl et al.*, 1977].

Let us first consider the constraint imposed by observed total ejecta volume (Figure 39*a*): for V_E = 125 km^3 one obtains d_e of 1280 m (Z = 2.5), 1570 m (Z = 2.7), and 1880 m (Z = 3). Corresponding values for V_E = 150 km^3 are d_e = 1460, 1670, and 1910 m, respectively, while for V_E = 200 km the excavation depths become unreasonably deep (as we will discuss via Figure 39*b*). The second observational constraint, i.e., 2 $R_0 \geq$ 12 km (Figure 39*b*), yields excavation depths of 1225 m (Z = 2.5), 1560 m (Z = 2.7), and 1940 m (Z = 3.0). The third observational constraint, i.e., the ratio of crystalline to sedimentary ejecta, provides a powerful boundary condition as illustrated in Figure 40: the observed 30–45 km^3 of crystalline material is typically associated with only 80–90 km^3 of total ejecta (e.g., an excavation depth of 1200 m and Z = 2.5 yields 32 km^3 of crystalline material but only 82 km^3 of total ejecta; the associated crater radius would be R_0 = 5.4 km, i.e., too small a diameter). Increasing the total volume to 130–140 km^3 would imply 62 km^3 of crystalline material (Z = 2.5, d_e = 1400 m, R_0 = 6.8 km) or 73 km^3 of crystalline material (Z = 2.7, d_e = 1625, R_0 = 6 km) and thereby approach or exceed a 1:1 ratio of crystalline to sedimentary ejecta. It is for this reason that we did not plot examples of Z = 3 in Figure 40; they would generate an intolerable ratio of crystalline versus sedimentary ejecta for reasonable choices of V_E or R_0.

Interestingly, *Engelhardt and Graup* [1981] use a completely different approach to calculate various Ries volumes, and yet their results are in good agreement with the above Z modeling. Their analysis follows the suggestions of *Kieffer and Simonds* [1980], which in turn are largely based on work by *Gault and Heitowit* [1963]. *Engelhardt and Graup* [1981]

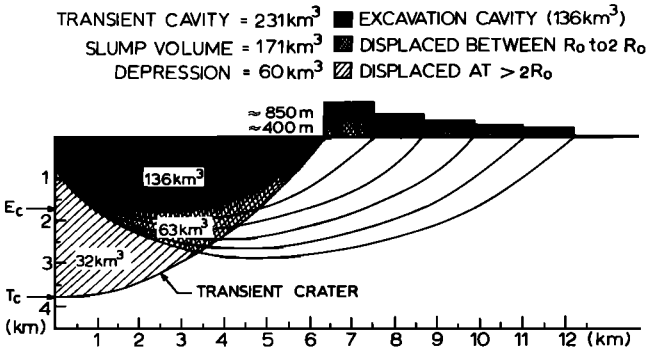

Fig. 41. Reconstruction of mass transport during the Ries event following a $Z = 2.7$ event. Note the difference in excavation and transient crater cavities. The suggestions by *Croft* [1980] were used in reconstructing the various volumes for uplifted and excavated materials.

constrain their calculations primarily via petrographic observations related to the absolute abundance of specific shock levels in crystalline rocks (from suevites, crystalline breccias, etc.). They calculate a pressure attenuation rate of $R^{-4.2}$ in the near field [see *Kieffer and Simonds*, 1980] and R^{-3} in the far field; having determined these attenuation rates, they generate an excavation cavity that experienced 25 GPa at its bottom (vertical axis of symmetry) and I GPa at its rim. A crater geometry akin to the above Z models results. Specifically, *Engelhardt and Graup* [1981] derive a total of 138 km^3 of ejecta, approximately divided 1:1 between crystalline basement (70 km^3) and sedimentary strata (68 km^3).

Thus, in a strict sense, the Z model as well as the approach suggested by *Kieffer and Simonds* [1980] appears to yield too much crystalline material. The geophysical constraints seem to be firm and the measured mass deficit [*Pohl et al.*, 1977] will not allow more than 45 km^3 of ejecta from below 600 m. We have thus tested the Z model within what are presently considered reasonable assumptions regarding the proper choice of Z and the absolute depth of EDOZ. It is possible, in principle, to design yet shallower transient cavities by assuming $Z < 2.5$ or by placing EDOZ closer to the surface, thus yielding better fits with the observations. But selection of these variables is not arbitrary. The present discrepancy between theory and observation most likely stems from the fact that the Ries target is not a homogeneous medium as is implicitly assumed in the model. The layered nature of the Ries target is well documented, and the contact between sediments and crystalline basement represents a major discontinuity in rheological properties. This discontinuity may significantly disturb material flow and affect the ratio crystalline/sedimentary ejecta.

Nevertheless, we feel that the Z model is usefully applied to the Ries and that it yielded some important insight. For example, very large total excavation volumes (e.g., >150 km^3) seem to be excluded, because for any reasonable exponent Z the relative proportion of crystalline ejecta will become intolerably large. Conversely, the crater diameter R_0 seems to be limited to <8 km, because the total displaced crystalline material will be too high (>50 km^3) and/or total ejecta volume becomes unrealistic (>200 km^3).

Transient Cavity

We consider it instructive to pursue some additional consequences of the Z model relating to the transient cavity of the Ries. Specifically, we wish to address the question of mass movement in the area below the excavation cavity and its consequences with regard to the 26-km-diameter "tectonic" rim.

Recall that the geometries of "transient" and "excavation" cavities differ dramatically (see Figure 37). Following *Croft* [1980], we have illustrated the Ries situation in Figure 41 for $Z = 2.7$. Streamlines are drawn that intersect the surface at 1.0, 1.2, 1.4, 1.6, 1.8 and 2.0 R_0, thus engulfing the masses uplifted (nonballistically) between the 13-km-diameter "inner ring" ($R_0 = 6.5$ km) and the 26-km-diameter tectonic rim ($R_D = 2\ R_0$). The volume contained between specific streamlines was calculated and is illustrated (to scale) as "uplifted" material. Taking an excavation volume of 136 km^3, the volume uplifted between 1 and 2 R_0 is about 63 km^3, and that displaced beyond 2 R_0 is 32 km^3. A transient cavity volume of about 230 km^3 results, of which approximately 60% is ballistically ejected and approximately 40% is merely displaced. The maximum depth of the resulting transient cavity is about 3.8 km. The average rim uplift between 1 and 1.2 R_0 is about 400 m and decreases with increasing radial distance; uplift at 2 R_0, i.e., at the tectonic rim, is still approximately 75 m. The dynamically uplifted material (62 + 32 km^3 = 94 km^3) is gravitationally unstable and should slump back into the transient cavity.

In addition, all ejecta deposited between R_0 and 2 R_0 must suffer slumping also, otherwise we would not have a present-day morphological depression at these radii. The average height of ejecta between 1 and 1.2 R_0 is approximately 450 m, and that at 2 R_0 is still about 90 m, yielding a total volume of ejecta between 1 and 2 R_0 of about 76 km^3 (according to Figure 35 and using $(r/R_0)^{-3}$). Adding the total volume of "displaced" materials (about 95 km^3) and the ejecta (76 km^3) between R_0 and 2 R_0, one obtains 171 km^3. This huge mass is gravitationally unstable and potentially involved in backfilling the transient cavity. A total volume deficit of about 60 km^3 for the entire Ries depression would result if the above mass (171 km^3) would quantitatively slide into the transient cavity (230 km^3). This calculated volume of the entire Ries depression (60 km^3) compares to 84 km^3 measured from present-day topographic analysis [*Pohl et al.*, 1977]. Significant slumping may have occurred only inside the present-day morphological crater rim, which has an average diameter of 24 km, and one may therefore subtract from the above ejecta volume about 6 km^3 (deposited between 12 and 13 km radius), obtaining then a total Ries depression of about 65 km^3.

In simplified form, these calculations are based on the following reasoning: all materials "uplifted" at radial ranges greater than R_0 are involved in restoring the transient cavity [*Croft*, 1980]. Therefore the total volume of the resulting, permanent depression corresponds only to the volume of all ejecta that reside beyond the morphologic rim, where slumping had ceased. We consider the agreement between observed volume (84 km^3) and calculated volume (about 60–65 km^3) fair. Incidentally, the initial crater radius ($R_0 = 6.5$ km) is also reduced by slumping and tilting of rim blocks to the presently observed value of 6 km for the inner ring.

Importantly, these calculations show that slumping can, if not must, be an important process in the Ries, contrary to *Chao* [1977*a*, *b*], who suggests a depth to diameter ratio for the Ries of 1:30 and minimal slumping on local scales only, if at all. *Dence et al.* [1977] and *Grieve* [1980] delineate slumping processes in large, Canadian craters that yields

apparent crater diameters of 2 R_0; similar conclusions were reached by *Pike* [1977] on the basis of lunar photogeologic studies and by *Croft* [1981]. The scenario depicted in Figure 41 is also compatible with the recent geoelectric sounding results of *Hüttner et al.* [1980], who inferred both relative outward movement of cubic kilometer sized blocks in the vicinity of the morphological Ries rim (radial motion while the area is being uplifted) and relative inward motion (while the material subsides).

All suevites at $r > 6$ km possess aerodynamically shaped melt bombs and are essentially identical otherwise; all suevites at $r < 6$ km, i.e., those lining the crater walls inside the initial R_0, do not possess aerodynamically shaped bombs and also contain relatively small amounts of melt [*Stöffler*, 1977]. These observations serve to demonstrate that genuine ballistic ejecta may be encountered inside the present-day morphological rim, and they strongly support our view that the megablock zone is partly made up of ballistic ejecta. Since these ballistic ejecta occur within the morphologic crater depression, i.e., at elevations below the level of the initial target surface, the conclusion appears inescapable that slumping must have been a major process, involving both ballistically and nonballistically displaced material.

Some additional comments regarding the transient cavity depicted in Figure 41 may be offered: seismic investigations indicate severely disturbed basement to depths of 5–6 km [*Pohl et al.*, 1977] (see also Figure 5). This again is taken as evidence for a relatively deep transient cavity as already postulated by *Pohl et al.* [1977]. Our present depth (3.8 km) is compatible with these seismic observations. An important aspect of the Z model is the fact that materials close to the impact point are driven downward and that a corresponding volume is displaced at some radial distance at the surface. This allows some Ries suevite generated at, say, 1000 m depth to be transported temporarily to a depth of >3 km, where it will line the growing cavity walls. By definition, this material will not leave the cavity, but instead it will form a suevite lens or injection dikes in the crystalline masses during restoration of the transient cavity. Some suevite (breccia) dikes may also be injected into the wall rocks during growth of the transient cavity [*Lambert*, 1981]. Such features are abundantly observed in a 1200-m drill core (Forschungsbohrung Nördlingen, 1973 [*Schmidt-Kaler*, 1977]). The Z model approach provides a natural answer to such dikes, now found at great depth (>1 km) relative to the restored crater.

Principally, the Z model also provides a good framework for understanding the occurrence of large amounts of suevite inside the morphologic crater cavity or impact melt in general [e.g., *Grieve*, 1980; *Stöffler*, 1977]. Inasmuch as suevite (impact melt) experienced demonstrably the highest peak pressures of all crater materials (excepting gaseous impact products), it should also have received the highest shock accelerations. Such materials, however, are typically concentrated inside the cavity or in the rim vicinity. Consulting the Z model (e.g., Figure 37 or 38), it follows that the critical streamline (at R_0) must pass through the target volume that is molten; parts of that volume reside above the critical streamline (and will be ejected), while others are below and will remain in the crater cavity. During their transport inside the crater cavity (regardless of whether they get ejected or not), these hot materials have ample opportunity to be mixed and mingled with materials from the temporary crater bottom and walls, thereby incorporating diverse mineral and lithic detritus, so typical for impact melts, and/or clasts of diverse shock histories, because the streamlines cut across isobars of the initial shock wave.

Summary

Despite extensive field investigations by generations of Ries geologists, important, first-order information regarding total crater volume, absolute excavation depth, total volume of Bunte Breccia, etc., is still poorly understood, unfortunately. Difficulties in obtaining such data relate partly to the variable degree of erosion during the past 15 m.y. and partly to the enormous difficulties in obtaining subsurface information of such detail that reconstruction of an excavation or transient cavity could be attempted with a high degree of confidence. It is difficult enough to characterize the present-day subsurface relationships in an exact fashion [e.g., *Pohl et al.*, 1977]. Thus comparison of field evidence with cratering theory is qualitative at present; within limits, certain observational constraints may be brought to bear. The present work attempted to provide a new constraint: the total amount of crater ejecta deposited between about 16 and 40 km from the impact center. In detail, this datum, however, did not result in a significantly better defined total ejecta volume.

Despite these shortcomings an attempt was made to compare the Ries findings with current cratering models that relate to (1) ejection processes and (2) the geometry of the Ries excavation, and transient cavities. The following results emerged:

1. The total thickness of crater material measured with increasing radial range is compatible with currently proposed primary ejecta decay models, although $(r/R_0)^{-2.5}$ and $(r/R_0)^{-4}$ seem to be bracketing limits; an $(r/R_0)^{-3}$ seems to be reasonable [*McGetchin et al.*, 1973], and so is the recent proposal of variable ejecta decay by *Schultz et al.* [1981].

2. None of the above primary ejecta models, however, adequately predicts the total thickness of Bunte Breccia. Total thickness can only be accomplished by addition of locally excavated materials as suggested by Oberbeck and co-workers.

3. An attempt was made to reconstruct the Ries excavation and transient cavities via the so-called Z model [*Maxwell*, 1973, 1977; *Orphal*, 1977; *Croft*, 1980; *Austin et al.*, 1981]. Average $Z > 2.7$ cannot account for some field observations, especially the low ratio of crystalline to sedimentary ejecta. The discrepancy between observation and theory most likely results from the rheological variability of the Ries target, which is prominently layered. Using $Z = 2.7$ and 136 km^3 total excavation cavity volume, one obtains a maximum excavation depth of about 1600 m and an initial crater radius of $R_0 = 6.5$ km. Initial radii of $R_0 < 5$ km and $R_0 > 8$ km can reasonably be excluded because they would yield not enough or too much excavation volume, respectively, and they would also violate the observed ratio of crystalline to sedimentary ejecta.

4. Additional consequences of an excavation cavity $Z = 2.7$ and $R_0 = 6.5$ km were explored. One calculates a total transient cavity of 230 km^3. Such a model also yields some 95 km^3 of stratigraphically uplifted volume at ranges greater than R_0. Depositing another 76 km^3 of ejecta between R_0 and 2 R_0, i.e., inside the presnt-day tectonic rim, yields a total volume of about 170 km^3 temporarily residing above the

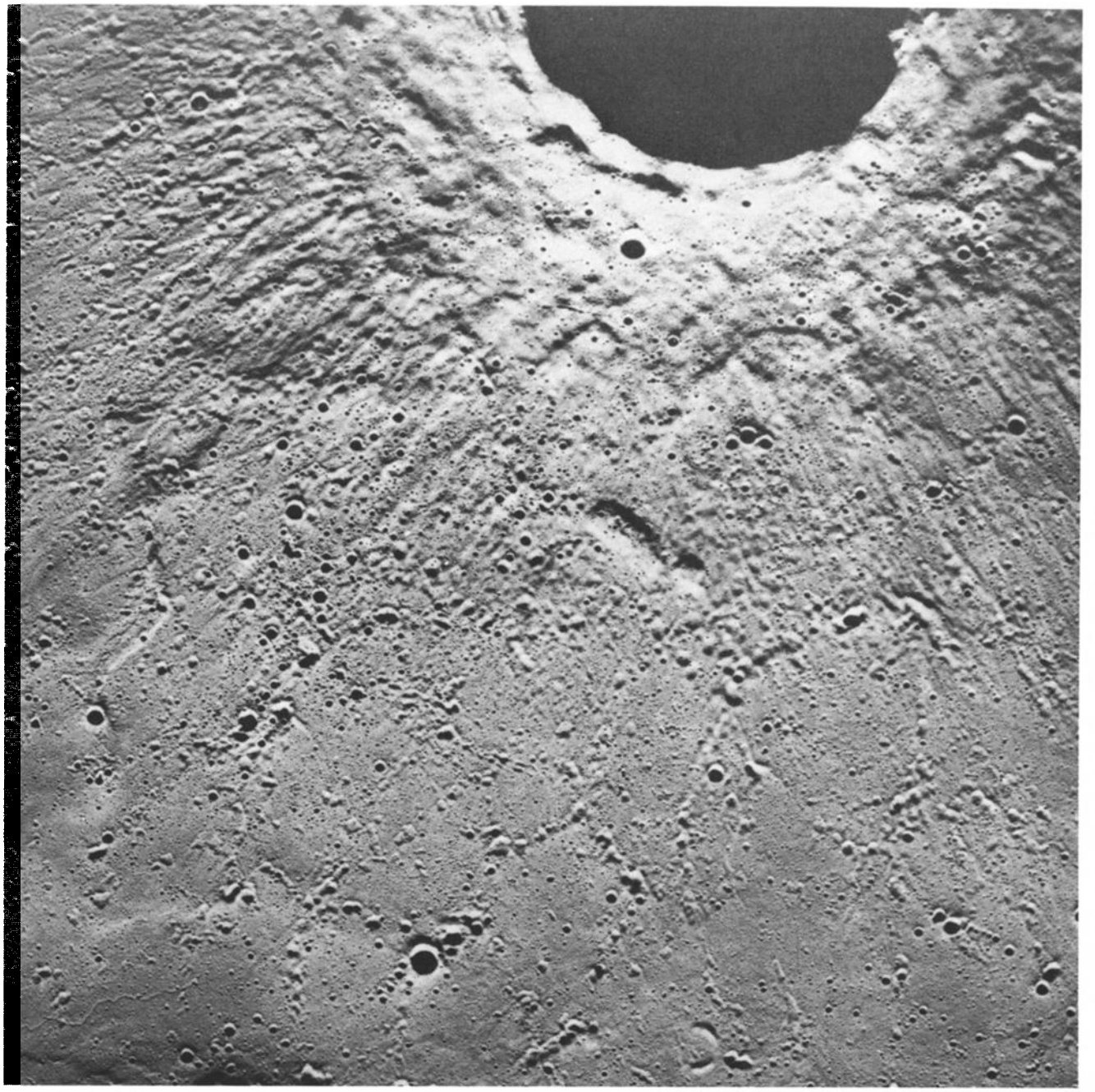

Fig. 42. Fresh lunar crater (Timocharis) surrounded by continuous deposits displaying evidence of secondary cratering and ground-hugging flow.

initial target plane. This volume may slump back into the transient cavity and will contribute to the restoration of this cavity to its more or less present-day configuration. The volume for the resulting topographic depression would be about 65 km^3, which compares reasonably well with the one existing at present (about 84 km^3 [*Pohl et al.*, 1977]). These calculations show that slumping is indeed a major factor in generating the Ries megablock zone.

In conclusion we find qualitative to fair agreement between observations and theory. Discrepancies and disagreements may result both from potential weaknesses in the theoretical approaches and from the somewhat qualitative nature of the observations. Oberbeck's secondary cratering hypothesis and Maxwell's Z modeling provide, however, extremely appealing tools to explain qualitatively a large number of field observations that otherwise and hitherto were not readily understood.

THE DEPOSITION OF BUNTE BRECCIA

The Secondary Cratering Hypothesis

All Bunte Breccia observations are consistent with, if not predicted by, the "secondary cratering" hypothesis as detailed and summarized best by *Oberbeck* [1975] and as applied specifically to the Ries by *Morrison and Oberbeck* [1978]. This hypothesis is based primarily on photogeologic lunar evidence (Figure 42), small-scale laboratory experiments (Figure 43), and diverse considerations regarding cratering mechanics [e.g., *Shoemaker*, 1962; *Oberbeck et*

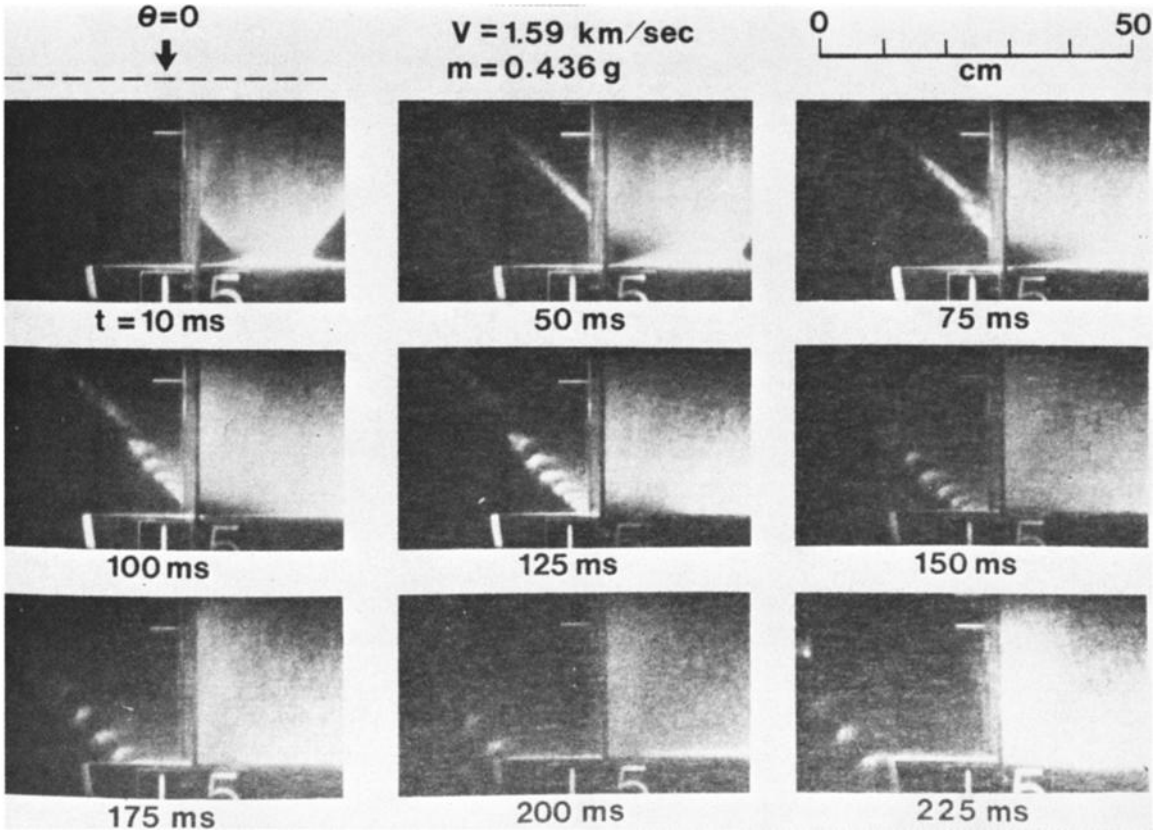

Fig. 43. The development and migration of an ejecta curtain during a small-scale laboratory experiment in quartz sand. Note that the growing ejecta plume (at t = 10 ms) is blocked by a slitted wall so as to allow only a small segment of the plume to pass unaffected; this segment not only shows the relatively thin nature of the ejecta curtain but also illustrates how it moves across the crater's surroundings to drop finally (at t = 225 ms) over the rim of the target bucket. The final crater diameter of this event was approximately 5 cm to the right of the slitted wall [from *Oberbeck and Morrison*, 1976]. (Reprinted by permission of Pergamon Press.)

al., 1974; *Oberbeck*, 1975]. The salient features of this hypothesis are illustrated in Figure 44. Ejecta emanate from the growing crater cavity along discrete ballistic trajectories; individual trajectories differ in takeoff angle as well as velocity, depending on specific fractional volume and its exact position relative to the point of impact. The projection of these discrete trajectories at any specific time t results in an "ejecta curtain," which is a sheetlike concentration of ejecta that expands in a truncated cone geometry. The top of this curtain is formed by relatively fast ejecta with relatively steep takeoff angles, while the lower sections of the curtain contain slow ejecta with rather shallow takeoff angles. This ejecta curtain sweeps across the crater surroundings. Particles contained at the base of the curtain reimpact onto the local substrate with terminal ballistic velocity, and they form secondary craters if they exceed a specific threshold velocity (about 100 m/s [see *Oberbeck*, 1975]). Since these ejecta fragments are closely associated in space and time, the resulting secondary ejecta will overlap and interfinger. Overall momentum of these secondary ejecta masses will be radially away from the crater because ejecta generated during oblique impacts have azimuthally asymmetric mass distributions and they possess a pronounced mass and momentum maximum downrange [*Gault*, 1973; *Oberbeck and Morrison*, 1974]. In the context of the secondary cratering hypothesis this implies that overlapping secondary ejecta will have dominant radial momentum and that primary and secondary ejecta combine into a massive, radial debris surge. It is important, however, to note that substantial masses of secondary ejecta may be expelled over a wide range of azimuthal angles relative to the center of the secondary cavity; unless one approaches extremely oblique trajectories (<15° [e.g., *Oberbeck and Morrison*, 1974; *Gault*, 1973]), a modest fraction of ejecta may even be propelled uprange, i.e., backward toward the parent crater. This diversity of azimuthal takeoff angles will lead to a great variety of collision velocities when ejecta from neighboring secondary craters start overlapping and colliding. Such collisions at vastly different relative velocities, in turn, are conducive for setting up highly turbulent flow regimes. We therefore must envision a turbulent flow with a significant net radial momentum (see Figure 47); this flow is an intimate mixture of primary and secondary ejecta.

Importantly, the primary ejecta curtain traverses the crater environs at essentially the ballistic velocity of its component clasts. The bulk of the secondary ejecta emanate at substantially lower velocities than these terminal ballistic speeds, and therefore the radial flow velocity of the debris surge is small compared to the ballistic velocities of primary ejecta. Therefore secondary crater growth at small radial ranges is well under way while the primary ejecta curtain initiates secondary cratering at large radial ranges. Thus a wide annulus must be envisioned in which secondary ejecta are being produced simultaneously, albeit in systematically different phases of total secondary crater growth. This implies that material is in motion simultaneously over sub-

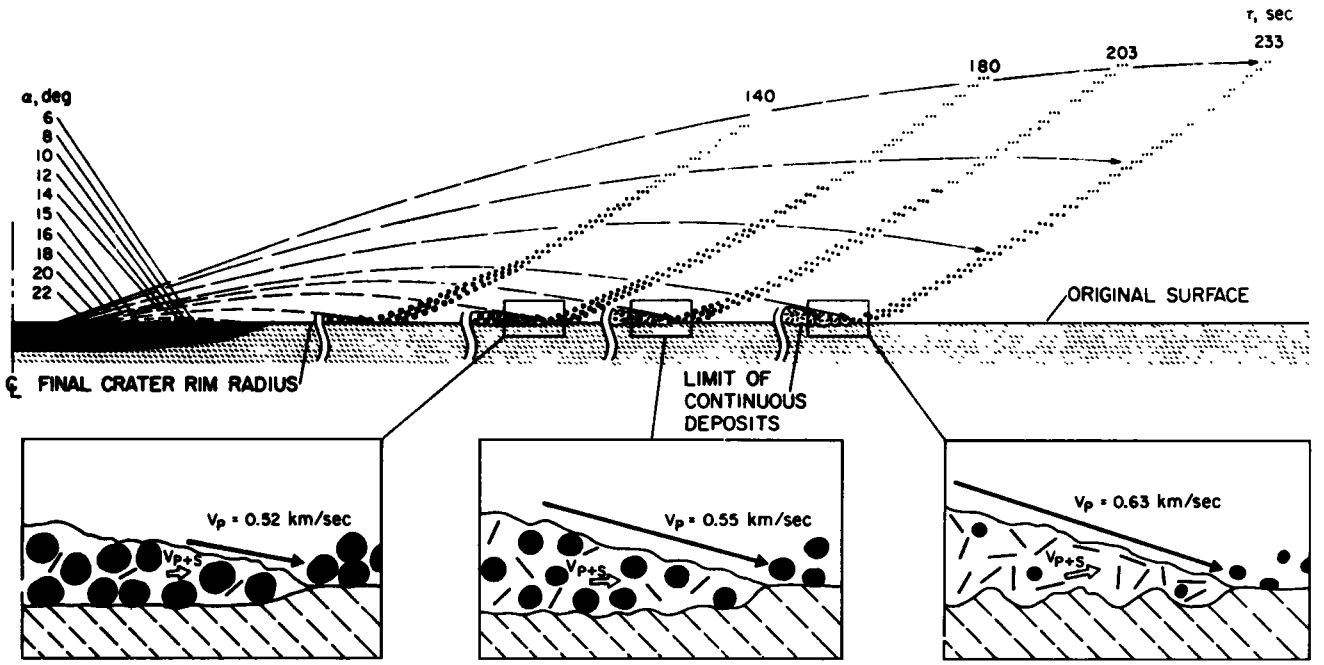

Fig. 44. Principal characteristics of ballistic crater ejecta and their interaction with the surrounding terrain. Note that the projection(s) of individual ballistic trajectories, at any specific time, form the so-called "curtain." Also at any given time the curtain is thickest at the base, which furthermore contains the largest and slowest particles. The inserts illustrate schematically the interaction of this curtain with the local crater environs: primary ejecta (solid symbols) become more fine grained and less abundant with increasing radial range; conversely, more and more local materials will be excavated and incorporated into the resulting debris flow. Note the high velocities of primary ejecta (solid vectors) versus the flow velocity (open vectors) of the ensuing debris surge. Numerical data are applicable to the 90-km-diameter lunar crater Copernicus [from *Oberbeck*, 1975].

stantial fractions of the entire radial range covered by continuous deposits. The debris surge of combined primary and secondary ejecta must be envisioned as one flow regime that is set in motion almost simultaneously at dramatically different ranges, because absolute times for initiating secondary cratering are small compared to total growth time of a specific secondary crater and to the times necessary for an ensuing debris surge to come to a halt.

We have presented in Figures 18, 25, 29, 30, and 35 the most diagnostic features supporting a secondary cratering regime in the Ries, i.e., the incorporation of substantial quantities of local substrate materials. We noted repeatedly that the observed thicknesses of Bunte Breccia are incompatible with any of the current views concerning distribution of primary ejecta alone. Predicted addition of local components [*Morrison and Oberbeck*, 1978] results in fair agreement with observations. We take these arguments as strong evidence that secondary cratering is indeed an important aspect of large-scale impact deposits.

In detail (e.g., equations (10)–(13)) one may argue that observations and predictions do not agree quantitatively (see also Figure 30). Many arguments may be advanced why this is to be expected; some of the major factors are as follows: (1) our statistical sample, i.e., small number of locations, may be inadequate, (2) the basic model has inherent limitations as described by *Oberbeck* [1975] and *Morrison and Oberbeck* [1978], and (3) Upper Jurassic, limestone clasts, "locally" dislodged from the Miocene cliff line (because of the presence of abundant mollusc boreholes), may now be found as far as 10 km from their original location and, incidentally, uplifted some 70 m above the cliff line's elevation [*Gall*, 1969; *Hüttner*, 1958, 1969]. These local tracers attest to mass transport of local components on the scale of one apparent crater radius, indeed very large, horizontal distances. Thus it is very likely that the materials encountered now at any specific radial range were actually produced farther uprange. The secondary cratering model (as well as any other ejecta emplacement model) presently does not account quantitatively for horizontal mass movement during ground-hugging debris flow, and it predicts only the specific mixtures initially generated at any specific range but not how far such a mixture may have been transported.

All in all, we recognize some potential discrepancy between prediction and observation. The potential discrepancy, however, does not overly alarm us, considering the vagaries of the secondary cratering process and the fact that real ejecta are clods and chunks that arrive locally in variable concentrations, thus causing considerable local variance. Considering that there is fundamental debate whether ballistic ejecta emplacement exists at all [*Chao*, 1977*a*, *b*] and whether incorporation of local materials is a geologically significant process [*Wilhelms*, 1981; *Schultz*, 1981], the observed agreement with predictions and observations for the Ries crater is highly significant and is exceedingly strong support for the ejecta emplacement scenarios developed by Oberbeck and co-workers.

We alluded in the core descriptions to a wide variety of deformational styles; and we have emphasized throughout this review the enormous variability of most parameters measured, i.e., the chaotic nature of the Bunte Breccia deposit. This, we feel, is also a natural consequence of secondary cratering. The variety of deformational styles observed in close juxtaposition requires highly variable, small-scale differences in deformational energy. We inter-



Fig. 45. Contact relationship of Bunte Breccia (bottom) and suevite (top) at the Otting quarry (courtesy of R. Hüttner). The hammer is at the exact contact; the bottom surface (to the right of the hammer) of the suevite is relatively competent because it is sintered; the Bunte Breccia remains unconsolidated. The contact surface dips steeply (about 50°), with suevite draping a freshly generated relief of the Bunte Breccia; this relief is typically on the order of a few meters, although it may occasionally approach some 20–30 m (e.g., Altenbürg quarry).

pret these features as signs of vastly different collision velocities of overlapping and interfingering secondary crater ejecta plumes, initiating turbulent motion but preserving radial momentum of the debris surge.

Further, the enormous variability of distinct polymict breccia types also requires conditions of formation compatible with, if not indicative of, secondary cratering action. Each breccia type requires its own, small-scale geologic environment of a rather specific mix. For example, matrices typically are mixtures of various OMM and OSM sediments, although occasionally one finds a matrix that may be pure OSM or OMM. This indicates that polymict breccia types were formed initially at distinctly (or subtly) different locations and subsequently transported to a common, final resting place. Additional mixing may have occurred, of course, during the ensuing turbulent debris surge, however, on sufficiently limited scales to prevent complete matrix homogenization. Considering the frequent facies changes of OSM and OMM on horizontal scales of <1 km and vertical scales of <10 m, such highly variable polymict breccias are the natural consequence of secondary cratering, each secondary crater cavity containing its own, specific mix of local and crater-derived materials.

The above observations can be rephrased: the Bunte Breccia does not possess at all a homogeneous "matrix." Instead, Bunte Breccia consists of a mixture of discrete, monolithic megaclasts and discrete volumes ("clasts") of specific polymict breccia types. On the linear scales observable in core profile the absolute dimensions (length) of polymict breccia sections are essentially the same as those of monolithic megaclasts, i.e., typically 1–5 m. The entire deposit must therefore be viewed as a mixture of monomict and polymict clasts. Bunte Breccia does not have a uniform matrix sensu stricto; it appears to be a mixture of discrete clasts.

Before concluding this section we estimate the absolute time necessary to deposit the entire Bunte Breccia. A field detail provides the crucial constraint [e.g., *Hüttner*, 1969]: where exposed, the suevite always rests on top of the Bunte Breccia; no exception to this rule is known in the Ries, thus demonstrating that suevite was universally deposited last. Most important, the contact between suevite and Bunte Breccia is stunningly, knife-edge sharp (Figure 45). "Mixing" of Bunte Breccia into the suevite is not observed. These contact relationships mandate a pronounced depositional hiatus. They also mandate that emplacement of the Bunte Breccia was completely terminated while suevite was still being transported (either in the crater cavity or in midair).

Using data of *Maxwell* [1977] and according also to *Pohl and Gall* [1977], the time required for the ejecta curtain to detach itself from the rim of a 13-km-diameter crater is of the order of 1 min ($T \approx 1$ min). Conservative ejection velocities for Ries ejecta traveling to $r > 40$ km are of the order of 500 m/s (see also *Morrison and Oberbeck* [1978]). This implies approximately one additional minute for secondary cratering action to commence at distal ranges ($T \approx 2$ min). Net flow velocity of the debris surge, V_s, is unknown but is significantly less than the ballistic velocity, e.g., about 100 m/s [*Oberbeck*, 1975]. The pholade-studded limestone clasts from the Miocene cliff line indicate flow distances as much as 10 km. For $d = 10$ km and $V_s = 100$ m/s one calculates an additional 2 min for the duration of such a flow ($T \approx 4$ min). Thus total emplacement times for the entire Bunte Breccia deposit must be of the order of a few minutes only. Clearly, these are crude estimates. The abundantly observed hiatus between suevite and Bunte Breccia provides the most powerful argument for extremely short absolute emplacement times for Bunte Breccia: Bunte Breccia was entirely emplaced with suevite still in "midair." Time scales of the order of minutes must be invoked.

Other Emplacement Scenarios

Taking the total evidence presented here, we maintain that the ballistic hypothesis adequately predicts some and most certainly accounts for all Bunte Breccia observations. In the following paragraphs we will discuss the major scenarios suggested against ballistic ejecta emplacement.

We will first turn to the nonballistic emplacement mechanism of *Chao* [1977*a*, *b*; *Chao et al.*, 1978]. After first subscribing to the existence of ballistic ejecta, but questioning the efficiency of secondary cratering [*Chao*, 1974], Chao now maintains that a ground-hugging flow of primary crater ejecta emanates at the crater rim and subsequently spills across the crater surroundings. The principal evidence for this view is derived from heavily striated Bunte Breccia components [*Chao*, 1976] from striated Upper Jurassic "substrate" surfaces [*Wagner*, 1964; *Chao*, 1977*a*] and from the basal mixing zone observed at the Guldesmühle outcrop [*Chao*, 1977*a*].

Core F reveals specifically that the Guldesmühle outcrop must be interpreted differently (see appendixes A and B). Our Bunte Breccia cores demonstrate that a universal, basal mixing zone does not exist in the Ries. Chao's generalizations of the Guldesmühle outcrop are incorrect for the entire Ries.

The considerable number of careful observations related to striation and deformation of Bunte Breccia components accumulated by Chao do indeed vividly attest to relative motion of a ground-hugging debris surge. In all of these observations we cannot, however, see evidence pertaining to the crucial question: how was this flow generated? The postulate, that the flow is primary ejecta emanating nonballistically out of the crater cavity, is an ad hoc assumption, and it completely neglects the existence of a debris surge following secondary cratering. In our view, Chao's observations pertain to and are consistent with a massive debris flow constituting the last phase of a ballistic emplacement scenario. It is this last phase that dominates many present-day field relations, including the observations of Chao.

Fundamental arguments against Chao's nonballistic emplacement may now be advanced, because the magnitude of interaction with the local substrate is quantified. Any primary flow emanating from the Ries cavity in a nonballistic fashion must rapidly dissipate energy if it is to interact with the substrate to depths now measured in tens of meters. This view is certainly valid if interaction with the substrate is by frictional forces only, an assumption on our part, because *Chao* [1977*a*, *b*] does not specify the detailed mechanism by which local substrate materials are dislodged. We find it difficult to "excavate" equivalent or multiple volumes of local materials via frictional forces of a "primary" debris surge. The fact that increasingly more local materials are excavated with progressive radial range argues conclusively that the specific kinetic energy per unit mass of primary ejecta increases with increasing r; this is not possible for any primary debris flow emanating from $r = R_0$; such a flow must progressively dissipate energy. Another fundamental argument against nonballistic ejecta transport is never addressed by *Chao* [1977*a*, *b*]: how can ejecta leave a crater cavity without becoming airborne? Launch velocities must be measured in hundreds of meters per second to reach radial ranges of 40 km; launch angles cannot be 0° if the materials move along the growing cavity walls. Such materials become airborne, as evidenced by secondary crater fields observed around fresh planetary impact structures.

We now turn to those viewpoints that principally subscribe to ballistic ejecta and that differ, however, with the specific predictions of Oberbeck and co-workers regarding the relative amount of local versus crater-derived materials. *Schultz et al.* [1980] and *Schultz* [1981] maintain that *Oberbeck* [1975] and *Morrison and Oberbeck* [1978] systematically overestimate the local contributions. On the basis of laboratory experiments using extended projectiles that yield relatively shallow craters, Schultz and co-workers maintain that Oberbeck generates too much secondary ejecta per unit mass of primary projectiles; the systematic error may be of the order of a factor 10 and thus, indeed, of serious geologic consequence. While some refinement of the mixing calculations of *Morrison and Oberbeck* [1978] is, of course, possible along the lines suggested by Schultz, we feel that Morrison and Oberbeck are correct within a factor of 2; an order of magnitude correction, as proposed by *Schultz* [1981], is not warranted because the amount of local substrate material incorporated into the Bunte Breccia is in essential agreement with data of Oberbeck and co-workers. We do, however, fully subscribe to *Schultz'* [1981] assertion that because of local vagaries of the ejection process and secondary cratering action, one may encounter local areas enriched (and conversely also depleted) in primary crater ejecta. This is observed abundantly in the Ries in the form of rays [e.g., *Graup*, 1978] and indeed is not surprising, much less detrimental to the general predictions of the ballistic model that only addresses idealized, "average" conditions.

Continuous Deposits and Target Stratigraphy

The only terrestrial impact crater where detailed field studies could relate ejecta to the crater's known stratigraphy is Meteor Crater, Arizona, 1.1 km in diameter [*Shoemaker*, 1963; *Roddy et al.*, 1975]. An "inverted" target stratigraphy is found in its continuous ejecta deposits; the "overturned flap" is particularly prominent in the rim vicinity. Similarly overturned flaps are described from explosion craters [*Roddy*, 1977; *Roddy et al.*, 1977*b*]. They are also well known from small-scale experimental impact craters [*Gault*

et al., 1968]. Experimental crater ejecta were analyzed in greatest detail by *Stöffler et al.* [1975] and *Stöffler* [1981]. Overturned flaps and resulting inverted target stratigraphies are generated in almost every theoretical calculations [*e.g.*, *Ahrens and O'Keefe*, 1978; *Orphal*, 1977; *Trulio*, 1977; *Cooper*, 1977]. As a consequence the concept of an inverted target stratigraphy established itself firmly and early as a major tool in planetary surface exploration, and it provided much of the primary mission rationale for lunar site selection during Apollo.

It is extremely important to note that observational evidence for this concept is based exclusively on relatively small scale impact craters ($\leq$1 km), where terminal ballistic velocities of the ejecta are generally insufficient to generate a secondary cratering regime. On the moon, very few secondary craters are observed around craters <1 km in diameter (see, for example, Figure 16 of *Oberbeck* [1975]). We wholeheartedly subscribe to the reality of an inverted target stratigraphy surrounding relatively small impact structures. We must, however, express caution when these small-scale phenomena are extrapolated to large-scale continuous deposits. Our data (e.g., Figures 24, 28, and 29) seemingly do not reflect such an inverted target stratigraphy.

First, it must be emphasized again that the Bunte Breccia constitutes indeed >90% (volume) of all Ries materials beyond the crater rim (Table 1) and that it is therefore the analog to photogeologically observed "ejecta blankets" surrounding large planetary craters. Second, it must also be emphasized that the Bunte Breccia is the only impact formation analyzed so far which contains significant components from local substrate sources. This is a fundamental difference from all previous ejecta studies, owing to the (large) size of the Ries crater. Keep in mind, however, the absolute or scaled radial ranges represented by the present core studies (e.g., Figures 4, 35, and 36). If R_0 approximates 6.5 km, then it is not surprising that primary ejecta at scaled radial ranges greater than 2.5 R_0 are indeed dominated by Upper Jurassic, i.e., the shallowest target stratigraphies. The presence of subordinate amounts of deep-seated target strata at all radial ranges investigated is most likely due to the highly turbulent flow regimes within the debris surge and to ricocheting of primary crater fragments during secondary cratering. These processes may mask or destroy the relatively orderly sequences existing during the ballistic phase.

Combination of the modal stratigraphic observations and the postulated degree of slumping of the Ries cavity (see, for example, Figure 41) results in an exceedingly important planetary implication: the mappable continuous deposits beyond the apparent rim of complex planetary craters, i.e., beyond the morphologic rim crest, are overwhelmingly dominated by rather shallow seated target materials. Such mappable continuous deposits represent only that fraction of ejecta that was initially transported beyond a radial range of approximately 2 R_0. The majority of the deep-seated strata are deposited at a range less than 2 R_0, i.e., in a relatively restricted annulus. Importantly, this annulus suffered slumping. Therefore deep-seated target strata occur predominantly inside the morphological rim of large, complex craters or multiringed basins. The modal stratigraphic makeup of the Ries "megablock zone" is consistent with this view, if not in strong support [*Pohl et al.*, 1977], and the inner "rim" of the Ries is almost exclusively characterized by crystalline blocks; not a single Upper Jurassic limestone block is known at $r < 8$ km. The important point of this discussion is that continuous deposits beyond the apparent rims of large planetary impact structures are composed largely of "local" materials followed by primary crater ejecta that furthermore predominantly originated from very shallow target depths.

Generalizing the Bunte Breccia observations, one may obtain crude guidelines for large-scale continuous deposits beyond the morphological crater rim: >90% of all crater materials derive from the uppermost 10% of the total depth of the excavation cavity (for $Z = 2.7$) and from the uppermost 4% of the transient cavity depth. If one includes the locally excavated materials, the total fraction (weight percent) of primary ejecta derived from deeper than 10% of the parent crater's excavation cavity is $\ll$5% of the entire deposit. Translating these values to a hypothetical impact basin of $d_e = 100$ km, $R_0 = 400$ km and an apparent rim crest diameter of about 800 km, one finds that >95% of its continuous deposits are derived from source depths of <10 km. If these Bunte Breccia findings are related to the apparent crater diameter R_D of large craters, the dominant source depth for most primary ejecta in the continuous deposits is $<0.01R_D$. These are indeed very shallow depths in terms of many planetary implications. The observations and conclusions presented above are, however, perfectly consistent with, if not the reason for, the apparent dominance of relatively shallow seated materials in the collection of lunar highlands rocks and breccias [*Papike and Merrill*, 1980; *James and Hörz*, 1981; *Taylor and Wilkening*, 1982]. Deep-seated rocks are rarities in the lunar sample collection [e.g., *Vaniman and Papike*, 1980]. The shallow excavation depths documented for the Ries ejecta thus provide potential clues to understanding the dominance of shallow source depths in the lunar sample collection. *Croft* [1980] stressed the compatibility of shallow excavation cavities with the lunar sample collection. We now suggest that Croft's arguments be refined in view of the Ries findings by specifically addressing the modal stratigraphic composition of continuous deposits beyond the apparent crater rim; after all, most of the lunar samples were collected from such exterior deposits (at least with regard to major impact basins that also would have produced ejecta from great crustal depths).

Taking all Ries ejecta beyond the tectonic crater rim, i.e., including the moldavite tektites and the suevites, one does, however, obtain a scenario crudely consistent with that of an inverted target sequence: the moldavites (of most shallow seated derivation [*David*, 1969; *Bouska et al.*, 1973; *Graup et al.*, 1981]) were clearly transported farthest, followed by the Bunte Breccia and the suevite (from the most deep-seated horizons [*Hörz*, 1965; *Engelhardt*, 1967; *Graup*, 1978; *Stöffler*, 1966, 1981]), the latter even in perfectly "inverted" position, always, and without exception, deposited on top of the Bunte Breccia [*Hüttner*, 1969]. The present occurrences of suevite may be erosional remnants of a once more continuous suevite blanket, but *Stöffler* [1977] argues against this and there appears little question that suevite or other deep-seated crystalline material was a minor component in the ejecta beyond the tectonic rim. *Schneider* [1971] extracted from individual 1:25,000 maps the information illustrated in Figure 46. It depicts the maximum areal extent of large clasts (>25 m) that were recognized and mapped individually by a large number of field workers. While this figure seemingly attests to relatively orderly ejection processes compatible with the concept of an inverted target stratigraphy, it

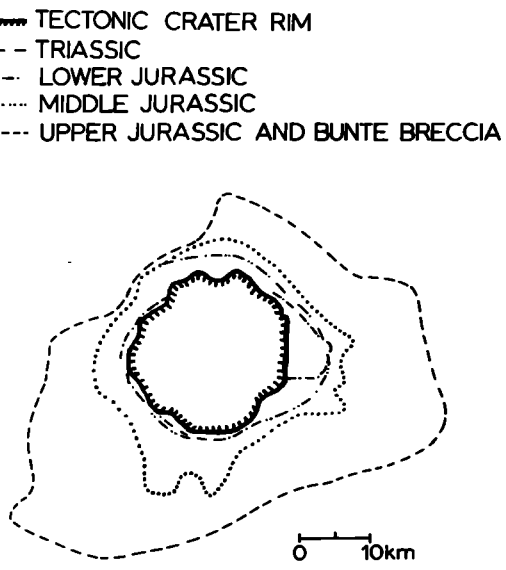

Fig. 46. Maximum areal extent of >25-m clasts associated with specific target horizons as synthesized by *Schneider* [1971] from 1:25,000 scale maps. It is important to note that these boundaries do not apply to <25 m clasts; relatively small clasts may in principle occur anywhere in the Bunte Breccia. Further, this summary does not contain information related to absolute and relative frequency of occurrence; with the exception of Upper Jurassic, all other target horizons and associated clasts larger than 25 m are relatively rare.

may not be used to infer the actual existence of stratigraphic inversion in the Bunte Breccia. The figure simply depicts maximum radial extent of large blocks from specific horizons and says nothing about their relative frequency. Other than Upper Jurassic, any >25-m clast of Triassic and Lower or Middle Jurassic is a rarity a few kilometers from the crater rim, and they are volumetrically not very significant. The general field relations in a volumetric sense (as mapped on 1:25,000 scales) as well as in vertical profile (as determined in our cores) do not argue for an orderly, inverted target stratigraphy in the Bunte Breccia. Where exposed at radial ranges of >15 km, the <25-m components of Bunte Breccia appear always dominated by Upper Jurassic clasts, and the more deep seated strata are of subordinate abundance; centimeter-sized clasts may in principle be observed everywhere.

Further, *Gall et al.* [1975] measured the ratio of Upper Jurassic delta + zeta (i.e., highest stratigraphic members) to "older" Upper Jurassic (i.e., the lower Upper Jurassic horizons). They find a systematic increase of the younger, higher horizons with radial range as illustrated in Figure 47. This is the most detailed evidence for inverse target stratigraphy accumulated to date. The data refer to clasts generally larger than 50 cm in dimension where positive assignment to any specific stratigraphy could be made; such assignment was not possible with our relatively small core clasts. The data illustrated in Figure 47 attest in a sense to relatively orderly ejection processes, but they do not refer, again, to absolute volume percent, and therefore they do not imply inverted target stratigraphy in a strict sense; small clasts (<50 cm) from very deep target sources can still be present.

The secondary cratering action and ensuing debris surge seem to modify the apparently orderly ejection systematics during large-scale cratering. This modification is particularly evident in vertical profiles, observations for the first time made possible by our continuous core sections in which we find no preferred concentration of any lithology. Our cores differ in this respect somewhat from those obtained by *Chao et al.* [1977] from Otting (17-km radial range, east of the impact center) and Itzing (21-km radial range, southeast of the impact center). These cores display only in their bottom sections Bunte Breccia akin to that encountered by us, i.e., rich in local Tertiary; the upper core sections are rich in crater materials, although diverse stratigraphic horizons may be mixed. Thus some crude inverted stratigraphy can be inferred from these cores. Detailed modal-stratigraphic analysis is not available. Our core analyses also differ in some aspects from the Bunte Breccia studies of *Schneider* [1971]. Schneider analyzed Bunte Breccia profiles, typically 1–2 m long and immediately below some suevite contacts. He finds, for example, that the quartz/feldspar ratio decreases from bottom to top and that the frequency of quartz grains displaying planar elements, i.e., evidence of shock greater than 10 GPa, also increases. He concludes that the upper sections of Bunte Breccia are enriched in deep-seated target lithologies. Schneider's observations probably apply to some transition zone (although the Bunte Breccia/suevite contacts are knife-edge sharp) characteristic for the top section of Bunte Breccia. For example, his profile from the Otting quarry is 2 m long, whereas the core of *Chao et al.* [1977] indicates 48 m total Bunte Breccia. Interestingly, *Schneider* [1971] also describes other Bunte Breccia samples collected south of the cliff line as being exclusively derived from local, Tertiary sources, and stratigraphic inversion is not observed.

The point of this discussion is that primary ejecta beyond the apparent rim of large complex craters are volumetrically dominated by shallow-seated target strata. Deep-seated target strata are predominantly deposited inside the morphologic rim, i.e., in an annulus that suffers slumping; such deep-seated ejecta are found in the Ries megablock zone, on occasion even in bona fide, inverted fashion [*Dressler and Graup*, 1974; *Gall et al.*, 1976]. Thus the concept of inverted target stratigraphy continues to be a valuable planetary exploration tool even for large impacts with the proviso that, according to our Ries studies, the ejecta beyond the morpho-

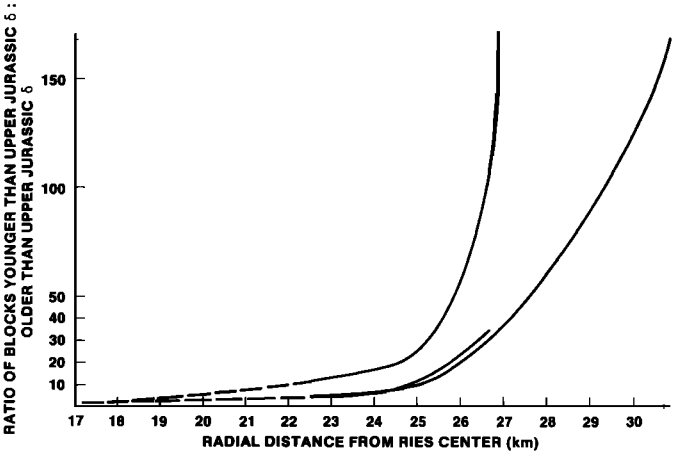

Fig. 47. The relative frequency of 0.5-m clasts from shallow-seated, young Upper Jurassic (delta and zeta) and those derived from more deep-seated, older Upper Jurassic horizons according to *Gall et al.* [1975]. Note that the younger members increase with increasing radial range. The three curves refer to three separate, radial traverses in the south and southeast continuous deposits.

logical rim crest represent but a fraction of the total ejecta. Such deposits are entirely dominated by shallow target horizons; the majority of deep-seated strata were initially deposited at radial ranges less than the apparent crater diameter; they now reside inside the morphological crater depression.

We now consider additional model predictions of continuous deposits and their possible relation to target stratigraphy. For example, *Ahrens and O'Keefe* [1978] extrapolate relatively early time, hydrodynamic flow phenomena to the ballistic phase and conclude that ejecta deposits may be stratified with regard to their internal energy; a layer of more severe shock history should be sandwiched between two relatively unshocked or mildly shocked strata. Figure 33 indicates that those clasts that have shock histories resolvable by optical means may be found anywhere in vertical profile; they are not concentrated in a discrete stratum.

Further, all shock levels in the Bunte Breccia may essentially occur at any given radial range (Figure 34), contrary to *Hawke and Head* [1978], who postulated concentric zoning of increasingly higher shock levels with increasing radial range. Again, we do not see any radial trends in the level of shock of our crystalline clasts. *Schultz et al.* [1981] present calculations indicating that a wide variety of shock levels may be found at any radial range. Our Bunte Breccia studies are in qualitative agreement with their results; the Bunte Breccia observations suggest, however, on the average significantly lower peak pressures than those indicated by *Schultz et al.* [1981].

These significant or modest departures from theoretical predictions are interpreted again as a consequence (at least in part) of secondary cratering action and the ensuing, turbulent debris surge which thoroughly mixes and destroys any systematic trends that may have existed during the ballistic phase.

It is important to stress that we do not disagree with many of these predictions, but we must warn against their uncritical application in lunar sample interpretation or remote sensing studies. The continuous planetary deposits sampled or remotely analyzed are the combined result of a ballistic transport phase, an ensuing secondary cratering action, and a massive, turbulent debris surge. Most models address the ballistic phase only and even that, in a strict sense, mostly via extrapolation of very early stage, hydrodynamic flow phenomena.

Schultz and Mendell [1978] postulate an increasing degree of ejecta comminution with increasing crater diameter. We concur and expand their findings to include that successively more deep-seated strata are progressively more comminuted (equations (5) and 6)). Unfortunately, we see no possibility in our Ries data of differentiating between comminution in the crater cavity and that due to secondary cratering processes.

Summary of Ejecta Emplacement Mechanisms

We take the Ries observations to be in strong support of the secondary cratering hypothesis as proposed by Oberbeck and co-workers. The magnitude of interaction with the local substrate, previously the subject of considerable, if not fundamental, debate, [*Chao*, 1974, 1977*a*, 1977*b*; *Schultz et al.*, 1980; *Schultz*, 1981; *Wilhelms*, 1981], is now quantified for the Ries. The Ries findings are in substantial agreement with the model predictions of *Morrison and Oberbeck* [1978]. There is no diagnostic evidence to support the nonballistic emplacement mechanisms advanced by *Chao* [1977*a*, *b*], nor is there evidence to decrease the efficiency of secondary cratering action by a factor of about 10 as suggested by *Schultz* [1981]. Also, systematic trends are found in neither vertical profile nor radial traverse regarding the occurrence of variously shocked clasts as postulated by some workers. Discrepancies between observations and predictions are largely ascribed to the highly turbulent conditions during ground-hugging debris flow. Deposition of some >200 km^3 of Bunte Breccia (including the locally derived components) was seemingly completed within minutes, i.e., while late stage ejecta (the suevites) were still being ejected.

Consideration of the stratigraphic source depth(s) of suevite, Bunte Breccia, and moldavite tektites, their respective ballistic ranges, and their associated areal distributions results in a picture grossly consistent with the concept of inverted target stratigraphy during the Ries event. The present Bunte Breccia studies and previous investigations of the megablock zone in the slumped parts of the Ries crater indicate, however, that >90% of a complex crater's continuous deposits beyond the apparent crater rim derive from depths that may be one-hundredth the depth of the apparent crater diameter; truly deep-seated ejecta are deposited in the areas subject to slumping, immediately following the excavation phase. Importantly, and as emphasized previously [*Hörz and Banholzer*, 1980], continuous deposits beyond the apparent rim are emplaced as relatively cold masses; the majority of hot ejecta either do not leave the crater cavity or will be deposited also in the area subject to slumping processes. The bulk of continuous deposits beyond the crater rim experienced modest to negligible shock stresses.

PLANETARY IMPLICATIONS

A variety of planetary implications result from the above Bunte Breccia studies. Such implications relate to remote sensing studies of planetary surfaces and to the interpretation of extraterrestrial materials such as lunar highland rocks and meteoritic impact breccias. Some broad implications are presented in the text, implict or explicit. Specific examples are emphasized below.

Throughout this review we have attempted to quantify our observations, where possible, and many observations were generalized, for example, by normalization to a crater diameter or crater depth. These generalizations are deliberate. On the other hand, we cannot imply that each and every detail observed in the Ries will be duplicated by each and every large planetary crater; such an implication would be unrealistic. As a consequence the Ries observations and their quantifications are offered as guidelines or order of magnitude estimates. This intent is justified because both laboratory experiment and theory are presently not capable of generating or duplicating, in toto, the complex processes responsible for the formation of a 26-km-diameter crater and its continuous deposits. Much of our knowledge regarding large impact structures derives from photogeologic studies of planetary surfaces, although subsurface, structural information relies almost exclusively on the terrestrial cratering record [e.g., *Grieve*, 1980]. Each approach has its specific limits, but we feel that field studies of large-scale terrestrial impact structures must continue to provide guidelines for improved experiments, theories, and photogeologic infer-

ences. The Bunte Breccia remains the premier example of large-scale continuous ejecta deposits, and it may be studied with superb field control. In this spirit, in the following paragraphs we apply our Ries findings to some current lunar and planetary "problems."

The Apollo 14 Landing Site

Contrary to the initial mission rationale, which intended to return primary Imbrium Basin ejecta, it is now widely agreed that the Apollo 14 samples represent a mixture of locally processed specimens as well as genuine Imbrium ejecta. *Head* [1976], *Head and Hawke* [1975], *Morrison and Oberbeck* [1975], and *Wilhelms et al.* [1978] describe abundant, local secondary craters associated with the Imbrium Basin formation. Present debate focuses on (1) how much Imbrium components might be present and (2) how they can be identified. On the basis of the Bunte Breccia studies (e.g., Figures 25 and 26) it will remain enormously difficult to answer these questions, although, as stated, the guidelines established by *Morrison and Oberbeck* [1975] appear to be reasonable. Rather than associating rocks or specific clasts with a parent source terrain, the Bunte Breccia studies seem to indicate that clues to local sample provenance may be gained by detailed characterization of Apollo 14 breccia matrices; >95% of the Bunte Breccia matrix is locally derived.

The Apollo 16 Landing Site

Qualitatively, similar problems exist at the Apollo 16 landing site [*James and Hörz*, 1981]. Additional complexity is introduced by the fact that primary ejecta emanating from the Imbrium Basin encountered as the local substrate the continuous deposits of the Nectaris Basin, formed earlier. The question therefore at Apollo 16 is to recognize materials added to the site by the Imbrium and Nectaris events, and possibly others, and to contrast them with distinctly local components, indeed a formidable task but again perhaps best approached by characterizing the breccia matrices. Because of the proximity of the Descartes landing site to the Nectaris Basin, materials ejected during formation of the Nectaris Basin should dominate the basin-related materials at Apollo 16 [*Maurer et al.*, 1979; *Wilhelms*, 1981]. We do not agree with the strictly photogeologic arguments of *Wilhelms* [1981] that a flow of essentially pure Imbrium Basin material was deposited at Apollo 16; we acknowledge the existence of an Imbrium-related flow, but we consider this flow part of a debris surge composed of both Imbrium and local substrate materials, the latter dominating volumetrically but essentially being composed of Nectaris ejecta. Further, the depositional scenario of *Muehlberger et al.* [1981], and particularly their cross section, is in conflict with the Ries and other observations from terrestrial craters [*Phinney and Simonds*, 1977; *Grieve*, 1980; *Stöffler*, 1981], which indicate that "hot" and "cold" ejecta are never mixed on the scales envisioned by *Muehlberger et al.* [1981]; specifically, all suevites (hot materials) always rest on top of the clastic (cold) Bunte Breccia. "Draining" of a melt fraction out of clastic impact deposits is simply not observed in terresterial craters and cannot be expected, if the rapid cooling rates for even voluminous impact melts by themselves are considered [e.g., *Onorato et al.*, 1976, 1978].

The Lunar Megaregolith

Estimates of the present lunar megaregolith thickness are approximately 1–2 km [*Short and Foreman*, 1972; *Morrison and Oberbeck*, 1978]; these estimates are based on the cumulative ejecta volume of all craters presently observed on the lunar surface. Significantly deeper megaregolith depths are obtained if it is assumed that this crater population represents but a fraction of the craters actually produced during lunar geologic history [*Hörz et al.*, 1976; *Hartmann*, 1980]. Therefore the absolute depth of the lunar megaregolith, presently unknown, is a measure of the moon's total cumulative bombardment history.

The Bunte Breccia observations reveal that the bulk of crater ejecta is modestly shocked, if at all. Similar observations apply to experimental craters [*Stöffler et al.*, 1975] or Meteor Crater, Arizona [*Kieffer*, 1971]. Thus the great majority of basin ejecta deposited at Apollo 14 and 16 should have suffered modest shock effects prior and during the Imbrium and Nectaris events, because most basin ejecta derive from below the 1- to 2-km-deep megaregolith, providing that these model depths are correct. This statement even holds for our preferred, very shallow excavation depths for most basin ejecta (<5 km); the fraction of relatively "pristine" rocks versus highly shock-processed "megaregolith" materials must increase if deeper excavation depths for basin ejecta are postulated. The important point is that if megaregolith thickness is indeed only 1–2 km, most basin ejecta should display minor shock effects, if any; they should be relatively pristine rocks.

As we all know, such pristine materials are generally rare in the lunar highland rock collection, including the Apollo 14 and 16 samples [*Warren and Wasson*, 1980; *Herzberg and Baker*, 1980]. Instead, the majority of lunar highland rocks are processed severely, if not multiply, by impact cratering (see *Ryder and Norman* [1980], *Taylor and Marvin* [1981], and many others). A major question arises: were these rocks brecciated and shock metamorphosed by impacts prior to or after ejection from their respective basin events? This question is clearly recognized and of central importance in deciphering absolute basin chronology (e.g., *Schaeffer et al.* [1976], *Horn and Kirsten* [1977], and many others). The question, however, bears crucially also on absolute thickness of the megaregolith: if(!) most lunar highland rocks were indeed shock processed and assembled into diverse breccias prior to basin formation, then one would have to postulate megaregolith thicknesses of >>1 km already at the time(s) of basin formation. If indeed most lunar highland rocks were shock processed prior to the Nectaris or Imbrium basin formation, megaregolith thicknesses of >5 km could be inferred. Thus the question of "where" did most of the breccias form is in a sense synonymous with "when," i.e., before or after basin formation. If the breccias and melt rocks were largely formed prior to basin formation, relatively deep megaregolith would be inescapable; this in turn would imply that the presently observed crater (and basin?) population [e.g., *Neukum and Wise*, 1976; *Woronow*, 1978] are but survivors of a significantly larger number of lunar impact events.

Lunar Basin Chronology

As already emphasized by *Hörz and Banholzer* [1980], the Ries continuous deposits are emplaced at essentially ambient temperatures. Review of the terrestrial cratering record

[Grieve, 1980; *Grieve et al.*, 1981], and specifically the Ries [*Stöffler*, 1977; *Engelhardt and Graup*, 1981], indicates that (1) generally <5% of the total crater volume is molten and (2) very little melt appears to be transported beyond the crater rim. Thus temperatures sufficient to completely reequilibrate isotope systems used in absolute chronological studies are confined to a relatively small volume that furthermore appears concentrated inside the crater cavity. Occurrence of photogeologically defined impact melts beyond the crater rims appears limited [*Hawke and Head*, 1977]. In addition, recent $^{40}Ar/^{39}Ar$ studies of clasts dislodged from suevite [*Jessberger et al.*, 1978; *Bogard et al.*, 1981; *Staudacher et al.*, 1982] demonstrate the inefficiency of thermal reequilibration of even a relatively mobile noble gas system(s) in the hottest ejecta known from the Ries. Essentially, none of the lunar mare basalt hand specimens is isotopically disturbed by impact cratering, although all of the specimens returned are crater ejecta.

We thus consider it unlikely that large-scale basin deposits, e.g., at the Apollo 14 and 16 landing sites, contain statistically significant numbers of specimens that experienced temperatures appropriate for complete isotopic equilibration during formation of the respective basin(s). We consider it statistically much more likely that the isotope systems were affected by numerous "local" impacts as suggested by *Kirsten and Horn* [1974], *Horn and Kirsten* [1977], and others. It is, however, not clear at present to what degree these frequent impacts predated or postdated the major basin-forming events. Some difficulty is also encountered in explaining the observed distribution of highland rock ages which differ characteristically from landing site to landing site [*Schaeffer and Schaeffer*, 1977; *Wetherill*, 1981]. Unless one invokes a small number of craters as local vagaries of an otherwise stochastic process, the differences in age distributions are not readily explained by the (frequent?) local resetting of isotope systems.

Planetary Impact Breccias

Our Bunte Breccia studies very generally reveal the possible importance of detailed matrix studies in deciphering the source terrain of lunar and meteoritic impact breccias. Provided the association of any hand specimen with a relatively large cratering event can be established and provided that the (unknown) crater stratigraphy differed from that of the local substrate, such a breccia should contain clastic material that must also give rise to the matrix. Clast lithologies that do not participate in matrix formation are excellent candidates to be from distant terrains. In reality, these are, however, rather idealized "field conditions" because many shallow target horizons in a planetary context are probably akin to or indistinguishable from the surrounding substrate; such a breccia may be characterized by the fact that all clast lithologies contribute to matrix formation. The important point is that clast materials that do not participate in matrix formation are volumetrically rare constituents of the local geologic setting and may be likely candidates for distant source areas.

The Formation of Lunar Light Plains

Oberbeck et al. [1974] postulated that the formation of lunar light plains, such as the Cayley deposits, are caused by mass wasting processes from the local topographic highs due to primary and secondary impact cratering. The large quantities of local materials now documented for the Ries continuous deposits, as well as the considerable horizontal mass movements, add credence to the hypothesis that ballistic crater ejecta constitute a significant erosional force perfectly capable of shedding large amounts of materials into local depressions, regardless of whether such depressions are filled by early volcanic deposits [*Schultz and Spudis*, 1979] or not. *Soderblom* [1970] and *Soderblom and Lebofsky* [1972] addressed the erosional forces of small-scale craters and come to similar conclusions: local depressions are gradually being filled up by impact deposits.

The Chemistry of Basin-Forming Projectiles

Again, terrestrial experience indicates that meteoritic contamination is preferentially, if not exclusively, concentrated in impact melts [*Palme*, 1982; *Grieve et al.*, 1981]. As a consequence, identical, essentially statistical arguments that were offered above in negating establishment of a firm basin chronology must also apply to the identification of basin-forming projectiles [e.g., *Hertogen et al.*, 1977]. The measured impactor chemistries in lunar rocks more likely reflect those of relatively small, local cratering events rather than big basins. The recent discovery of a siderophile-rich layer at the Cretaceous/Tertiary boundary [e.g., *Alvarez et al.*, 1980; *Smit and Hertogen*, 1980; *Kyte et al.*, 1980] may, however, demonstrate that the transport mechanism(s) for large(?) fractions of relatively massive projectiles may not be related to the transport mechanism of molten or solid crater ejecta; much of the projectile may be vaporized and subsequently condensed, thus allowing relatively global distribution [e.g., *O'Keefe and Ahrens*, 1982; *Hörz*, 1982]. Nevertheless, this potential(?), terrestrial analog for global distribution of impactor materials reveals that its meteoritic "contamination" is contained in a discrete, relatively thin layer. The meteoritic contamination on the moon is, however, not surface correlated, but disseminated throughout the volume of a specific rock. In this sense its mode of occurrence is similar, if not identical, to terrestrial impact melt sheets. Present evidence indicates meteoritic contamination to be present only if the rock mass (or its progenitor) resided at or close to the projectile/target rock interface. Meteoritic contamination is not known from terrestrial impact formations that could be considered analogues of continuous ejecta deposits. We therefore believe that the siderophile contamination observed in lunar rocks relates to numerous local or regional impact events, rather than to basin-forming bolides.

Flow Phenomena and Impact Melts in Distal Crater Deposits

The existence of flow morphologies as part of large-scale continuous deposits, especially lunar basins, is well established. In particular, the flows observed in association with the relatively young and thus well-preserved Orientale Basin event are taken as analogs to infer similar flow phenomena on the more degraded deposits of, for example, Mare Imbrium or Nectaris [*Head*, 1974; *Moore et al.*, 1974; *Wilhelms*, 1981]; such analog studies of the least degraded basin ejecta are, beyond question, valid, necessary, and useful. We caution, however, against the common and popular inference of associating all flow morphologies with "liquid" ejecta, i.e., hot impact melts, especially in the distal ejecta. A number of arguments may be advanced to caution against such inferences: (1) The Bunte Breccia studies indicate that the Ries continuous deposits are anything but warm, and there is certainly no impact melt

present. (2) The total melt transported beyond the crater rim is a small fraction relative to the total volume of continuous deposits, although *Schultz et al.* [1981] illustrate that relatively more melt will be ejected to large radial ranges in a basin-forming event as opposed to a relatively small crater; the total mass is nevertheless very small. (3) Cooling rates determined for massive, terrestrial impact melt sheets such as the 300-m-thick melt layer inside the Manicouagan Crater are measured to drop below the liquidus in a few seconds [*Simonds et al.*, 1976; *Onorato et al.*, 1978]; similarly rapid cooling rates were calculated for lunar impact melts or melt bearing fragmental breccias [*Onorato et al.*, 1976, 1978]. As a consequence, cooling times to below the liquidus of lunar impact melts, even those that may have crystallized from large melt pools inside crater cavities, are of very short time scales. On the basis of these cooling rates it is therefore questionable whether highly liquid melts will even be arriving at the large radial ranges from which "melt flows" are reported by, for example, *Moore et al.* [1974], *Muehlberger et al.* [1981], and *Wilhelms* [1981]. Importantly, all Ries bombs cooled to <700°C during ballistic transport [*Hörz*, 1965]; they were rigid bodies when they landed. (4) Small-scale "flow" phenomena are frequently seen on relatively small scale, lunar land slides in the absence of any liquid phase [e.g., *Howard*, 1973; *Lucchitta*, 1977]. Such observations, in part prompted *Melosh* [1979] to propose fluidization of particulate materials by accoustical energy. (5) *Mendell* [1976] argues on the basis of IR observations (which essentially relate to bulk cooling properties of discrete, mappable formations inside relatively fresh lunar craters, such as Copernicus) that "impact melts" identified via flow morphologies may not be coherent rocks. The cooling properties of even classical impact melts are more compatible with particulate, loose materials that are shed from the crater walls according to *Mendell* [1976]. Thus there is reasonable doubt, based on IR observations, that "melts" are responsible for many flow phenomena. (6) Flow lobes and flow fronts are frequently observed in association with secondary craters in the absence of liquid melts [*Oberbeck*, 1975]. Some, although not all, of the melt flows observed on the continuous deposits of Mare Orientale also appear to emanate from large secondary craters.

We therefore caution against the frequent association of flow phenomena with liquid impact melts on the moon, especially at the large radial ranges proposed by, for example, *Moore et al.* [1974], *Wilhelms* [1981], and *Muehlberger et al.* [1981]. Such flows may represent nothing else but fluidized, particulate materials, perhaps due to acoustical fluidization [*Melosh*, 1979]. It may also be possible that the high-velocity, turbulent debris surge generated by secondary cratering action will develop a laminar boundary layer during deceleration, thus displaying flow features on the surface [*Hsü and Heim*, 1978].

Continuous Deposits on Mars

Because of terrestrial gravity, the presence of abundant volatiles in the target, and the existence of an atmosphere, the Ries Crater is actually a much better analog for large-scale Martian impacts than it is for lunar ones. Many Martian impact structures are surrounded by multiple ejecta lobes [e.g., *Carr et al.*, 1977; *Greeley et al.*, 1980; *Schultz and Singer*, 1980; *Mouginis-Mark*, 1979].

In general, there is widespread consensus that these characteristic Martian morphologies are caused by volatiles contained in the target; such volatiles appear to provide the necessary lubrication for development of pronounced flow morphologies within the continuous deposits. The relative paucity of secondary craters on continuous deposits on Mars relative to the moon [*Schultz and Singer*, 1980] is most likely due to this enhanced lubrication, because increased ability to flow will lead to less pronounced "herringbone" patterns, typical for secondary craters, and will furthermore cause the secondary crater cavities to be filled more readily. Therefore the continuous deposits surrounding large-scale Martian craters should display a different morphology relative to the moon because of their effectively decreased viscosity (see, for example, *Greeley et al.* [1980]). This decreased viscosity is largely responsible for the pronounced lineations, discrete terminal flow lobes, and other morphologies indicating a highly fluidized medium. Much of the volatiles contained in these flows may actually be liberated also during secondary cratering. Peak shock pressures during secondary impact on Mars may be sufficient to liberate H_2O, CO_2, and possibly other cold-trapped volatiles [*Kieffer*, 1975; *Kieffer and Simonds*, 1980]. Thus we postulate similar processes to operate on Mars that we described during emplacement of the Bunte Breccia. We know of no Martian observation that would negate, in principle, the existence and importance of secondary cratering for the deposition of continuous deposits.

Nevertheless, we also do have difficulties in understanding the multiple nature of Martian flow lobes. There is nothing in our Ries cores indicating distinct, multiple, relatively large scale flow regimes, although drill locations were placed purposely such that vertical profiles as complete as possible could be recovered. Details of the surface morphology are, of course, eroded in the Ries continuous deposits. Do our Ries observations indicate that the Martian flow morphologies are indeed very surficial features, barely "skin deep"? Are they a laminar boundary layer resulting during deceleration of the turbulent debris surge? But then, why are there multiple flows? Is it possible that some lithologic discontinuity in the target stratigraphy also causes multiple ejection regimes akin to the suevite/Bunte Breccia dichotomy? Was a second or third ejection regime generated from more deep-seated target zones which had a pronounced hiatus relative to the major ejecta curtain? Clearly, there is no ready explanation for the existence of temporally and spatially distinct flow regimes observed around many Martian craters. As detailed by *Hörz* [1982], suevite and Bunte Breccia do have distinctly different ejection and depositional histories; thus at least two "phases" of ejecta do exist at the Ries, the detailed surface morphologies of which are, however, not preserved.

Schultz and Gault [1979] address the effects of aerodynamic sorting upon Martian crater ejecta and the possible effects thereof on the morphology of continuous deposits. The present state of preservation of the Ries ejecta does not exclude the existence of such effects, because a thin, surficial layer would, of course, be eroded. Indeed the Forschungsbohrung Nördlingen, 1973 [*Stettner*, 1974; *Stöffler*, 1977; *Pohl et al.*, 1977] revealed a layer, 7 m thick, that represents aerodynamically sorted suevite; this layer rests on normal crater suevite (260 m deep), and the top layer is clearly the last material deposited. This is the only occurrence of aerodynamically sorted materials in the Ries. The grain size distributions for Bunte Breccia and especially the suevites beyond the tectonic rim, however, are character-

ized by extremely poor grain size sorting (see Figure 20). While one can argue that significant comminution may have occurred during secondary cratering and in the ensuing debris surge, such comminution by ground hugging can be excluded for the ballistically transported suevites. The aerodynamically shaped bombs, frequently of very delicate shapes, are only rarely broken upon landing [*Hörz*, 1965]. Coarse- (>5 cm) and fine-grained (<1 mm) suevite components were emplaced simultaneously to yield poorly sorted deposits throughout. The lack of any aerodynamic sorting in suevite deposits that contain aerodynamically shaped melt bombs appears to require some dense, radially expanding vapor clouds capable of transporting coarse- and fine-grained debris with equal ease and over distances of >10 km (see also *Hörz* [1982]). These suevite observations appear to argue against aerodynamic sorting on the scales envisioned by *Schultz and Gault* (1979). In all likelihood the ambient atmosphere was severely disturbed, temporarily displaced by a radially expanding vapor cloud, and only after dissipation of this cloud was the atmosphere restored to give rise to an aerodynamically sorted fallback suevite of very limited volumetric significance that furthermore is known only from inside the crater cavity ($R_0 < 6$ km). None of the deposits beyond the morphological Ries rim displays evidence of aerodynamic sorting.

CONCLUDING REMARKS

Our Bunte Breccia core studies yielded a number of qualitative and quantitative insights into impact cratering and especially into the depositional mechanisms for large-scale continuous crater deposits. We reemphasize the suggestion of *Oberbeck* [1975] to utilize the term "continuous deposits" for these formations, because they contain abundant, locally derived materials; the terms "crater ejecta," "ejecta blanket," etc., should be restricted to only those materials that originated in the excavation cavity of the parent crater.

The superb field control with which the Bunte Breccia may be studied is unique for all known large terrestrial craters. The Ries is the only large crater where continuous deposits may be investigated in vertical profile on occasion as thick as 100 m. As emphasized throughout the text, such deposits are poorly sorted, massive formations. They must be viewed as a chaotic assemblage of monomict and polymict clasts. Pronounced or subtle variability is observed for virtually every parameter measured on scales that approach those of hand specimens returned from planetary impact formations. The Ries observations point toward the enormous difficulties when such extraterrestrial samples must be used as the only clues to reconstruct a potential planetary target stratigraphy and the associated geologic history and processes. On the other hand, it is equally important and highly comforting to know that almost any target horizon may occur anywhere in the continuous deposits. A typical 1-kg sample of polymict Bunte Breccia may contain materials from virtually any target horizon, albeit some of them perhaps as small grains and in minute quantities. Such a sample most likely would suffice to recognize igneous and possibly metamorphic processes to have existed and to characterize the regional, first-order sedimentary processes for the past 250 m.y. This is indeed an encouraging outlook for all students concerned with planetary impact formations.

Clearly, the actual observations refer only to the very specific conditions prevailing during the Ries event: very little is known about the impactor (velocity, mass, composition), just as we know very little about the impactor of specific planetary impact craters. On the other hand, the target stratigraphy of the Ries is exceedingly well documented, in contrast to the planetary case, where target stratigraphy generally also is completely unknown. We therefore do not subscribe to the occasional argument of some colleagues that the Ries crater is an "anomaly." As long as specific impactor conditions and planetary stratigraphies remain in essence unknown, and as long as computational methods are limited (by resources(!) and not by principal capabilities) to perfectly homogeneous target media, it seems difficult to argue which case is "anomalous," if any. The Ries crater happens to be the only large impact structure where detailed field studies and associated laboratory investigations, such as the ones presented, can be pursued. The results, we suggest, will provide reasonable guidelines of general validity for large-scale planetary impact processes.

Some of our findings seemingly conflict with certain theoretical details and/or with some photogeologic inferences, as detailed in the text. It is these areas of discrepancy and incomplete understanding where future work must concentrate. We are thoroughly convinced that theory, photogeology, terrestrial field studies, and laboratory experiments will have to combine for ultimate understanding of the complex impact process at small and large scales.

In this spirit we propose that the following Ries observations and associated interpretations have general validity:

1. Large-scale continuous deposits are chaotic mixtures of diverse monomict and polymict clasts.
2. Specific members of the target stratigraphy may be found anywhere in the continuous deposits, although the most shallow-seated materials are the dominant species; these dominant lithologies may be derived from depths as little as one-hundredth the depth of the morphological crater diameter. Most deep-seated ejecta are deposited in an area that undergoes slumping, and they therefore reside inside the actual crater depression.
3. Large-scale continuous crater deposits are emplaced by ballistic ejecta which cause secondary cratering and an ensuing, turbulent debris surge. The fraction of locally dislodged components may easily exceed the primary crater ejecta.
4. The bulk of large-scale continuous deposits is deposited at essentially ambient temperatures.

APPENDIX A: RATIONALE FOR SPECIFIC SITE SELECTION

As detailed in the text, a variety of criteria were employed in making specific site selections. Initially, we had expected to explore approximately 30 sites, as we assumed an average thickness of Bunte Breccia of 30 m. The actual depths encountered were significantly deeper, and thus significant trade-offs had to be made in real time between fiscal constraints and optimum scientific return. The rationale for each site was as follows:

Core A: Located purposely north of the cliff line, this site was therefore suitable as a reference point regarding incorporation of OMM sediments. The core was located in the center of a suevite deposit, thus ensuring an uneroded Bunte Breccia profile.

Core B: This was the first location south of the cliff line, again capped by suevite and thus assuring recovery of a complete vertical profile of Bunte Breccia. Judging from the general dip of the Upper Jurassic limestone plateau, one could expect 10–20 m of OMM sediments if they were unaffected by ejecta emplacement.

Core C: Located on a N-S striking ridge that was some 2–3 km wide and 7–8 km long and that had a relief of 60–100 m relative to the valleys on either side, this site was selected primarily to test the "thin draping" hypothesis or to obtain, on the other hand, a relatively uneroded, long Bunte Breccia profile.

Core D: Located on the same ridge system as core C (some 3 km farther to the south), this site was selected essentially for the same reasons as for core C. The specific drill site was located in a patch of OMM (30 × 60 m in extent) to ascertain whether it represents allochthonous or autochthonous OMM.

Core E: This site is on a different local promontory and next to an OMM sand quarry. This OMM occurrence was traditionally also interpreted as autochthonous until H. Gall (unpublished data, 1971) demonstrated that it is but a single OMM megaclast of at least 50 × 30 × 10 m in dimensions (see also *Chao et al.* [1978]).

Core F: This site constitutes one of the most prominent locations for evaluating "thin" versus "thick" Bunte Breccia deposits. The drill site was located on the upper slopes of the Eger river valley, believed to predate the Ries event [*Hüttner*, 1958, 1969]. Indeed, this valley was thought to have channeled the flow of ejecta as evidenced by (1) Upper Jurassic limestone clasts (≈100 m in size) "plastered" against the seemingly autochthonous valley slopes and (2) an apparent change in the direction of megascopic striae in the underlying Upper Jurassic limestone surfaces [*Wagner*, 1964; *Hüttner*, 1969], signaling deflection of the onrushing ejecta surge from a generally NE direction into one striking NNE, with the preexisting valley exerting a channeling effect. In addition, the Guldesmühle outcrop, some 800 m to the south of the drill site, beautifully displays the contact relationships of Bunte Breccia and genuine in situ OMM. Its description [*Hüttner*, 1969] led to considerable interpretative controversies concerning ballistic versus nonballistic emplacement mechanisms [*Hörz et al.*, 1974; *Oberbeck et al.*, 1975; *Chao*, 1974, 1977*a*, *b*; *Chao et al.*, 1978].

Core G: Again, this is a location on a modest, local topographic high. The major objective here was to recover the most southerly occurrence of Bunte Breccia.

Core H: This site is located on an isolated hill of 60 m relief that displays along its entire circumference (following an isohyps) a bank of competent OSM freshwater limestone, and thus autochthonous OSM materials. How much additional OSM and/or Bunte Breccia does occur above this in situ limestone?

Core I: This is by far the most westerly and distal occurrence of Bunte Breccia in the entire Ries. Although located north of the cliff line (see Figure 5), a very distinct facies (Oggenhauser Sande) of OSM occurs to the NE of this location, i.e., between crater rim and drill site. Were these sands incorporated into the Bunte Breccia?

Viewing the nine drill sites together, cores A–D represent a well-controlled N-S traverse; cores E–G may be projected onto this traverse. Additionally, cores G–I approximate a concentric traverse and thus may assist in evaluating the characteristics of distal Bunte Breccia deposits at approximately equal radial ranges (see Figure 4).

APPENDIX B: DETAILED CORE DESCRIPTIONS

Core A: It is by far the most coarse grained core and possibly somewhat anomalous, considering more "typical" Bunte Breccia exposed in its vicinity. The core is dominated by two Upper Jurassic limestone megaclasts, 20 and 29 m long. Both clasts were highly fractured, unconsolidated rock flour, called "Gries" [*Hüttner*, 1969]. The larger clast contained some pockets of Tertiary, lateritic soil, indicating that the entire clast was dislodged from the upper most target surface; the possibility that it was dislodged from the local crater environs rather than in the crater cavity cannot be excluded. Unfortunately, core A did not bottom out in autochthonous bedrock and terminated in highly coherent limestone megaclast. Therefore Bunte Breccia at location A is >80 m deep. (The above limestone was initially interpreted in the field to be bedrock (by Hörz), but vertically oriented, platy sponges recognized by Hüttner and Gall later revealed its allochthonous nature.)

Core B: After penetrating some 4.70 m of suevite, a 30-cm-thick layer of extremely crystalline-rich Bunte Breccia was encountered, akin to that described by *Chao et al.* [1977] from the Otting suevite quarry. The remainder of the Bunte Breccia contains relatively abundant crater materials, the most noteworthy being relatively frequent Lower Jurassic and Triassic clasts. The local bedrock is Upper Jurassic limestone. It displays a decreasing intensity of fracturing with depth; i.e., it changes over a 3-m vertical distance from essentially highly cataclastic "rock flour" (at the immediate contact) to "normal," competent Upper Jurassic limestone. This intense fracturing of in situ limestone vividly attests, albeit on modest scales, to some interaction between bedrock and incoming ejecta during emplacement of the latter.

Core C: Although this core constitutes one of the longest profiles obtained, it appears relatively homogeneous to the naked eye and has only few megaclasts. The polymict matrix sections contain unusually abundant, fine-grained (1–5 cm) Upper Jurassic limestone clasts. The core encountered in situ clays and silts of OSM at 77.2 m and penetrated OMM silts at 82.0 m.

Core D: This core was taken from essentially the same geological setting (same ridge system) as core C, just 3 km farther to the south. Nevertheless, core D has distinctly more megaclasts. The OMM encountered from 0 to 6 m is a dislodged clast rather than an erosional remnant of in situ OMM; the true bedrock, at 52.2 m, is OSM. Of all the materials recovered, this core is the most intensely studied [*Ostertag*, 1978; *Gasse*, 1981].

Core E: This is the longest continuous core of the entire drilling program. Inasmuch as it was located on the slope of a ridge some 40 m below the ridge crest, a Bunte Breccia deposit of >120 m can be demonstrated for this area. This enormous thickness totally confirms the postulate of H. Gall (personal communication, 1971) that the "Goldbergalm" sand quarry near Lutzingen is indeed confined to one gigantic OMM megaclast that is furthermore uplifted >80 m relative to autochthonous OMM in the vicinity.

Core F: This core has a rather heterogeneous mixture of megaclast lithologies; the largest megaclast is 12 m long (OSM). The impact deposit is in contact with OSM freshwater limestone at 47.15 m. This core demonstrates that the

nearby Guldesmühle outcrop exposes but a small fraction (6 m vertical profile) of the total, local Bunte Breccia profile. We therefore consider the inferences and associated generalizations offered by *Chao* [1974, 1977*a*, *b*] regarding the total Bunte Breccia deposit unwarranted. The Guldesmühle outcrop exposes only some 15% of the total, local Bunte Breccia profile, i.e., the bottom section.

Core G: The southernmost drill site is characterized by a very high content of Tertiary silts and sands (at the expense of clays). The core terminated in autochthonous OSM sands at 21.28 m.

Core H: Macroscopically, this is the most homogeneous core recovered. It lacks any clasts larger than 1 m; even clasts a few tens of centimeters in length are rare. Bunte Breccia overlies OSM sands at 27.80 m. The freshwater limestone was not penetrated.

Core I: This location represents the westernmost occurrence of Bunte Breccia, some 37 km from the impact center. It contains local "Oggenhauser Sande" in great quantities. There is little clay in the matrix. The core encountered autochthonous OSM marls at 15 m. Again the drill site was placed for practical reasons at a relative low elevation; thus Bunte Breccia in the general area may be as deep as 20–25 m.

Acknowledgments. Numerous people contributed to this project from its inception (V. R. Oberbeck, R. H. Morrison), through the field work (R. Hüttner, H. Gall, H. Vidal), the laboratory analysis and data reduction (G. B. Banholzer, D. Pratt, S. Langer), and typing (E. Stockton). Comments on draft manuscripts or other suggestions at various stages of this project were received from S. Croft, W. Engelhardt, H. Fechtig, G. Graup, R. A. F. Grieve, W. C. Phinney, J. Pohl, R. B. Schaal, and D. Stöffler, and H. Zook. Mark Cintala's technical comments and superb penmanship markedly improved this report. Considerate and helpful reviews were provided by T. J. Ahrens and P. Spudis. The drilling expertise of Prakla Seismos, Hannover, Germany, was instrumental. Most of the funding was provided by NASA. All of the above deserve our warm thanks. F. Horz is grateful to the Max Planck Gesellschaft and various staff members of the Max Planck Institut für Kernphysik, Heidelberg, especially H. Fechtig, for generous support and pleasant working conditions while finalizing this review; R. Ostertag was, in part, supported by the Deutsche Forschungsgesellschaft and the Lunar and Planetary Institute. A document containing the detailed data from which many of the averaged or otherwise synthesized figures and summaries were derived was assembled in 1981 (about 400 plots and 500 pages). Unfortunately, limited resources did not allow printing of a NASA technical memorandum for wider distribution and reference; a few copies are available (contact the senior author).

REFERENCES

Abadian, M., Petrographie, Stosswellenmetamorphose und Entstehung Polymikter kristalliner Breccien im Nördlinger Ries, *Contrib. Mineral. Petrol., 35*, 245–262, 1972.

Ahrens, T. J., and J. O'Keefe, Energy and mass distribution of impact ejecta blankets on the moon and Mercury, *Proc. Lunar Planet. Sci. Conf. 9th*, 3787–3802, 1978.

Alvarez, L. E., W. Alvarez, F. Asaro, and H. V. Michel, Extraterrestrial cause for the Cretaceous-Tertiary extinction, *Science, 208*, 1095–1108, 1980.

Ammon, L. V., Die Bahnaufschlüsse bei Fünfstetten am Ries und an anderen Punkten der Donauwörth-Treuchtlinger Linie, *Geogn. Jahresh., 16*(1903) 145–184, 1905.

Austin, M. G., et al., Z-model analysis of impact cratering: An overview, *Proc. Lunar Planet. Sci., 12A*, 197–205, 1981.

Birzer, F., Molasse und Ries-Schutt im westlichen Teil der südlichen Frankenalb, *Geol. Bl. Nordost Bayern, 19*, 1–28, 1969.

Bogard, D. D., F. Hörz, P. Johnson, and D. Stöffler, Resetting of $^{40}Ar/^{39}Ar$ ages in suevite ejecta from the Ries Crater (abstract), *Lunar Planet Sci., XII*, 92–94, 1981.

Bouska, V., J. Benada, Z. Randa, and J. Kuncir, Geochemical evidence for the origin of moldavites, *Geochim. Cosmochim. Acta, 37*, 121–132, 1973.

Carr, M. H., et al., Martian impact craters and emplacement of ejecta by surface flow, *J. Geophys. Res., 82*, 4055–4065, 1977.

Chao, E. C. T., Geologic implications of the Apollo 14 Fra Mauro breccias and comparison with ejecta from the Ries Crater, Germany, *J. Res. U.S. Geol. Surv., 1*, 1–18, 1973.

Chao, E. C. T., Impact cratering models and their application to lunar studies—A geologist's view, *Proc. Lunar Planet. Sci. Conf. 5th*, 35–52, 1974.

Chao, E. C. T., Mineral produced high pressure striac and clay polish: Key evidence for nonballistic transport of ejecta from Ries Crater, *Science, 194*, 615–618, 1976.

Chao, E. C. T., The Ries Crater of southern Germany: A model for large basins on planetary surfaces, *Geol. Jahrb. Reihe A, 43*, 81 pp., 1977*a*.

Chao, E. C. T., Preliminary interpretation of the 1973 Ries research deep-drill core and a new Ries cratering model, *Geol. Bavarica, 75*, 421–441, 1977*b*.

Chao, E. C. T., R. Hüttner, and H. Schmidt-Kaler, Vertical section of the Ries sedimentary ejecta blanket as revealed by 1976 drill cores from Otting and Itzing, *Lunar Sci., VII*, 163–165, 1977.

Chao, E. C. T., R. Hüttner, H. Schmidt-Kaler, Principal exposures of the Ries meteorite crater in southern Germany, report, Bayer. Geol. Landesamt, München, Federal Republic of Germany, 1978.

Cooper, H. F., A summary of explosion cratering phenomena relevant to meteor impact events, in *Impact and Explosion Cratering*, edited by D. J. Roddy, R. O. Pepin, and R. B. Merrill, pp. 11–44, Pergamon, New York, 1977.

Croft, S. K., Lunar crater volumes: Interpretation by models of impact cratering and upper crustal structure, *Proc. Lunar Planet. Sci. Conf. 9th*, 3711–3733, 1978.

Croft, S. K., Cratering flow fields: Implications for the excavation and transient expansion stages of crater formation, *Proc. Lunar Planet. Sci. Conf. 11th*, 2347–2378, 1980.

Croft, S. K., The excavation stage of basin formation: A qualitative model, *Proc. Lunar Planet. Sci., 12A*, 207–225, 1981.

David, E., Das Ries-Ereignis als physikalischer Vorgang, *Geol. Bavarica, 61*, 350–378, 1969.

Dence, M. R., R. A. F. Grieve, and P. B. Robertson, Terrestrial impact structures: Principal characteristics and energy considerations, in *Impact and Explosion Cratering*, edited by D. J. Roddy, R. O. Pepin, and R. B. Merrill, pp. 247–275, Pergamon, New York, 1977.

Dressler, B., and G. Graup. Gesteinskundliche Untersuchungen am Suevit der Bohrung Wörnitzostheim I im Nördlinger Ries, *Aufschluss, 25*, 404–411, 1974.

Dressler, B., G. Graup, and K. Matzke, Die Gesteine des kristallinen Untergrunds im Nördlinger Ries, *Geol. Bavarica, 61*, 2nd ed., 201–229, 1969.

Engelhardt, W., Chemical composition of Ries glass bombs, *Geochim. Cosmochim. Acta, 31*, 1677–1689, 1967.

Engelhardt, W., and G. Graup, Ries Crater, Germany: Petrography of the suevite and conclusions on crater formation, paper presented at Meteoritical Society Meeting, Bern, Switzerland, Aug. 1981.

Ernstson, K., The structure of the Ries Crater from geoelectric depth soundings, *J. Geophys., 40*, 639–659, 1974.

Förstner, U., Petrographische Untersuchungen des Suevit an den Bohrungen Deiningen und Wörnitzostheim im Ries von Nördlingen, *Contrib. Mineral. Petrol., 15*, 281–307, 1967.

French, B. M., and N. M. Short (Eds.) *Shock Metamorphism of Natural Materials*, Mono, Baltimore, Md., 1968.

Füchtbauer, H., Sedimentpetrographische Untersuchungen in der kontinentalen Trias der Bohrung Scherenstetten, 1, *Geol. Bavarica, 24*, 99, 1955.

Füchtbauer, H., Sedimentpetrographische Untersuchungen in der älteren Molasse nördlich der Alpen, *Eclogae Geol. Helv., 57*, 157–298, 1964.

Gall, H., Geologische Untersuchungen im südwestlichen Vorries: Das Gebiet des Blattes Wittislingen, Ph.D. thesis, Univ. München, München, Federal Republic of Germany, 1969.

Gall, H., Neue Daten zum Verlauf der Klifflinie der Oberen Meeresmolasse (Helvet) im südlichen Vorries, *Mitt. Bayer, Staatssammlung Palaeontol. Hist. Geol., 14*, 81–101, 1974.

Gall, H., and D. Müller, Der Riesgries bei Wellheim: Eine aufges-

churfte Scholle in Bunten Trümmermassen, *Neues Jahrb. Geol. Palaeontol. Monatsh., 1971,* 271–284, 1974.

Gall, H., D. Müller, and D. Stoffler, Verteilung, Eigenschaften und Entstehung der Auswurfsmassen des Impaktkraters Nördlinger Ries, *Geol. Rundsch., 64,* 915–947, 1975.

Gall, H., E. Hollous, and J. Trischler, Obermiozäne Seesedimente und Bunte Trümmermassen der Forschungsbohrung Wörnitzostheim I im Nördlinger Ries, *Geol. Bl. Nordost Bayern, 26,* 188–206, 1976.

Gall, H., R. Hüttner, and D. Müller, Erläuterungen zur geologischen Karte des Ries 1:50 000, *Geol. Bavarica, 76,* 191 pp., 1977*a*.

Gall, H., D. Müller, and J. Pohl, Zum geologischen Bau der Randzone des Impaktkraters Nördlinger Ries, *Neues Jahrb. Geol. Palaeontol. Monatsh., 1977,* 65–94, 1977*b*.

Gasse, W., Die tertiären Foraminiferen der NASA Forschungsbohrung Demmingen (SW Vorries), M.S. thesis, Univ. Münster, Münster, Federal Republic of Germany, 1981.

Gault, D. E., Displaced mass, depth, diameter, and effects of oblique trajectories for impact craters formed in dense crystalline rocks, *Moon, 6,* 32–44, 1973.

Gault, D. E., and E. D. Heitowit, The partition of energy for hypervelocity impact craters formed in rock, *Proc. Hypervelocity Impact Symp. 6th,* 420–456, 1963.

Gault, D. E., W. L. Quaide, and V. R. Oberbeck, Impact cratering mechanics and structures, in *Shock Metamorphism of Natural Materials,* edited by B. M. French, and N. M. Short, pp. 87–100, Mono, Baltimore, Md., 1968.

Gentner, W., and A. W. Wagner, Altersbestimmungen an Riesgläsern und Moldaviten, *Geol. Bavarica, 61,* 296–303, 1969.

Graup, G., Das Kristallin im Nördlinger Ries, Ph.D. thesis, 197 pp., Univ. Tübingen, Tübingen, Federal Republic of Germany, 1975.

Graup, G., *Das Kristallin im Nördlinger Ries: Petrographische Zusammensetzung und Auswurfmechanismus der kristallinen Trümmermassen, Struktur des Kristallinen Untergrundes und Beziehungen zum Moldanubikum,* vol. V, 190 pp., Ferdinand Enke, Stuttgart, 1978.

Graup, G., P. Horn, H. Köhler, and D. Müller-Sohnius, Source materials for moldavites and bentonites, *Naturwissenschaften, 67,* 616, 1981.

Greeley, R., et al., Impact cratering in viscous targets: laboratory experiments, *Proc. Lunar Planet. Sci. Conf. 11th,* 2075–2097, 1980.

Grieve, R. A. F., Cratering in the lunar highlands: Some problems with the process, record and effects, in *Proceedings of the Conference on Lunar Highlands Crust,* edited by J. J. Papike and R. B. Merrill, pp. 173–196, Pergamon, New York, 1980.

Grieve, R. A. F., P. B. Robertson, and M. R. Dence, Constraints on the formation of ring impact structures, based on terrestrial data, *Proc. Lunar Planet. Sci., 12A,* 37–57, 1981.

Hartmann, W. K., Dropping stones in magma oceans: Effects of early lunar cratering, in *Proceedings of the Conference on Lunar Highlands Crust,* edited by J. J. Papike and R. B. Merrill, pp. 155–171, Pergamon, New York, 1980.

Hawke, B. R., and J. W. Head, Impact melt on lunar crater rims, in *Impact and Explosion Cratering,* edited by D. J. Roddy, R. O. Pepin, and R. B. Merrill, pp. 815–841, Pergamon, New York, 1977.

Hawke, B. R., and J. W. Head, Criteria for the identification of the Imbrium ejecta and local components in the Apollo 14 samples (abstract), *Lunar Planet. Sci., IX,* 477–479, 1978.

Head, J. W., Orientale multi-ringed basin interior and implications for the petrogenesis of lunar highland samples, *Moon, 11,* 327–356, 1974.

Head, J. W., Evidence for the sedimentary origin of Imbrium sculpture and lunar basin radial texture, *Moon, 15,* 445–462, 1976.

Head, J. W., and B. R. Hawke, Geology of the Apollo 14 region (Fra Mauro): Stratigraphic history and sample provenance, *Proc. Lunar Sci. Conf. 6th,* 2483–2501, 1975.

Heiken, G. H., et al., Preliminary stratigraphy of the Apollo 15 core, *Proc. Lunar Sci. Conf. 4th,* 191–213, 1973.

Hertogen, J., et al., Lunar basins and craters: evidence for systematic compositional changes of bombarding population, *Proc. Lunar Sci. Conf. 8th,* 17–45, 1977.

Herzberg, C. T., and M. B. Baker, The cordierite-to spinel-cataclasite transition: Structure of the lunar crust, in *Proceedings of the Conference on Lunar Highlands Crust,* edited by J. J. Papike and R. B. Merrill, pp. 113–132, Pergamon, New York, 1980.

Homilius, J., and H. Schmidt-Kaler, Ein Profil vom Riesrand südlich Wemding in das östliche Vorries nach geoelektrischen Tiefensondierungen, *Geol. Jahrb. Reihe E, 14,* 3–10, 1979.

Horn, P., and T. Kirsten, Lunar highland stratigraphy and radiometric dating, *Philos. Trans. R. Soc. London Ser, A, 285,* 145–150, 1977.

Hörz, F., Untersuchungen an Riesgläsern, *Beitr. Mineral. Petrogr., 11,* 621–661, 1965.

Hörz, F. (Ed.), Special issue on meteorite impact and volcanism, *J. Geophys. Res., 76,* 5381–5798, 1971.

Hörz, F., Ejecta of the Ries Crater, Germany, *Spec. Pap. Geol. Soc. Am., 190,* 39–56, 1982.

Hörz, F., and G. S. Banholzer, Deep-seated target materials in the continuous deposits of the Ries Crater, Germany, in *Proceedings of the Conference on Lunar Highlands Crust,* edited by J. J. Papike and R. B. Merrill, pp. 211–231, Pergamon, New York, 1980.

Hörz, F., V. R. Oberbeck, and R. H. Morrison, Remote sensing of the Cayley Plains and Imbrium Basin deposits (abstract), *Lunar Sci., V,* 357–359, 1974.

Hörz, F., R. V. Gibbons, R. E. Hill, and D. E. Gault, Large scale cratering of the lunar highlands: Some Monte Carlo model considerations, *Proc. Lunar Sci. Conf. 7th,* 2931–2945, 1976.

Hörz, F., H. Gall, R. Hüttner, and V. R. Oberbeck, Shallow drilling in the Bunte Breccia impact deposits, Ries Crater, Germany, in *Impact and Explosion Cratering,* edited by D. J. Roddy, R. O. Pepin, and R. B. Merrill, pp. 425–448, Pergamon, New York, 1977.

Howard, K. A., Avalanche mode of motion: Implications from lunar examples, *Science, 180,* 1052–1055, 1973.

Hsü, K. J., and A. Heim, Observations on landslides and relevance to modern interpretations, in *Rock Slides and Avalanches,* edited by B. Voigt, pp. 71–93, Elsevier, New York, 1978.

Hüttner, R., Geologische Untersuchungen im SW Vorries auf Blatt Neresheim und Wittislingen, Ph.D. thesis, 347 pp., Univ. Tübingen, Tübingen, Federal Republic of Germany, 1958.

Hüttner, R., Bunte Trümmermassen und Suevit, *Geol. Bavarica, 61,* 142–200, 1969.

Hüttner, R., Impaktgesteine des Rieses, *Geol. Bavarica, 76,* 108–158, 1977.

Hüttner, R., E. Brost, J. Homilius, and H. Schmidt-Kaler, Struktur des Ries-Kraterrandes auf Grund geoelektrischer Tiefensondierungen, *Geol. Jahrb., Reihe E, 19,* 95–117, 1980.

James, O. B., and F. Hörz, Workshop on Apollo 16, *LPI Tech. Rep. 81-01,* 157 pp., Lunar and Planet. Inst., Houston, Tex., 1981.

Jessberger, E. K., et al., Limited response of the K-Ar-system to the Nördlinger Ries giant meteorite impact, *Nature, 271,* 338, 1978.

Kieffer, S. W., Shock metamorphism of the Coconino Sandstone at Meteor Crater, Arizona, *J. Geophys. Res., 76,* 5449–5473, 1971.

Kieffer, S. W., From regolith to rock by shock, *Moon, 13,* 301–320, 1975.

Kieffer, S. W., and C. H. Simonds, The role of volatiles and lithology in the impact cratering process, *Rev. Geophys. Space Phys., 18,* 143–181, 1980.

Kirsten, T., and P. Horn, Chronology of the Taurus-Littrow Region III: Ages of mare basalts and highland breccias and some remarks about the interpretation of lunar highland ages, *Proc. Lunar Sci. Conf. 5th,* 1451–1475, 1974.

Kyte, F. J., Z. Zhou, and J. T. Wasson, Siderophile-enriched sediments from the Cretaceous-Tertiary boundary, *Nature, 288,* 651–655, 1980.

Lambert, P., Breccia dikes: Geological constraints on the formation of complex craters, *Proc. Lunar Planet. Sci., 12A,* 59–78, 1981.

Lemcke, E., W. Engelhardt, and H. Füchtbauer, Geologische und sedimentpetrographische Untersuchungen im Westteil der ungefalteten Molasse des süddeutschen Alpenvorlandes, *Geol. Jahrb. Beih., 11,* 1953.

Lindsay, J. F., Depositional processes on the lunar surface, *Lunar Sci., V,* 450–452, 1974.

Löffler, R., *Beiträge zur Riesenstehungs Hypothese, Jahresber. Mitt. Oberrheinischen Geol. Ver.,* vol. 14, 1926.

Lucchitta, B. K., Crater clusters and light mantle at the Apollo 17 site: A result of secondary impact from Tycho, *Icarus, 30,* 80–96, 1977.

Maurer, P., et al., Preimbrian craters and basins: Ages, compositions and excavation depths of Apollo 16 breccias, *Geochim. Cosmochim. Acta, 42,* 1687–1720, 1979.

Maxwell, D. E., Cratering flow and crater prediction methods, *Tech. Memo. TCAM 73-17,* Phys. Int. Corp., San Leandro, Calif., 1973.

Maxwell, D. E., Simple *Z* model of cratering, ejection and the overturned flap, in *Impact and Explosion Cratering,* edited by D. J. Roddy, R. O. Pepin, and R. B. Merrill, pp. 1003–1008, Pergamon, New York, 1977.

McGetchin, T. R., M. Settle, and J. W. Head, Radial thickness variation in impact crater ejecta: Implication for lunar basin deposits, *Earth Planet. Sci. Lett., 20,* 226–236, 1973.

Melosh, H. J., Acoustic fluidization: A new geological process?, *J. Geophys. Res., 84,* 7513–7520, 1979.

Mendell, W. W., Degradation of large, period II lunar craters, *Proc. Lunar Sci. Conf. 7th,* 2705–2716, 1976.

Moore, H. J., C. A. Hodges, and D. H. Scott, Multiringed basins—Illustrated by Orientale and associated features, *Proc. Lunar Sci. Conf. 5th,* 71–100, 1974.

Morrison, R. H., and V. R. Oberbeck, Geomorphology of crater and basin deposits—Emplacement of the Fra Mauro formation, *Proc. Lunar Sci. Conf. 6th,* 2503–2530, 1975.

Morrison, R. H., and V. R. Oberbeck, A composition and thickness model for lunar impact crater and basin deposits, *Proc. Lunar Planet, Conf. 9th,* 3763–3785, 1978.

Mouginis-Mark, P., Martian fluidized crater morphology: Variations with crater size, latitude, altitude, and target material, *J. Geophys. Res., 84,* 8011–8022, 1979.

Muehlberger, W. R., G. E. Ullrich, and C. A. Hodges (Eds.), Geology of the Apollo 16 area, central lunar highlands, *U.S. Geol. Surv. Prof. Pap., 1048,* 1981.

Neukum, G., and D. U. Wise, Mars: A standard crater curve and possible new time scale, *Science, 194,* 1381–1387, 1976.

Oberbeck, V. R., The role of ballistic erosion and sedimentation in lunar stratigraphy, *Rev. Geophys. Space Phys., 13,* 337–362, 1975.

Oberbeck, V. R., and R. H. Morrison, Laboratory simulation of the herringbone pattern associated with lunar secondary crater chains, *Moon, 9,* 415–455, 1974.

Oberbeck, V. R., and R. H. Morrison, Candidate areas for in situ ancient lunar materials, *Proc. Lunar Sci. Conf. 7th,* 2983–3005, 1976.

Oberbeck, V. R., et al., Effects of formation of large craters and basins on emplacement of smooth plains materials (abstract), *Lunar Sci., V,* 568–570, 1974.

Oberbeck, V. R., et al., On the origin of lunar smooth plains, *Moon, 12,* 19–54, 1975.

O'Keefe, J. D., and T. J. Ahrens, The interaction of the Cretaceous-Tertiary extinction bolide with the atmosphere, ocean and solid earth, *Spec. Pap. Geol. Soc. Am., 190,* 103–120, 1982.

Onorato, P. I. K., D. R. Uhlmann, and C. H. Simonds, Heat flow in impact melts: Apollo 17, station 6, boulder and some applications to other breccias and xenolith-laden melts, *Proc. Lunar Sci. Conf. 7th,* 2449–2468, 1976.

Onorato, P. I. K., D. R. Uhlmann, and C. H. Simonds, The thermal history of the Manicouagan impact melt sheet, Quebec, *J. Geophys. Res., 83,* 2789–2798, 1978.

Orphal, D. L., Calculations of explosion cratering, II, Cratering mechanics and phenomenology, in *Impact and Explosion Cratering,* edited by D. J. Roddy, R. O. Pepin, and R. B. Merrill, pp. 907–917, Pergamon, New York, 1977.

Ostertag, R., Sedimentologische Untersuchungen der NASA Forschungsbohrung Demmingen in der Ejektadecke des Impakt Kraters Nördlinger Ries, M.S. thesis, Univ. Münster, Münster, Federal Republic of Germany, 1978.

Palme, H., Identification of projectiles of large terrestrial impact craters and some implications for the interpretation of Ir-rich Cretaceous/Tertiary boundary layers, *Spec. Pap. Geol. Soc. Am., 190,* 223–234, 1982.

Papike, J. J., and R. B. Merrill (Eds.), *Proceedings of the Conference on Lunar Highlands Crust,* 499 pp., Pergamon, New York, 1980.

Phinney, W. C., and C. H. Simonds, Dynamical implications of the petrology and distribution of impact melt rocks, in *Impact and Explosion Cratering,* edited by D. J. Roddy, R. O. Pepin, and R. B. Merrill, pp. 771–790, Pergamon, New York, 1977.

Pike, R. J., Apparent depth/diameter relation for lunar craters, *Proc. Lunar Sci. Conf. 8th,* 3427–3436, 1977.

Pohl, J., and G. Angenheister, Anomalien des Erdmagnetfeldes und Magnetisierung der Gesteine im Nördlinger Ries, *Geol. Bavarica, 61,* 327–336, 1969.

Pohl, J., and H. Gall, Bau und Entstehung des Ries-Kraters, *Geol. Bavarica, 76,* 159–175, 1977.

Pohl, J., D. Stöffler, H. Gall, and K. Ernstson, The Ries impact crater, in *Impact and Explosion Cratering,* edited by D. J. Roddy, R. O. Pepin, and R. B. Merrill, pp. 343–404, Pergamon, New York, 1977.

Preuss, E., and H. Schmidt-Kaler, Das Ries; Geologie, Geophysik und Genese eines Kraters, *Geol. Bavarica, 61,* 478 pp., 1969.

Raikes, S. A., and T. J. Ahrens, Post shock temperatures in minerals, *Geophys. J. R. Astron. Soc., 58,* 717, 1979.

Roddy, D. J., Large scale impact and explosion craters: Comparisons of morphological and structural analogs, in *Impact and Explosion Cratering,* edited by D. J. Roddy, R. O. Pepin, and R. B. Merrill, pp. 185–246, Pergamon, New York. 1977.

Roddy, D. J., J. M. Boyce, G. W. Colton, and A. L. Dial, Meteor Crater, Arizona, rim drilling with thickness, structural uplift, diameter, depth, volume and mass balance calculations, *Proc. Lunar Sci. Conf. 6th,* 2621–2644, 1975.

Roddy, D. J., R. O. Pepin, and R. B. Merrill, (Eds.), *Impact and Explosion Cratering,* Pergamon, New York, 1977*a*.

Roddy, D. J., G. W. Ullrich, F. Sauer, and G. H. S. Jones, Cratering motions and structural deformation in the rim of the Prairie-Flat multi-ring explosion crater, *Proc. Lunar Sci. Conf. 9th,* 3389–3407, 1977*b*.

Ryder, G., and M. D. Norman, Catalog of Apollo 16 rocks, *NASA Johnson Space Center Curatorial Branch Publ. 52, JSC 16904,* 1980.

Schaeffer, G. A., and O. A. Schaeffer, $^{39}Ar/^{40}Ar$ ages of lunar rocks, *Proc. Lunar Sci. Conf. 8th,* 2253–2300, 1977.

Schaeffer, O. A., L. Hussain, and G. A. Schaeffer, Ages of highland rocks: The chronology of lunar highlands revisited, *Proc. Lunar Sci. Conf. 7th,* 2067–2092, 1976.

Schmeer, D., Sedimentpetrographische Beobachtungen aus der oberen Süsswassermolasse im Bereich von Freising bis Landshut, *Z. Dtsch. Geol. Ges., 105,* 496–516, 1955.

Schmidt-Kaler, H., Keuper and Jura in der Tiefbohrung Riedenburg, *Geol. Bl. Nordost Bayern, 19,* 97–112, 1969.

Schmidt-Kaler, H. (Ed.), Ergebnisse der Ries-Forschungsbohrung 1973: Struktur des Kraters und Entwicklung des Kratersees, *Geol. Bavarica, 75,* special issue, 470 pp., 1977.

Schmidt-Kaler, H., W. Treibs, and R. Hüttner, Exkursionsführer zur Geologischen Übersichtskarte des Ries 1:100 000, 68 pp., Bayer, Geol. Landesamt, München, Federal Republic of Germany, 1970.

Schneider, W., Petrologische Untersuchungen der Bunten Breccie im Nördlinger Ries, *Neues Jahrb. Mineral. Abh., 114,* 136–180, 1971.

Schnitzer, W. A., Sedimentpetrographische Untersuchungen an den postjurassischen Überdeckungsbildungen der mittleren südlichen Frankenalb, *Geol. Bl. Nordost Bayern, 3,* 121–134, 1953.

Schnitzer, W. A., Der Schwermineraliengehalt der Randfacies des fränkischen mittleren Keupers in Tiefbohrungen, *Erlanger Geol. Abh., 11,* 49–66, 1954.

Schultz, P. H., Evidence and mechanisms for the non-local contribution to ejecta deposits, Apollo 16 Workshop, *LPI Tech. Rep. 80-01,* edited by O. B. James and F. Hörz, pp. 120–122, Lunar and Planet. Inst., Houston, Tex., 1981.

Schultz, P. H., and D. E. Gault, Atmospheric effects on Martian ejecta emplacement, *J. Geophys. Res., 84,* 7669–7687, 1979.

Schultz, P. H., and W. Mendell, Orbital infrared observations of lunar craters and possible implications for impact ejecta emplacement, *Proc. Lunar Planet. Conf. 9th,* 2857–2883, 1978.

Schultz, P. H., and R. B. Merrill (Eds.), Multi ring basins, *Proc. Lunar Planet. Sci., 12A,* 1981.

Schultz, P. H., and J. Singer, A comparison of secondary craters on the moon, Mercury and Mars, *Proc. Lunar Planet. Sci. Conf. 11th,* 2243–2259, 1980.

Schultz, P. H., and P. D. Spudis, Evidence for ancient mare volcanism, *Proc. Lunar Planet. Sci. Conf. 10th,* 2899–2918, 1979.

Schultz, P. H., D. E. Gault, and M. Mendenhall, Multiple body impacts: Implications for secondary impact processes (abstract), *Lunar Planet. Sci., XI,* 1006–1007, 1980.

Schultz, P. H., et al., Multi ring basin formation: Possible clues from impact cratering calculations, *Proc. Lunar Planet. Sci. Conf., 12A*, 181–195, 1981.

Settle, M., The role of fallback ejecta in the modification of impact craters, *Icarus, 42*, 1–19, 1980.

Settle, M., and J. W. Head, The role of rim slumping in the modification of impact craters, *J. Geophys. Res., 84*, 3081–3096, 1979.

Shoemaker, E. M., Interpretation of lunar craters, in *Physics and Astronomy of the Moon*, edited by Z. Kopal, pp. 283–330, Academic, New York, 1962.

Shoemaker, E. M., Impact mechanics at Meteor Crater, Arizona, in *The Moon, Meteorites and Comets*, edited by B. M. Middlehurst and G. P. Kuiper, pp. 301–336, University of Chicago Press, Chicago, Ill., 1963.

Short, N. M., and M. L. Foreman, Thickness of impact crater ejecta on the lunar surface, *Mod. Geol., 3*, 69–91, 1972.

Simonds, C. H., J. C. Warner, W. C. Phinney, and P. E. McGee, Thermal model for impact breccia lithification: Manicouagan and the moon, *Proc. Lunar Sci. Conf. 7th*, 2509–2528, 1976.

Smit, J., and J. Hertogen, An extraterrestrial event at the Cretaceous-Tertiary boundary, *Nature, 285*, 198–200, 1980.

Soderblom, L. A., A model for small-impact erosion applied to the lunar surface, *J. Geophys. Res., 75*, 2655–2661, 1970.

Soderblom, L. A., and L. A. Lebofsky, Technique for rapid determination of relative ages of lunar areas from orbital photography, *J. Geophys. Res., 77*, 279–296, 1972.

Staudacher, T., et al., $^{40}Ar/^{39}Ar$ ages of rocks and glasses from the Nördlinger Ries Crater and the temperature history of impact breccias, *J. Geophys., 51*, 1–11, 1982.

Stettner, G., Das Grundgebirge in der Forschungsbohrung Nördlingen 1973 im regionalen Rahmen und seine Veränderungen durch den Impakt, *Geol. Bavarica, 72*, 35–51, 1974.

Stöffler, D., Zones of impact metamorphism in the crystalline rocks of the Nördlinger Ries, *Contrib. Mineral. Petrol., 12*, 15–24, 1966.

Stöffler, D., Deformation and transformation of rock-forming minerals by natural and experimental shock processes, I, Behavior of minerals under shock compression, *Fortschr. Mineral., 49*, 50–113, 1972.

Stöffler, D., Research drilling Nördlingen 1973: Polymict breccias, crater basement, and cratering model of the Ries impact structure, *Geol. Bavarica, 75*, 443–458, 1977.

Stöffler, D., Cratering mechanics: Data from terrestrial and experimental craters and implications for the Apollo 16 site, Workshop on Apollo 16, *LPI Tech. Rep. 81-01*, edited by O. B. James and F. Hörz, pp. 132–141, Lunar and Planet. Inst., Houston, Tex., 1981.

Stöffler, D., D. E. Gault, J. Wedekind, and G. Polkowski, Experimental hypervelocity impact into quartz sand: Distribution and shock metamorphism of ejecta, *J. Geophys. Res., 80*, 4062–4077, 1975.

Taylor, G. J., and U. B. Marvin, How, when and where did the Apollo 16 impact breccias and melt rocks form? Workshop on Apollo 16, *LPI Tech. Rep. 81-01*, edited by O. B. James and F. Hörz, pp. 9–15, Lunar and Planet Inst., Houston, Tex., 1981.

Taylor, G. J., and L. L. Wilkening (Eds.), Workshop on lunar breccias and soils and their meteoritic analogs, *LPI Tech. Rep. 82-02*, 172 pp. Lunar and Planet. Inst., Houston, Tex., 1982.

Trulio, J. G., Ejecta formation: Calculated motion from a shallow-buried nuclear burst, and its significance for high velocity impact cratering, in *Impact and Explosion Cratering*, edited by D. J. Roddy, R. O. Pepin, and R. B. Merrill, pp. 919–957, Pergamon, New York, 1977.

Vaniman, D. T., and J. J. Papike, Lunar highland melt rocks: Chemistry, petrology and silicate mineralogy, in *Proceedings of the Conference on Lunar Highlands Crust*, edited by J. J. Papike and R. B. Merrill, pp. 271–337, Pergamon, New York, 1980.

Wagner, G. H., Kleintektonische Untersuchungen im Gebiet des Nördlinger Ries, *Geol. Jahrb., 81*, 519–600, 1964.

Warren, P. H., and J. T. Wasson, Early lunar petrogenesis, oceanic and extraoceanic, in *Proceedings of the Conference on Lunar Highlands Crust*, edited by J. J. Papike and R. B. Merrill, pp. 81–99, Pergamon, New York, 1980.

Wetherill, G. W., Nature and origin of basin-forming projectiles, *Proc. Lunar Planet. Sci., 12A*, 1–18, 1981.

Wilhelms, D. E., V. R. Oberbeck, and H. R. Aggarwal, Size-frequency distribution of primary and secondary lunar impact craters, *Proc. Lunar Planet. Sci. Conf. 9th*, 3735–3762, 1978.

Wilhelms, D. E., Primary ejecta origin of Apollo 16 samples, Apollo 16 Workshop, *LPI Tech. Rep. 81-01*, edtied by O. B. James and F. Hörz, pp. 150–154, Lunar and Planet. Inst., Houston, Tex., 1981.

Woronow, A., A general cratering history model and its implications for the lunar highlands, *Icarus, 34*, 76–88, 1978.

F. Hörz, NASA Johnson Space Center, Sn4/Experimental Planetology Branch, Houston, TX 77058.

R. Ostertag, Mineralogisches Institut, Universität Münster, 4400 Münster, Federal Republic of Germany.

D. A. Rainey, 4317 E. 17th Avenue, Parkway, CO 80220.

(Received February 17, 1983;
accepted April 4, 1983.)